NTNU

Norwegian University of
Science and Technology

Overtopping of embankment dams from landslide generated waves

Joël Biedermann

Civil and Environmental Engineering
Submission date: July 2017
Supervisor: Fjola Gudrun Sigtryggsdottir, IBM
Co-supervisor: Leif Lia, IBM

Norwegian University of Science and Technology
Department of Civil and Environmental Engineering

NTNU
Norwegian University of
Science and Technology

Faculty of Engineering
Science and Technology
Department of Civil and
Environmental Engineering

M.Sc. THESIS ASSIGNMENT

Candidate: Joël Biedermann

Title: Impact of landslide generated waves on embankment dams.

1   BACKGROUND

Landslide generated impulse waves may cause damages as they run-up shores, or against dams retaining a reservoir. Large such waves may overtop dams with hazardous consequences for the downstream area. The hazard may be intensified in the case of an embankment dam, considering that this may erode and even completely fail during such extreme loading conditions, thereby releasing more water from the reservoir.

It was with this background that the Norwegian Water Resources and Energy Directorate (NVE), in collaboration with NTNU, initiated a research program on the impacts of landslide generated wave action on embankment dams, particularly rockfill dams. For this, an experimental work has been carried out on a physical model in the hydraulic laboratory at NTNU.

In 2014, the experimental tests were carried out for different landslide scenarios, by varying slide parameters. The physical processes and interaction between the landslide generated waves, and dam overtopping was studied. A comparison was also made between the results obtained from the experimental test with results from the computational method recommended by Heller et al. (2009).

As a continuation of the project, an experimental study was also carried out in 2015 and spring 2016 using the model in the hydraulic laboratory. The experimental test was mainly focused on the slide volume and dam characteristics and was performed under several different scenarios by varying the parameters of the slide volume, the reservoir water levels, and the upstream dam face slope, and the dam alignment. A test program was also carried out with rough and smooth upstream dam face, respectively.

During fall 2016, a study into the different parameter was continued, also varying the speed of the landslide. Additionally, the ramp for the landslide was moved to the other side of the test basin to investigate potential laboratory effects in the previous setup. In the new landslide setup only a so-called Chevron dam has been used hitherto.

In general, the project study has enhanced the understanding of the effect of the landslide generated waves and dam parameters. However, the new landslide setup provides an opportunity for further studies to be conducted as a part of this thesis.

2   MAIN QUESTIONS FOR THE THESIS

The thesis will be composed of a number of tasks related to assessing relevant literature and preparing and running an experimental study on the existing physical model. The main objective of the study is to use the scale model in the hydraulic laboratory, in order to investigate the effect of landslide generated waves on embankment dams. This knowledge should contribute to the process of developing a method to calculate the size of the overtopping over an embankment dam as a result of landslide generated wave in reservoirs.

2.1 The specific tasks are as follows

1. Review current literature, an important aspect of the review will be to find examples of the previous study on landslide generated wave impacts on embankment dam and studied the governing parameters, their characteristics and interaction. The literature review will provide the basis for planning the model study.

2. Study the existing model set-up and the installed instrument. Carry out a model test to study the effect of the impulse of a landslide on wave generation, propagation and embankment dam overtopping. The effect of the impulse will be represented by an impulse product parameter, which considers the following parameters: the slide speed, the still water depth in the slide impact zone, relative slide mass, and the slide impact angle.
   A wave will be generated using a different slide size/volume/speed and the corresponding wave height, overtopping volume and overtopping depth above the dam crest in the model will be monitored and studied. The speed of the slide will be varied by adjusting the initial location of the slides.
   Two different dam arrangements will be used: the Chevron dam to repeat tests executed previously and a straight dam to analyse new results. Thus, the main focus will be on a straight dam with an upstream slope of 1:1.5 and potentially also of 1:2 or similar. Freeboard will be in accordance with Norwegian regulations (6 m and 4,5 m).
   Additionally, but depending on conditions in the laboratory, the effect of an energy breaker at the crest level will be investigated.

   The experimental results will be used to study the physical processes and the relationship between
   - The slide impulse and generated wave height
   - The slide impulse and dam overtopping volume, and discharge.
   - The slide impulse and pattern of wave propagation, with a focus on its influence on the overtopping depth at the dam crest.
   - Freeboard and dam overtopping volume, and discharge.

Sensors will be added to the model setup so that the overtopping depth at the dam crest can be investigated in more detail than previously, and for an estimate of the overtopping discharge with time.

3. Perform a sensitivity and uncertainty analysis of the parameters, and identify the limitations and/ possibility for improvement and also draw recommendation for practical application.

3   SUPERVISION, DATA AND INFORMATION INPUT

Associate Professor Fjola Gudrun Sigtryggsdottir will be the supervisor of the thesis work. Professor Leif Lia will be a co-supervisor, as well as research scientist Kiflom Belete, who will provide guidance on the model tests and the process of the study.

Discussion with, and input from colleagues and other research or engineering staff at NTNU, SINTEF, power companies or consultants are recommended. Significant inputs from others shall, however, be referenced in a convenient manner.

The research and engineering work carried out by the candidate in connection with this thesis shall remain within an educational context. The candidate and the supervisors are therefore free to introduce assumptions and limitations, which may be considered unrealistic or inappropriate in a contract research or a professional engineering context.

4   REPORT FORMAT AND REFERENCE STATEMENT

The report should be written with a text editing software, and figures, tables, photos, etc. should be of good quality. The report should contain an executive summary, a table of content, a list of figures and tables, a list of references and information about other relevant sources. The report should be submitted electronically in B5-format .pdf-file in DAIM, and three paper copies should be handed in to the institute.

The executive summary should not exceed 450 words and should be suitable for electronic reporting.

The Master's thesis should be submitted within **28th of July 2017**

<div align="center">

Trondheim 21th of February 2017

_____
Fjóla G. Sigtryggsdóttir
Associate Professor

</div>

Acknowledgements

After having been in exchange in Stockholm during my third year of bachelor, I am really grateful to have had the chance to come back to Scandinavia to write my master thesis in Norway. I would like to express my deepest thanks to Prof. Anton Schleiss of EPFL in Switzerland and Prof. Leif Lia of NTNU in Norway for giving me this opportunity. Furthermore, I really appreciated the warm welcoming in Trondheim, and Prof. Lia's availability throughout the semester as a co-supervisor.

I am sincerely grateful to my main supervisor Prof. Fjola Gudrun Sigtryggsdottir for always being helpful, supportive and enthusiastic along my master thesis. Prof. Sigtryggsdottir gave space for my ideas, but her door was always open whenever I needed advice or had question about my research or writing.

Many thanks and gratitude go also to Researcher Kiflom Belete, Eng. Geir Tesaker and Netsanet Nigatu for their advices and valuable help during the test phase in the laboratory. I would also like to thank a lot Žofie and Gonzalo for the help with their correction of my thesis. Furthermore, I would like to thank all my friends who made the five past years of university turn into awesome memories.

Finally, I would like to express my profound gratitude to my parents and siblings for providing me with endless support and encouragement throughout my years of studies.

Trondheim, 28th July 2017   Joël Biedermann

Abstract

A landslide entering a reservoir transforms its kinetic energy into an impulse wave. This wave propagates across the basin, runs up the shores and may overtop the dam. The consequences of such event are damages to nature and infrastructure, as well as a risk of human life losses. Due to their topographies, this danger threatens both Norway and the Alps areas: reservoirs, lakes or fjords are often located below steep shores with potentially unstable sliding masses.

This thesis is a parametrical study on landslide generated impulse waves, based on experiments conducted in a laboratory on a 1:190 scale model. The landslide is simulated by blocks sliding down a ramp on the reservoirs sides, entering the water, creating a wave running up on the opposite shore and propagating towards the dam. The resulting overtopping is thereby also influenced by the run-up waves along the lake shore.

The primary objective of this thesis is to use the scale model to investigate the overtopping of embankment dams due to landslide generated impulse waves. In order to better understand the parameters influencing the overtopping volume, height and discharge, different parameters were varied over the tests. Dam roughness, dam upstream slope, freeboard, landslide volume, shape and impact velocity were investigated, as well as the influence of a wave wall integrated into the upper part of the dam. Furthermore, overtopping speed and discharge, plus wave generation and propagation pattern were observed and described.

The lateral position of the landslide in the reservoir has caused a complex wave reflection phenomenon resulting in an uneven overtopping along the dam crest. The results of the tests indicate a major influence of the freeboard on the dam overtopping as well as, an additional impact of landslide volume on the overtopping volume, and landslide length on the overtopping height. The best way to mitigate the hazard is therefore by lowering the water level in the reservoir. Additionally, the implementation of a vertical wave wall has also shown to have an influence on the overtopping volume and needs to be further analysed. Finally, it is observed that the lateral landslide model makes it harder to apply impulse wave equations established in flume or wave basin.

Keywords

Résumé

Un glissement de terrain terminant sa course dans un plan d'eau transforme son énergie cinétique en vague d'impulsion. Celle-ci se propage à travers le lac, remonte les rives et crée potentiellement un débordement par-dessus le barrage. Un tel événement causerait des dommages à la digue, à l'environnement et aux infrastructures en aval, avec un risque de pertes humaines. En raison de leur topographie accidentée, ce danger menace à la fois la Norvège et les pays alpins : les retenues, lacs ou fjords sont en effet souvent situés en aval de pentes raides potentiellement instables.

Ce travail de master étudie les paramètres influençant les vagues d'impulsions générées par des glissements de terrain sur la base d'expériences menées dans un laboratoire sur un modèle à l'échelle 1 : 190. Le glissement de terrain, situé en rive droite de la retenue et simulé par des blocs, glisse sur un plan incliné, finit sa course dans l'eau et génère une vague d'impulsion. Cette dernière remonte la rive opposée et se propage vers le barrage. Le mouvement en résultant est donc influencé par la réflexion de la vague sur les rives. S'il est d'ampleur suffisante, il peut causer un débordement.

L'objectif principal de cette thèse est d'utiliser le modèle pour étudier le débordement de barrages en remblai suite à une vague d'impulsion générée par un glissement de terrain. Afin de mieux comprendre les éléments influençant le volume, la hauteur, la vitesse et le débit du débordement, les paramètres suivants ont été variés au cours des tests : la revanche, la rugosité et l'inclinaison de la pente amont du barrage, ainsi que le volume, la forme et la vitesse d'impact du glissement de terrain. De plus, l'effet d'une paroi verticale intégrée sous le couronnement du barrage est analysé.

Les résultats des simulations démontrent l'influence primordiale de la revanche sur le débordement par-dessus le barrage, une corrélation entre le volume du glissement de terrain sur le volume de débordement et de la longueur du glissement sur la hauteur de débordement. La meilleure façon d'atténuer le risque consiste en une réduction du niveau d'eau dans la retenue. En outre, la mise en œuvre d'une paroi verticale au couronnement a également montré une influence sur le volume débordant, mais doit être analysé plus en détail pour pouvoir en tirer des conclusions plus précises. Finalement, il est difficile d'appliquer les équations d'ondes d'impulsion en réservoir existantes à ce

modèle en raison de la position du glissement de terrain en rive latérale ce qui cause un phénomène complexe de réflexion d'ondes.

Mots-clés

Glissement de terrain, vague d'impulsion, débordement, revanche

Contents

Content

List of Figures

List of Tables

Notations / Abbreviations

Notations

a Wave amplitude [m]

b Landslide width [m]

b_c Crest section width [m]

c Wave celerity [m/s]

d_0 Overtopping height [m]

E_k Kinetic energy [J]

F Landslide Froude number; $F = V_s/(g/h)^{1/2}$ [-]

g Gravitational acceleration; $g = 9.81$ [m/s^2]

H Wave height in front of the dam [m]

h Still water depth [m]

h_c Measured overtopping height [m]

L   Length unit

L Wave length in front of the dam [m]

M Mass unit

M Relative landslide mass; $M = \rho_s V_s/(\rho_w bh^2)$ [-]

n Landslide porosity [-]

q_c Overtopping discharge [m^3/s]

r Radial distance from the impact location in the wave basin [m]

R^2 Coefficient of determination

S Relative landslide thickness; $S = s/h$ [-]

s Landslide thickness [m]

T   Time unit

T Wave period [s]

t Time step; $t = 1/200$ [s]

V Volume [l]

V_s Landslide impact velocity [m/s]

$V\!\!\!\!\!/_s$ Landslide volume [m^3]

X Relative streamwise distance from the impact location; $X = x/h$ [-]

X_M Relative streamwise distance of the maximum wave amplitude from the impact location; $X_M = x_M/h$ [-]

x Streamwise distance from the impact location [m]

x_M Streamwise distance of the maximum wave amplitude; $x_M = (11/2)P^{(1/2)}h$ [m]

w Dam height [m]

α Landslide impact angle [°]

β Run-up angle / dam front face angle [°]

γ Wave propagation angle (Figure 2.4) [°]

λ Scale factor

μ Average

ρ Correlation factor

ρ_s Landslide density [kg/m^3]

ρ_w Water density [kg/m^3]

Σ Sum

σ Standard deviation

Abbreviations

DW   Dam with wave wall and 1:1.5 slope

DWH   Dam with wave wall and horizontal part and 1:1.5 slope (Figure 4.6)

IPP   Impulse product parameter

RD   Rough dam with 1:1.5 slope

SD   Smooth dam with 1:1.5 slope

SD2   Smooth dam with 1:2 slope

2H   Landslide configuration with two blocks placed next to each other

2V   Landslide configuration with two blocks placed behind each other

4-block Landslide configuration with four blocks

6-block Landslide configuration with six blocks

Chapter 1 Introduction

In mountainous regions, reservoirs are often built to store water in altitude for power production and water supplies. Along these infrastructures, rock falls, avalanches, glacier carving and landslides are common. When these rapid masses fall into reservoirs, they generate an impulse wave by transferring their momentum to the water (ICOLD, 2002). Once the wave has propagated through the reservoir and reached the shores, the water runs up the shores and may cause a dam overtopping. Damages to the downstream populations, infrastructure and nature are then unavoidable. In western Norway, rock slides into the Lake Loen triggered impulse waves of 40.5 m, 74 m and 12-15 m in 1905, 1936 and 1950 respectively. Loss of lives and significant damages along the lake are reported for the two first events (Jørstad, 1968). In the Alps, the sadly well-known Vajont tragedy occurred in 1963. A landslide generated a wave flooding the village Erto along the reservoir and overtopping the dam of the reservoir by approximately 100 meters (Kiersch, 1964). The water ran down the Piave Valley and destroyed the town of Longarone. More than 2 000 lives were lost. During the elaboration of this master thesis, a small landslide occurred in the famous Geiranger fjord. The generated wave was about 1 m high and damaged some docks in the town of Geiranger (Gamlem, 2017; Gamlem & Brunstad, 2017; Petley, 2017). This recent event shows that the threat remains actual, enhanced by climate change or intensive precipitations.

Such catastrophes led to the beginning of investigations in this topic. Most of the research was executed in laboratories, in flume channels or large reservoirs, to simplify the phenomenon. In this way, only one impulse wave overtops the dam, and no reflections occur. Heller (2007) introduced the use of the impulse product parameter and Heller, Hager, & Minor (2009) wrote a guide for impulse wave calculations. However, landslides are mostly situated on the sides of the reservoir and create waves with reflections, which are not considered in these equations.

In 2008, the laboratory of the Department of Hydraulic Engineering at NTNU in Trondheim built a scaled model of Storfjord to predict the wave height due to the Åkerneset landslide. Once the tests were finished, the model was transformed into a generic model of a reservoir with a lateral landslide.

This model studies, therefore, the effect of an impulse wave and reflected waves. Thus, this model is closer to reality due to the landslide positioned on the side shore and a reservoir transversal profile with a trapezoidal shape.

This thesis is a parametrical study investigating mainly the overtopping height, volume and discharge over the dam crest. Different parameters of the model are considered, namely dam roughness, dam slope, freeboard, landslide impact velocity and landslide shape. Which one of these parameters influences the overtopping the most? Would a wave wall reduce considerably the overtopping? Is the overtopping uniform over the dam crest? Can previous research be applied to this model?

The thesis introduces first a summary of the impulse wave theory by Heller, Hager & Minor (2009) in Chapter 2, and a short presentation of the different studies already done on the model in Chapter 3. In Chapter 4 the physical model is described, before the test procedure is explained in Chapter 5. Finally, the analysis of the results is presented in Chapter 6. The report is written in a compact form with many appendices providing additional information for a better understanding.

Chapter 2 Impulse wave theory

This chapter presents first a summary of the currently applied theory for impulse waves due to landslides. In the second section, a recent study to calculate the overtopping due to an impulse wave based on the wave properties is given.

2.1   Impulse wave theory by Heller et al.

This section introduces the work of Heller et al. (2009) at the Laboratory of Hydraulics, Hydrology and Glaciology at ETH Zurich based on the work of Müller (1995), Ramsden (1996) and Heller (2007). According to Heller et al., the impulse waves can be generated in three different ways illustrated in Figure 2.1. The differentiation is determined by the initial landslide position – above, partially in the water or completely submerged. This thesis only considers subaerial landslides, the first of the three cases.
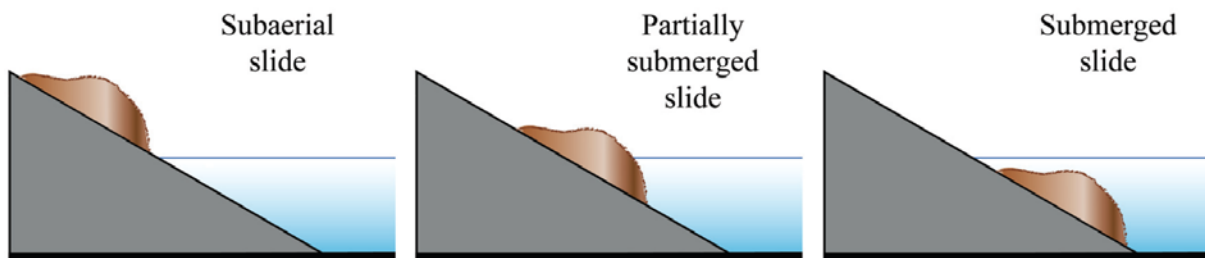
Figure 2.1. Different ways of impulse wave generation (Heller et al., 2009)

The impulse wave process is separated into three phases illustrated in Figure 2.2. First, the wave generation occurs through the transfer of the momentum of the landslide to the water, then the wave propagates through the reservoir, and finally the wave runs up the shore with a possible overtopping of the dam. Phases one and two are studied together in literature, whereas third is considered separately.
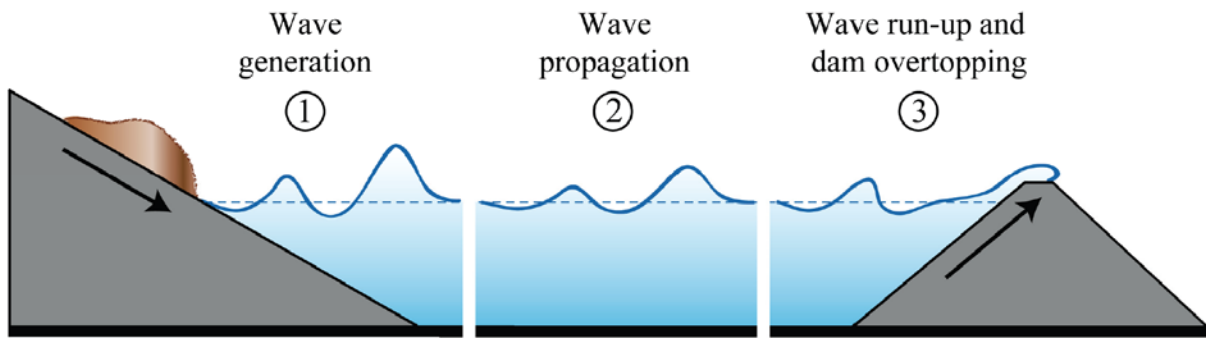
Figure 2.2. Three impulse wave phases (Heller et al., 2009)

2.1.1 Wave generation and propagation

The landslide transfers his momentum to the water when crashing into it, creating an impulse wave. The impulse wave generation equations are elaborated for two different reservoir geometries (Figure 2.3). The first one considers a prismatic wave channel where the wave is propagating only longitudinally, not laterally (2D). The attenuation of the wave by the bottom and internal friction is small. Therefore, the wave energy, i.e. the wave height, is preserved, and only a slight reduction of the wave is observed when propagating through the reservoir. The second geometry, a rectangular wave basin, generates a radial propagation of the wave. In this case, the wave height decreases when propagating as the energy is distributed over an increasing area.
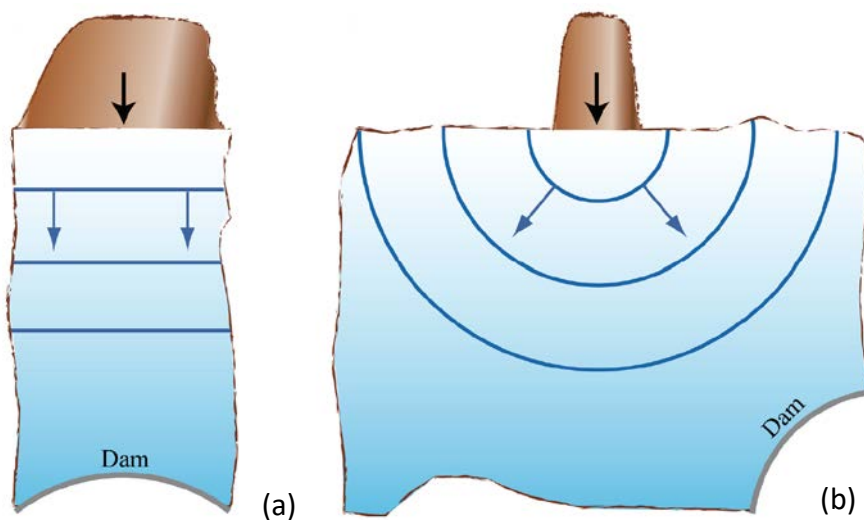
Figure 2.3. Reservoir geometries investigated with 2D and 3D equations (Heller et al., 2009)

Relevant parameters influencing the wave generation are identical for the 2D and the 3D case. They are listed below and illustrated in Figure 2.4 :

- still water depth h,
- landslide impact velocity V_s,
- landslide volume V_s,
- landslide thickness s,
- landslide width b,
- landslide density ρ_s,
- landslide porosity n,
- landslide impact angle α.

Research was also done on the following parameters, but they were found to have a negligible impact: the slide front angle ϕ, the slide length l and the grain size distribution (Heller, 2007). The underwater slide duration was studied by Panizzo, De Girolamo, & Petaccia (2005) but the parameter was hard to define and was for this reason deducted from other remaining governing parameters.

The propagation of the wave is influenced by the following governing parameters considering the channel (2D) and the basin (3D) setup presented in the list below and in Figure 2.4.

- streamwise distance x (2D),
- radial distance r (3D),
- wave propagation angle γ (3D).
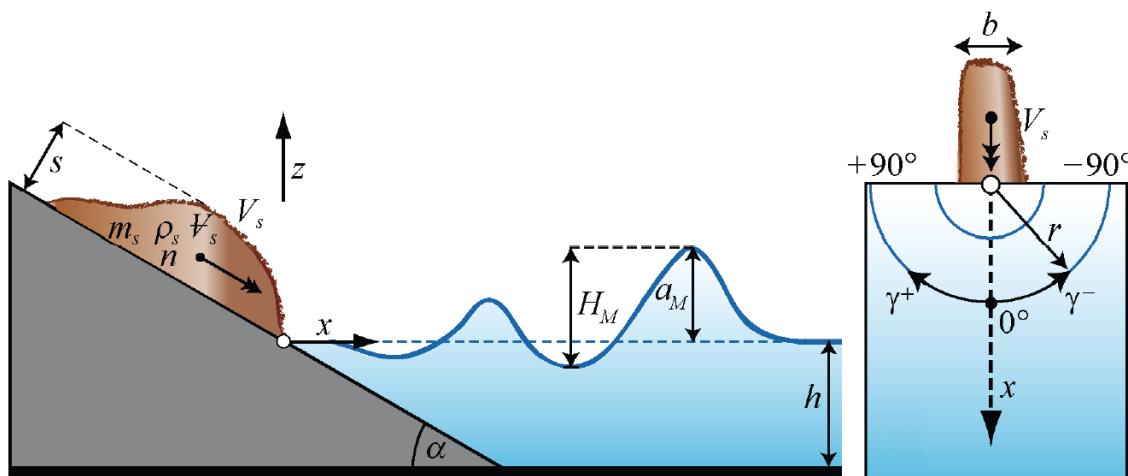
Figure 2.4. Governing parameters for landslide generation and wave propagation (Heller et al., 2009)

5

Equations are given for the calculation of the landslide velocity V_s based on the drop height, the slide angle α and the gravitational acceleration. However, they are not relevant for this thesis and thus not presented here.

The **wave celerity c** for an impulse wave is determined from the celerity of a solitary wave, as shown by Kamphuis & Bowering (1972):

$$c = \sqrt{g \cdot (h + a)} \qquad (2.1)$$

where: h [m]   Still water depth

a [m]   Wave amplitude

Heller (2007) defined an **impact product parameter P** to estimate the wave generated by the landslide. Equations are suggested to calculate the wave height, wave period and the distance of the maximal wave height. The impact product parameter is given in Equation (2.2).

$$P = F \cdot S^{\frac{1}{2}} \cdot M^{\frac{1}{4}} \cdot \sqrt{\cos(6/7\alpha)} \qquad (2.2)$$

where: F [-]   Slide Froude number; $F = V_s/(g/h)^{1/2}$

V_s [m/s]   Landslide impact velocity

g [m/s^2]   Gravitational acceleration; $g = 9.81\ m/s^2$

h [m]   Still water depth in the slide impact zone

S [-]   Relative slide thickness; $S = s/h$

s [m]   Slide thickness

M [-]   Relative slide mass; $M = \rho_s V_s/(\rho_w b h^2)$

ρ_s [kg/m^3] Landslide density

V_s [m^3]   Landslide volume

ρ_w [kg/m^3] Water density

b [m]   Landslide width

α [°]   Slide impact angle

The limitations which must be respected while using the impulse product parameter are given in Table 2.1.

Term	Range	Meaning
Slide Froude Number	$0.86 \leq F \leq 6.83$	$F = V_s/\sqrt{gh}$
Relative slide thickness	$0.09 \leq S \leq 1.64$	$S = s/h$
Relative slide mass	$0.11 \leq M \leq 10.02$	$M = \rho_s V_s/(\rho_w bh^2)$
Relative slide density	$0.59 \leq D \leq 1.72$	$D = \rho_s/\rho_w$
Relative granular density	$0.96 \leq \rho_g/\rho_w \leq 2.75$	ρ_g/ρ_w
Relative slide volume	$0.05 \leq V \leq 5.94$	$V = V_s/(bh^2)$
Bulk slide porosity	$30.7\% \leq n \leq 43.3\%$	n
Slide impact angle	$30° \leq \alpha \leq 90°$	α
Relative slide width	$0.74 \leq B \leq 3.33$	$B = b/h$
Relative radial distance	$5 \leq r/h \leq 30$	r/h
Wave propagation angle	$-90° \leq \gamma \leq 90°$	γ
Relative streamwise distance	$2.7 \leq X \leq 59.2$	$X = x/h$
Impulse product parameter	$0.17 \leq P \leq 8.13$	$P = FS^{1/2}M^{1/4}\sqrt{\cos[(6/7)\alpha]}$

Table 2.1. Limitations for the calculations of the impulse wave generation (Heller et al., 2009)

Other equations are available to calculate the maximal wave height and the period of the maximal wave height. Different equations describe the setup with a channel (2D) and with a basin (3D). However, these equations are not relevant to this thesis and thus are skipped. For places located further from the impact zone than the place of the maximal wave height occurrence, equations estimating the wave height (Equations (2.3) and (2.4)), wave period and wave length are suggested for the 2D and the 3D setup.

The **wave height $H(x)$** at a distance x from the impact zone (2D) or in a place described by coordinates r and γ (3D) can be determined depending on the impulse product parameter as follows.

$$\text{2D:} \qquad H(x) = (3/4)\left(PX^{-1/3}\right)^{4/5} \cdot h \qquad \text{for } X > X_M \qquad (2.3)$$

where: X [m]   Relative streamwise distance from the impact location; $X = x/h$

X_M [m]   Relative streamwise distance of the maximum wave amplitude; $X_M = x_M/h$

x_M [m]   Streamwise distance of the maximum wave amplitude; $x_M = (11/2)P^{(1/2)}h$

$$3\text{D:}\quad H(r,\gamma) = 3/2 \cdot P^{4/5} \cos^2(2\gamma/3)(r/h)^{-2/3} \cdot h \qquad \text{for } r/h > X_M \qquad (2.4)$$

where: r [m]   Radial distance from the impact location in the wave basin

γ [°]   Wave propagation angle (Figure 2.4)

2.1.2   Wave run-up and overtopping

Once the wave is generated, it propagates through the reservoir and reaches the shores. A run-up of the shore occurs, which eventually leads to an overtopping in case the top of the dam is reached. This subsection gives a quick overview of the methods suggested by Heller et al. (2009) to estimate the wave run-up and overtopping. These equations are taken from Müller (1995).

The **run-up height R** formula is presented in Equation (2.5) and the limitations are given in Table 2.2.

$$R = 1.25 \left(\frac{H}{h}\right)^{\frac{5}{4}} \left(\frac{H}{L}\right)^{-\frac{3}{20}} \left(\frac{90°}{\beta}\right)^{\frac{1}{5}} h \qquad (2.5)$$

where: h [m]   Still water depth in front of the dam

H [m]   Wave height in front of the dam

L [m]   Wave length in front of the dam

β [°]   Run-up angle equal to the dam face slope

Term	Range
Relative wave height	$0.011 \leq H/h \leq 0.521$
Wave steepness	$0.001 \leq H/L \leq 0.013$
Relative angle	$1.0 \leq 90°/\beta \leq 4.9$

Table 2.2. Limitations of the run-up equation by Müller (1995)

The overtopping volume formula from Müller (1995) is described but it is not given here, as a new method by Kobel, Evers, & Hager (2017) is presented in Section 2.2. Müller (1995) determines the overtopping volume in a two-step procedure. First, the overtopping volume without considering the freeboard is calculated, and then this value is reduced to take into account the freeboard. To determine the height of the freeboard necessary to avoid an overtopping, an iterative procedure has to be carried out.

2.1.3   Other effects on the impulse wave phenomenon

Research on impulse wave uses a simplified model to be able to understand these events. However, it is important to keep in mind the parameters which are not taken into account in any equations and require a qualitative assessment. A short overview of these parameters influencing the impulse wave is given here.

The **mass movement type** is modelled by solid or granular bodies in the laboratories, but it could be of more complex types as shown in Figure 2.5.
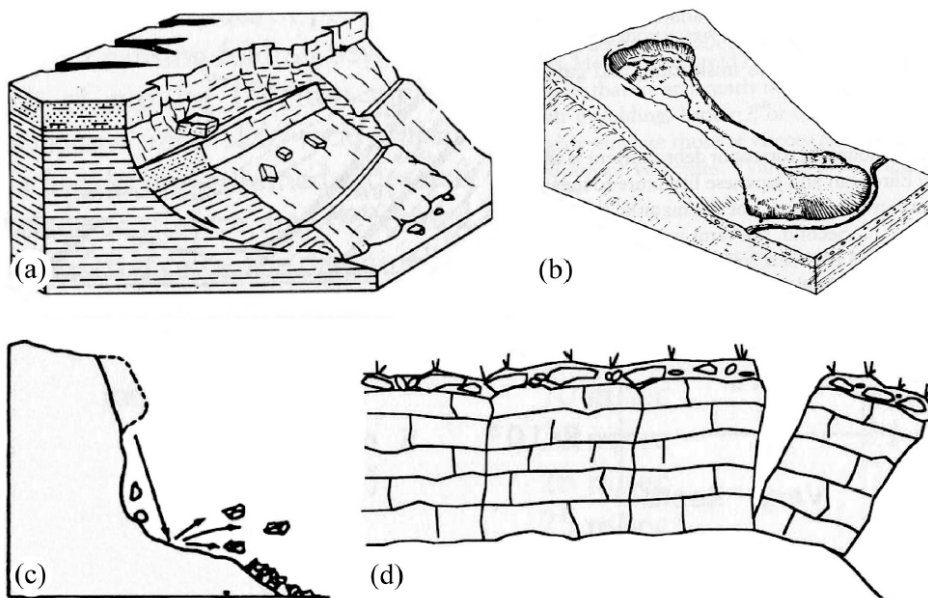
Figure 2.5. Mass movement types: (a) sliding, (b) flowing, (c) falling, (d) toppling
(Heller et al., 2009)

The **reservoir geometry** affects the wave propagation through the following phenomenon. *Refraction* acts on waves in shallow water by making them change their direction to move as frontally as possible onto the shore. *Diffraction* occurs when the wave passes around an obstacle and propagates behind it (Figure 2.6a). *Shoaling* appears when the wave gets into shallower water: the wave height increases while the wave length decreases. *Constriction* develops when the wave energy gets concentrated on the side of a dam as shown in Figure 2.6b. Finally, *reflection* occurs when the wave reaches a shore and returns in the opposite direction with reduced energy.
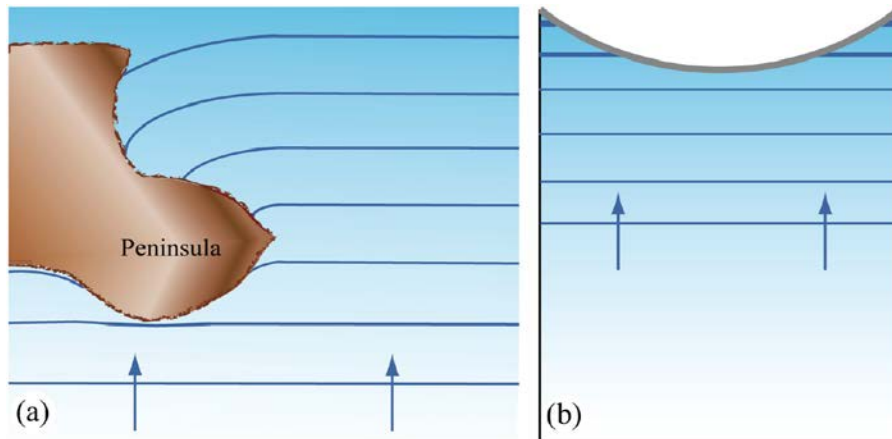
Figure 2.6. Effects of the reservoir geometry on waves: (a) Refraction and diffraction, (b) Constriction
(Heller et al., 2009)

2.2 Maximal overtopping height by Kobel et al.

A recent article written by Kobel et al. (2017) was released in June 2017. This research investigates the overtopping of rigid dam structures by solitary waves in a two-dimensional (2D) perspective. This section presents the conclusions of Kobel et al., which are compared to the results of the tests performed during this thesis. Over the 19 different setups tested, 13 tests were considered to elaborate equations. The others could have been subject to scale effects due to small overtopping depths. In this newly released report, the term *overtopping depth* is used. In this thesis, this overtopping depth corresponds to the *overtopping height*.

Kobel et al. investigated the overtopping volume and the overtopping height, and suggested to estimate them using different equations based on the characteristics of the impulse wave in front of the dam. The results for the overtopping volume include a condition which was not always verified during the performed tests in this thesis: the top of the wave has to be above the dam crest level. Therefore, the overtopping volume part is not further developed here and is not compared to the tests of this thesis.

Kobel et al. suggested two equations to estimate the maximum overtopping height at the dam crest. In both of them they put into relation the overtopping height d_0 and the dam height w versus the relative wave amplitude $\varepsilon \, (= a/h)$, the relative still water depth h/w, and the dam front face angle β. This Equation (2.6) shows an excellent empirical fit with their results ($R^2 = 0.95$).

$$\frac{d_0}{w} = 1.34 \left[\varepsilon \left(\frac{h}{w}\right)^{1.7} \left(\frac{\beta}{90°}\right)^{0.25} \right] = 1.34 \cdot E_1 ; \quad 0.40 < E_1 < 0.70 \tag{2.6}$$

An extended fit equation shows even better results ($R^2 = 0.99$).

$$\frac{d_0}{w} = 1.32 \left[\varepsilon \left(\frac{h}{w}\right)^{4[(\beta/(90°))^{-0.21} - \varepsilon]} \left(\frac{\beta}{90°}\right)^{0.16} \right] = 1.34 \cdot E_2 ; \quad 0.10 < E_2 \tag{2.7}$$
$$< 0.75$$

Chapter 3 Review of previous studies

Different studies have already been written on this model since it was transformed after the Åkerneset landslide study on the request of the Norwegian Water Resources and Energy Directorate (NVE). At that time, the model was a scaled replicate (1:158) of the Viddals reservoir with landslide generating an impulse wave. This chapter gives an overview of the different tests and results over the time.

The first students to investigate the model were Lorås (2014) and Svendsby (2014). A total of 12 tests, varying the landslide shape, volume, speed and density, were carried out. The aim was to define which characteristics of an avalanche influence the wave generation and the dam overtopping. The results showed that the volume of the landslide, as well as its shape, have a considerable impact on the overtopping volume. The overtopping volume is found as inversely proportional to the landslide porosity. Furthermore, it was observed that the first wave overtops the dam evenly, but the next ones are only spilling on one side. This was assumed to be a result of reflections in the reservoir. Besides, a comparison between the model results and the empirical method of Heller et al. (2009) was carried out. It was recommended to analyse further the results of the experimental tests by conducting more tests and detailed measurements.

The next thesis was written by Bolzoni (2015). In total, 17 tests were conducted, changing the slide volume, freeboard, dam slope and dam roughness. The wave run-up height and the overtopping volume were analysed. Again, the conclusions show a strong correlation between the landslide volume and the overtopping volume, a little impact of the dam slope on the overtopping volume, but a strong effect of the dam roughness. However, this last conclusion is based on two tests only and needs to be confirmed. Again, the empirical method by Heller et al. (2009) could not be verified on the model, giving significant discrepancies. Bolzoni (2015) recommended straightening the edges

and the shores of the reservoir to obtain a generic model less influenced by the particular shape of Viddals reservoir.

In 2016, previous recommendations were followed, and the model was transformed into a setup closer to the ideal shape of a reservoir. Ramírez (2016) wrote a bachelor thesis about the model based on 63 tests. Varying the dam profile, freeboard and the landslide size, she concluded a high, nonlinear correlation between the landslide volume and the overtopping volume. Besides, the influence of the water level in the reservoir on the overtopping volume was also noticed.

During the same semester, (Mortensen, 2016a) and Hammeren (2016) ran the model in 40 different constellations to get a statistical background for their master thesis. Landslides size, freeboard and dam shape were varied over 211 attempts. Landslide impact velocity, wave height, overtopping volume, and overtopping height were recorded and compared to a numerical model based on GloBouss and MOST. In opposition to previous attempts failing to fit the model with the Heller et al. (2009) empirical formula, the results showed a good prediction of the overtopping by the numerical model.

The task of Gardoni & Ponziani (2017) was to evaluate the influence of an abrupt level change in the reservoir bottom and of a small wall between the landslide impact area and the dam, allowing only reflected waves to overtop the dam. This was achieved by comparing the initial setup to a new one with the landslide being moved to the opposite side and towards the dam. Different landslide shapes, volumes, impact speeds and freeboards were simulated in both setups. Their results showed a difference in the wave propagation and the overtopping volume between the two model configurations. Furthermore, they analysed in detail the wave propagation with the help of a model in Matlab.

This thesis aims to build a reliable statistical background for the new model setup and analyse the parameters influencing the wave generation and overtopping. At the time the thesis draft was elaborated, the work of the antecedent students was not submitted. It turned out that their research on the generated wave height was advanced. Therefore, it was decided in accordance with the supervisor to focus on a new dam profile, instead of repeating the work and confirming the conclusions of the same model. The model was run over 200 times to collect reliable data for 135 tests in 46 different setups. Results and knowledge of the thesis are transferred to Netsanet Nigatu, who uses the model for her dissertation thesis and continues performing tests on the model.

Chapter 4 Physical model

This thesis is based on a model which was built in 2008 as a large-scale physical model of the Storfjord in a laboratory of the Department of Hydraulic Engineering at NTNU in Trondheim. The shore of this fjord is unstable and is going to collapse eventually, forming a landslide plunging directly into the water. A tsunami wave is going to be triggered, devastating the shores of the fjord. The model showed that several communities are going to be destroyed. Amongst them, the touristic village Geiranger is threatened by an up to 70m wave (Harbitz et al., 2014). Later, the model was transformed several times and is now a generic model. Different studies were carried out in this model, but undesired effects of its shape were observed. In the semester preceding to this thesis, two Italian students Ponziani & Gardoni (2017) studied these effects and concluded changing the position of the landslide in order to reduce them.

For this thesis, the so-called Chevron dam was replaced by a straight dam to reduce constriction effects. Besides, the dam crest was divided into five sections and sensors were added in each section to observe the differences of dam overtopping along the crest. In addition, improvements were brought to the model and to the way of processing the data, to enhance the accuracy of the results and to reduce the time needed to run the tests and analyse the results. The time needed in order to run a test was decreased from more than 40 min/test performed by two persons (Ponziani & Gardoni, 2017) to around 15 min/test performed by one person. Further details on the modifications and improvements are available in Appendix C.

The model is composed of three main parts illustrated in Figure 4.1. They are described in the following subchapters: Landslide, Reservoir and Dam. Different sensors used in each part of the model are presented as well, but the calibration process is described in Appendix B.

Figure 4.1. Picture of the model with the landslide (1), the reservoir (2) and the overtopped dam (3)

The current experimental setup models an embankment dam in a scale of 1:190. The Froude similarity is applied for scaling as it reproduces a free surface flow where the gravity and inertial forces are central. Two rules need to be followed to avoid scale effects: the still water depth at the bottom of the landslide area should be $h \geq 0.2$ m (Heller, Hager, & Minor, 2008) and the wave period should be $T \geq 0.35$ sec (Hughes, 1993). These two conditions are fulfilled in this model. In this thesis, all results are given in the scale of the model. To scale them up to the prototype size, Table 4.1 gives the conversion factors for the different parameters.

Parameters	Units	Scale factor ($\lambda = 190$)	
Distance	L	λ	190
Area	L^2	λ^2	36'100
Volume	L^3	λ^3	6'859'000
Density	M/L^3	1	1
Time	T	$\lambda^{0.5}$	≈ 13.78
Velocity	L/T	$\lambda^{0.5}$	≈ 13.78
Acceleration	L/T^2	1	1
Water flow	L^3/T	$\lambda^{2.5}$	$\approx 497'604$

Table 4.1. Scale factors

4.1 Landslide

The landslide is modelled as solid blocks entering the waterbody of the reservoir. The front blocks have a 45° bevel in the front, and the following ones are rectangular prisms attached to the first ones, as shown in Figure 4.2 (more details in Appendix A). The blocks are held in place by a quick release

hook which allows the triggering of the landslide. In this section, the sliding plane is described, as well as different sensors installed on the landslide part of the model.

The landslide is gliding into the water along a sliding surface. For each test, the blocks are first placed on a wooden board inclined by 50°. When released, the blocks slide down on this board and continue on a plexiglass board to ease the transition from the steep part to the flat reservoir bottom, as shown in Figure 4.3. This plastic part prevents an abrasion between the blocks and the concrete bottom of the reservoir. During the experiments, the plexiglass broke due to fatigue and needed to be replaced. This change could affect the results. Thus, one needs to pay attention when comparing the tests before and after test n°76.
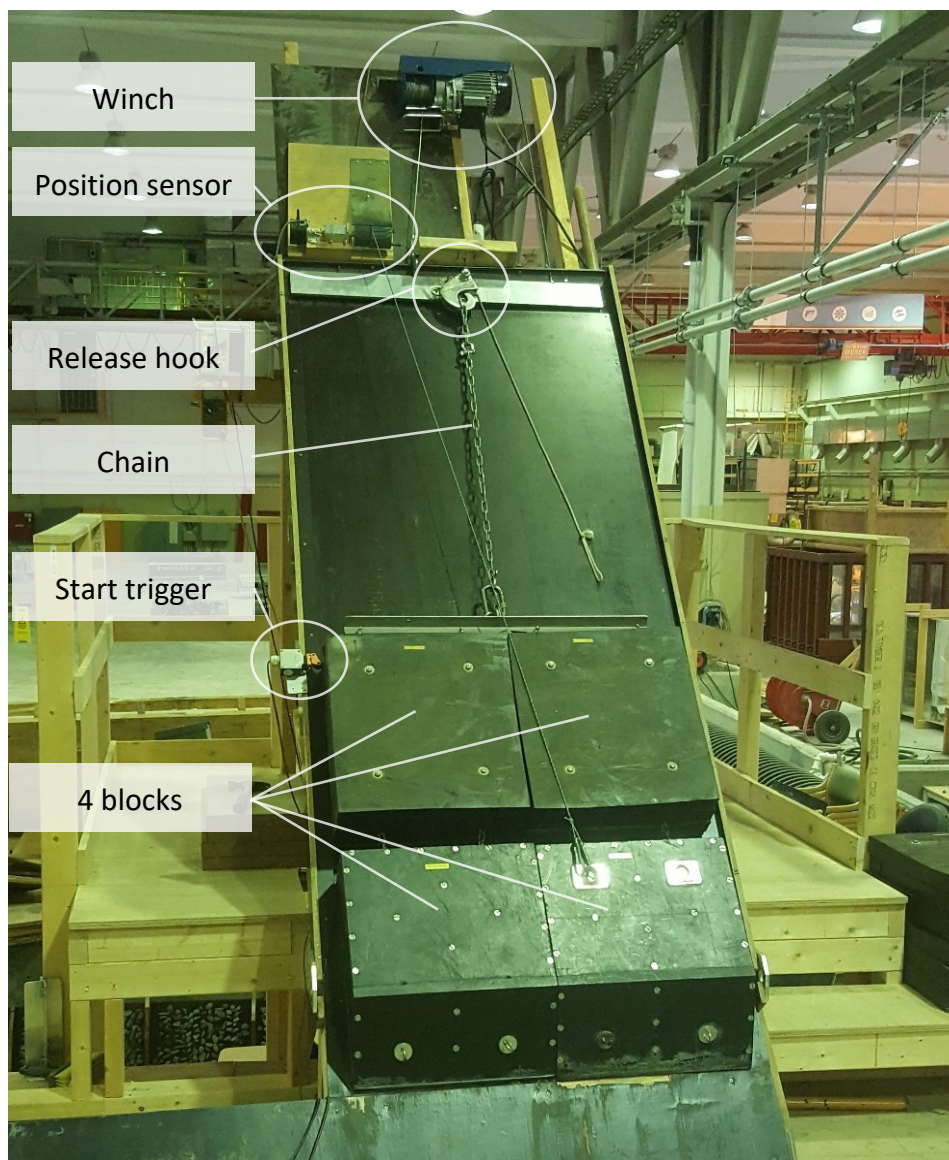
Figure 4.2. Landslide with four-block configuration, ready for start

One of the important parameters in these experiments is the velocity of the landslide when colliding with the water. Higher velocity is obtained by shortening the retaining chain and releasing the blocks higher above the water. In this thesis, the landslide impact velocity is characterised by the release distance, which is measured between the water level and the front of the blocks, as illustrated in Figure 4.3.
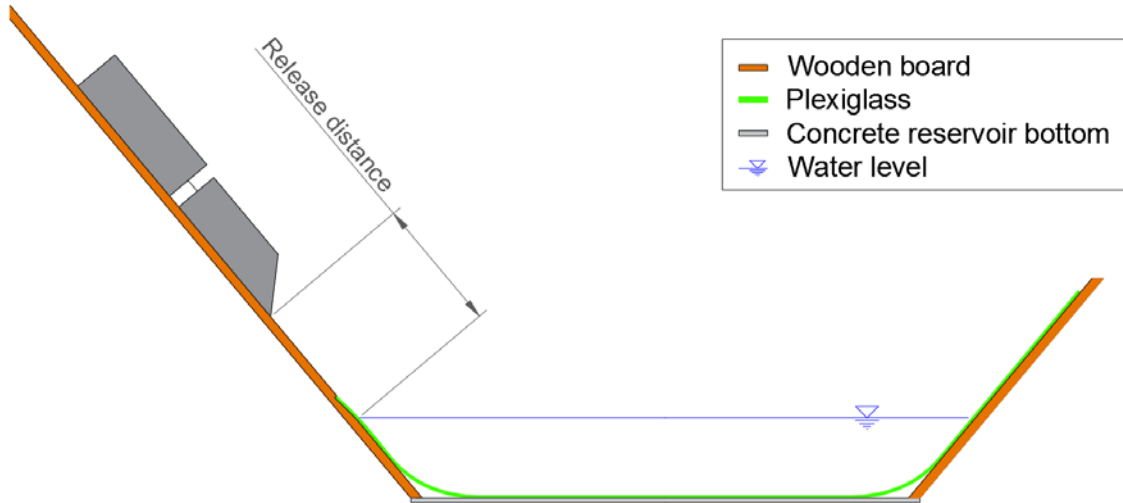
Figure 4.3. Detail of the sliding surface and the plexiglass

The landslide is composed of blocks which are arranged in different configurations to estimate the impact of landslide shape on the overtopping. Each block weights about 40 kg. The tests are carried out with four different block configurations: two blocks aligned horizontally (2H) and vertically (2V), four blocks and six blocks. Figure 4.4 illustrates the different landslide block configurations in starting position.

A start trigger is placed on the side of the landslide (Figure 4.2). This trigger is a push detector which gives a signal when it is released. Like other sensors of the model, it is connected to a computer running an Agilent program for data recording. Measurements are transmitted continuously to the software, which begins recording them at 200 Hz when the start signal is received.

As specified previously, the velocity of the landslide is one of the analysed parameters of this thesis. The landslide velocity is derived from a position measurement of the slide at 200 Hz. The position is monitored by a rotational sensor connected to the landslide with a string and giving a voltage value corresponding to the position. The position to speed conversion is done in a post-processing step and is described in Appendix C.
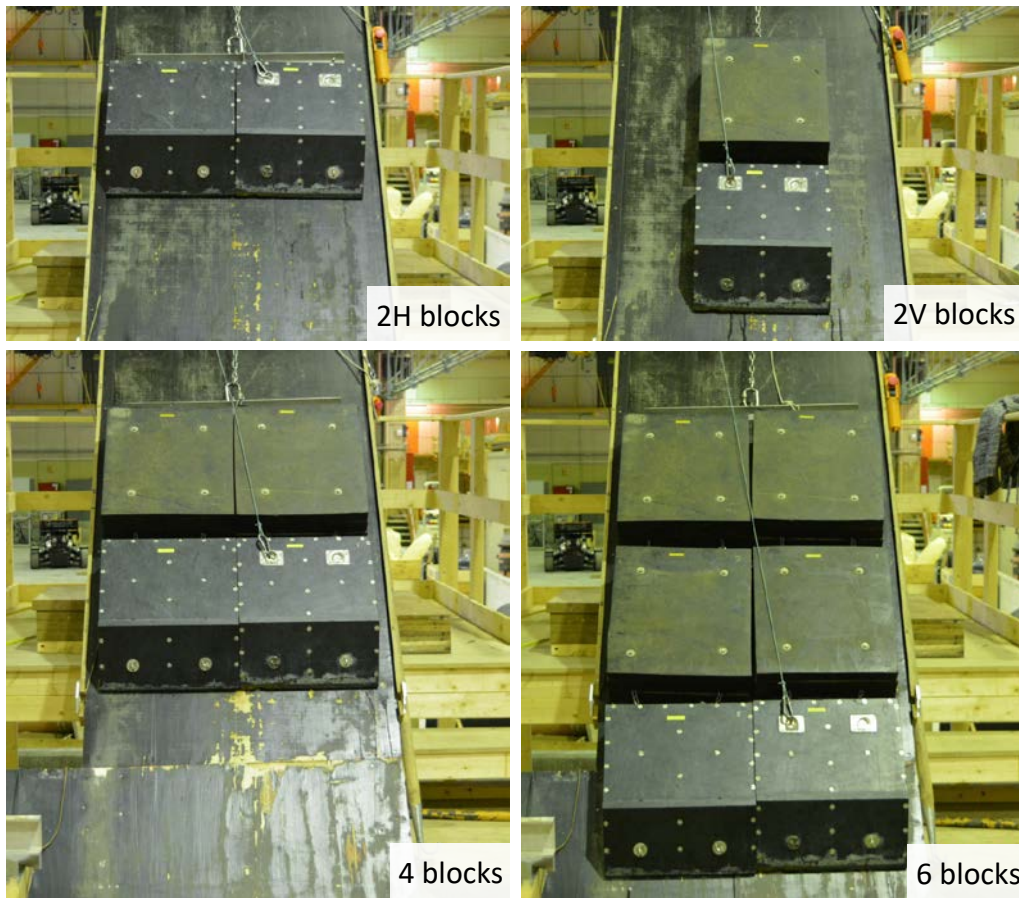
Figure 4.4. Different block configurations

4.2   Reservoir

The wave generated by the landslide entering the water propagates through the reservoir. The reservoir has a trapezoidal shape of dimensions given in Figure 4.5 below. Its sides are made of wooden boards with a plastering to simulate roughness. Waves are monitored by wave gauges, measuring a different conductivity for various water heights at the sensor. Before each test, these gauges need to be reset to zero and calibrated. Numbering and positions of the gauges are given in the summary in Figure 4.7.
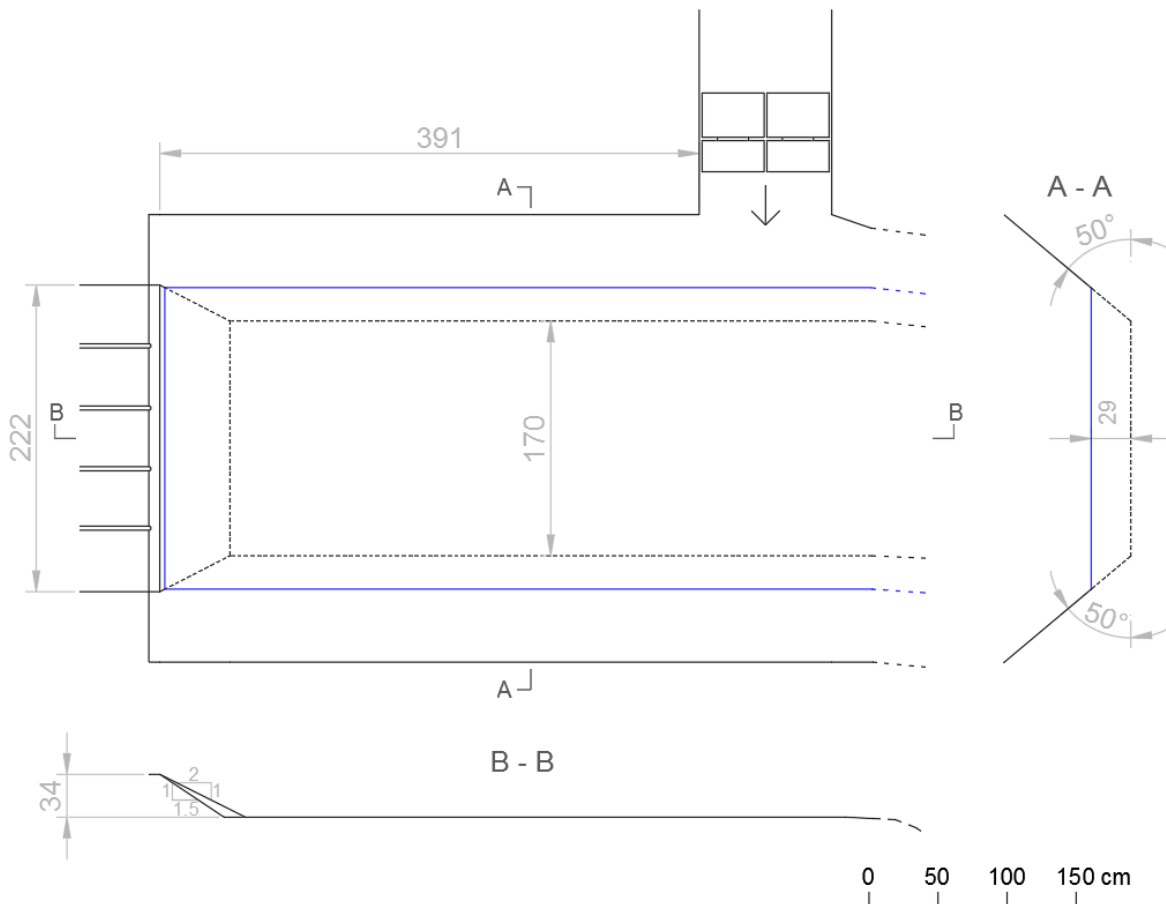
Figure 4.5. Plan of the model

Another important parameter is studied in this thesis and influencing the overtopping is the freeboard. It is the height difference between the dam crest and the water level. In Switzerland, the freeboard is set according to the highest possible flood, different for each dam (Schleiss & Pougatsch, 2011). The approach of the Norwegian Water Resources and Energy Administration (NVE) is different. The dams are categorised into four classes, considering a risk-based philosophy. Various requirements, including the freeboard, apply for each class. The Norwegian guidance (NVE, 2012) sets the maximum water level to 4.5 m below crest for dam belonging to class 3, and 6 m for dams belonging class 4. These two freeboard values are applied throughout the tests. To set these two different freeboards, the water level in the reservoir was adjusted to 23.6 mm before each test, i.e. 31.6 mm below the dam crest level, corresponding to 4.5 m, i.e. 6 m freeboard. For a precise regulation of the water level, a piezometer with a point gauge was used (Appendix B).

4.3   Dam

The model represents a 64-meter high embankment dam. The upstream side consists of a wooden board which assures that the shape of the dam remains constant over the different tests. The dam profile was varied over the tests to analyse the effects of different dam surfaces and shapes on the overtopping. In Figure 4.6, the different dam profiles tested are presented. The basic setup is the dam with 1:1.5 slope and smooth surface. The influence of the dam surface on the impulse wave is analysed by gluing 16-35 mm stones simulating roughness (first illustration to the left). Different dam profiles are tested by including a wave wall in the dam height. A further new setup with a horizontal part in front of the wave wall is also investigated. The aim of this shape is to diminish the overtopping volume by reducing the angle between the dam run-up surface and the wall. Thus, the impulse wave would dissipate more energy by crashing into the vertical part and reflects more energy back into the reservoir. Finally, the effect of the upstream dam slope is studied.
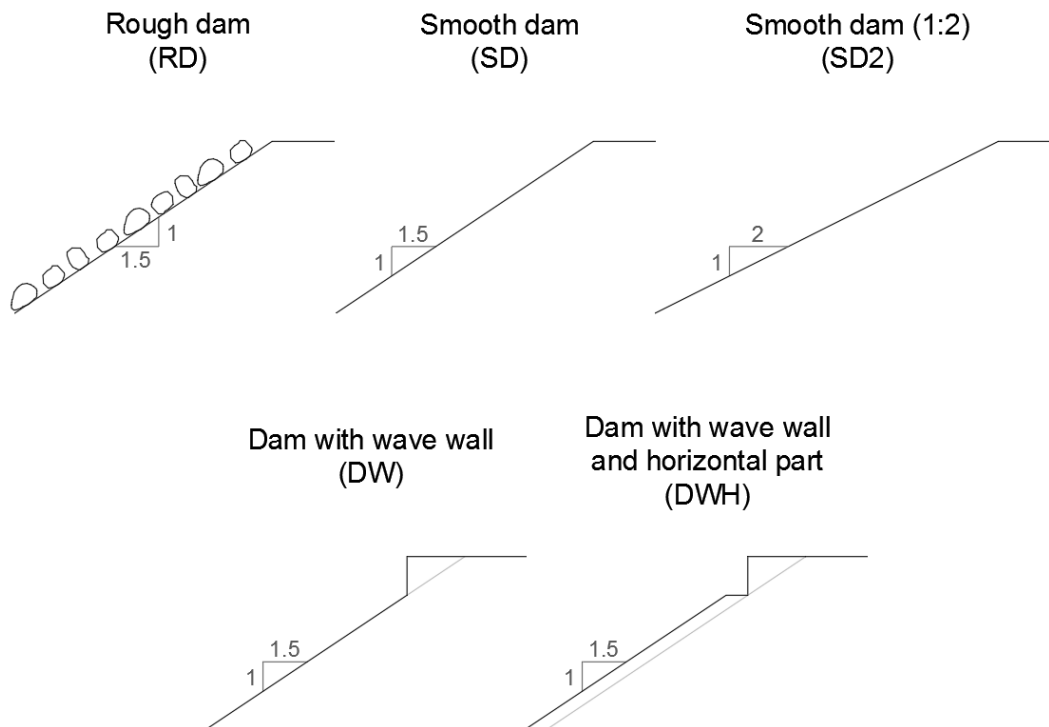
Figure 4.6. Different dam profiles analysed, along with used abbreviations

The thesis focuses on the overtopping of the dam, and therefore the model part of biggest interest is the dam crest. For a better understanding of the overtopping, the dam crest is divided into five sections, and measurements are carried out at each section separately. The following subchapters describe, how the various parameters are measured.

Overtopping height

Overtopping height over dam crest is measured by five ultrasonic sensors placed in accordance with each section of subdivided crest length. The different dam profiles do not have the dam crest at the same place, and therefore it is not possible to compare the overtopping heights of different dam profiles.

Overtopping volume

Water overtopping the dam is separated directly after the dam crest and is collected in individual buckets for each crest section. The overtopping volume is derived from a freeboard measurement performed with an ultrasonic sensor placed on top of each bucket. The description of the calibration and the precision of the measurement is available in Appendix B.

Wave speed

A new measurement, not conducted before on this model, was introduced within the framework of this thesis. In the middle of the dam crest, sensors 13 and 14 are aligned perpendicularly to the dam crest, i.e. parallel to the wave direction. Both sensors record the same wave at two spots by 53 mm from each other. By subtracting the times at which the wave passed respective sensors, the velocity is derived.

4.4   Sensor map

Different sensors used in the model, presented in detail in Appendix B, are illustrated in the map below (Figure 4.7). The recording begins when the start trigger (yellow) detects a landslide movement. Then the landslide impact velocity is monitored by a position sensor (grey). When the landslide hits the water, waves are generated and observed via the wave gauges (blue). The height of the overtopping wave is recorded by the overtopping sensors (green), and water flow is separated into five parts which lead to the buckets V1 to V5 (orange). The collected water volume needs to be measured manually afterwards.
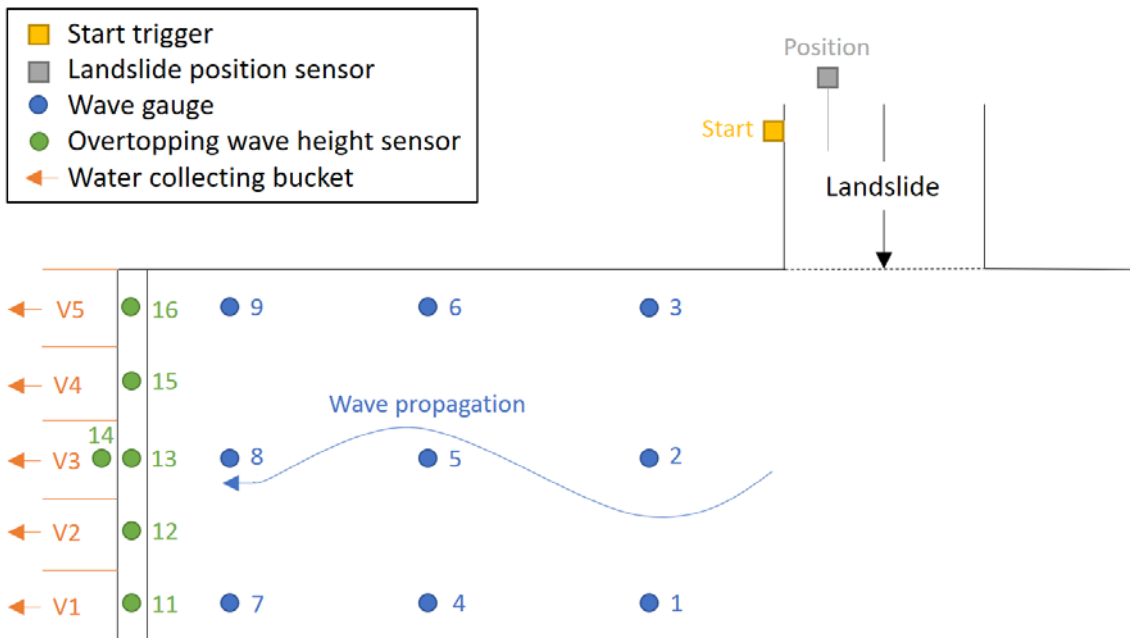
Figure 4.7. Sensor map with sensor numbers

Chapter 5 Test procedure

Chapter 5 describes the standard procedure carried out for each test, explains the requirements for considering the tests reliable and presents the performed tests.

5.1   Procedure

Each test follows an identical procedure as described in these subsections. In each test, the first step consists of the preparation of the model. Afterwards, the landslide is released, and the data are collected. Finally, these data are treated for further analysis. The first two steps are always carried out together and take around 15 minutes. Data treatment is usually executed at the end of a series of tests.

5.1.1   Model preparation

The first step of the model preparation is arranging the chosen block configuration for the landslide, fixing it at the proper release height and verifying the right position of the start sensor. Then the freeboard needs to be set by regulating the water level in the reservoir, either by pumping out water or by refilling the reservoir. The precise value of the water height is obtained by reading the installed piezometer. The next step consists of adding 1 litre of water into the collecting buckets V1 to V5 and measuring the water level. This action is necessary to flatten the bottom of the buckets (see Appendix B). Finally, once the water in the reservoir is completely still, the wave sensors are set to zero and calibrated.

The tests need to be executed each time under the same conditions to enable comparison in the analysis. Because the dam and other parts of the model are dry before the first test of each half-day, these measurements are not recorded.

5.1.2   Release of the landslide and data collection

Once the model is ready for the test, a camera, as well as Agilent program, are activated, and the landslide is released. The program continuously receives data from the landslide position sensor, the wave sensors and the overtopping height sensors and records them at a rate of 200 Hz after the start is given by the start trigger. When the overtopping of the dam is finished, and all water has arrived at the buckets, overtopping volumes are recorded manually.

5.1.3   Data treatment

The data treatment process is carried out in an excel sheet template elaborated for the model. For each test, landslide position and derived velocity, wave propagation along the centre and the sides of the reservoir, and wave overtopping heights are plotted. In Figure 5.1, the results for test n°20 are shown (more graphs given in Appendix D).
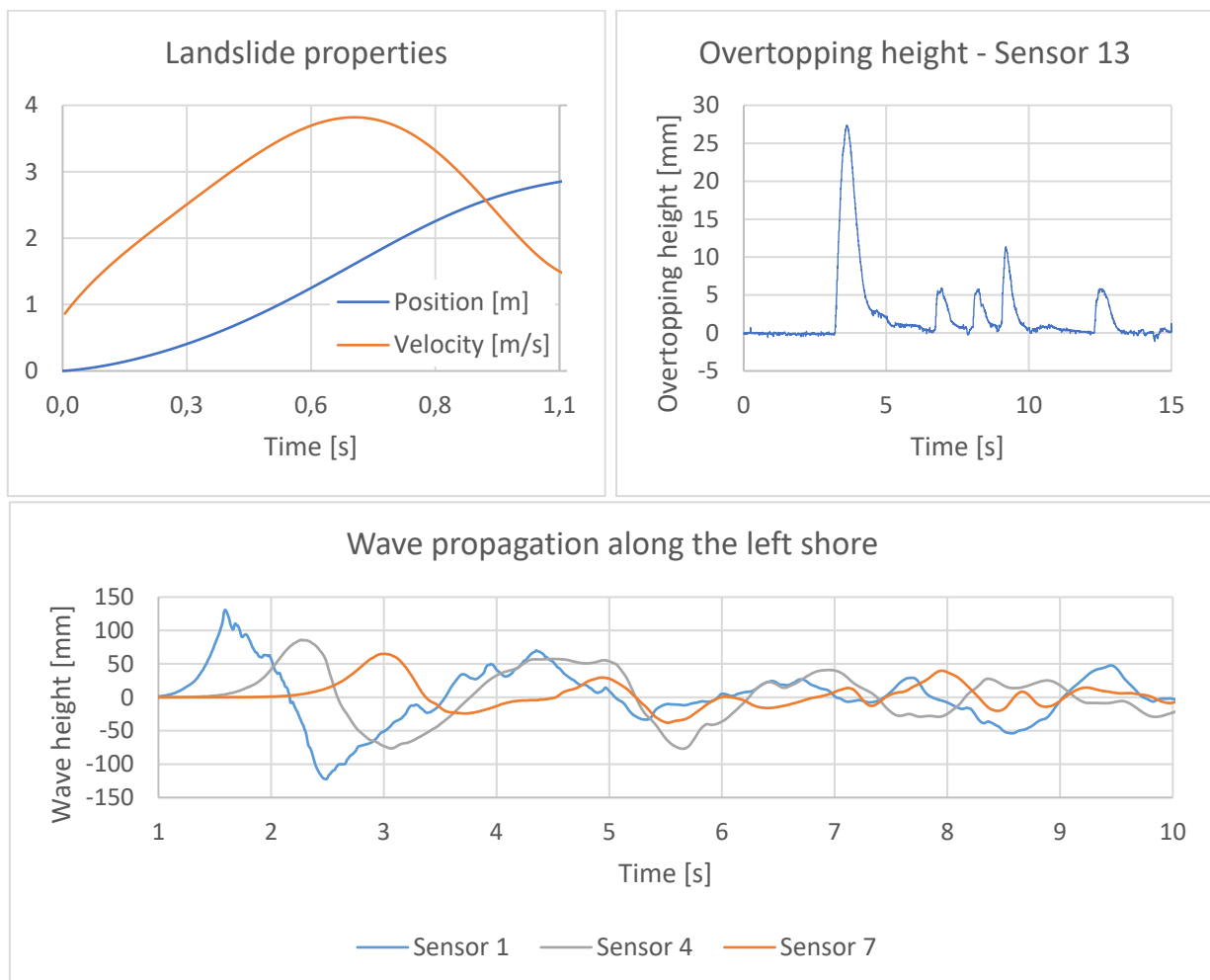
Figure 5.1. Different graphs resulting from data treatment (test n°20)

Besides these graphs, average overtopping speed between sensor 13 and 14, theoretical wave speed and discharge (further explained in Section 6.3) and impulse product parameter are calculated for each test. All the important data are resumed for each test in Appendix A and are compared in Chapter 6.

5.2   Reliability test

Reliability of the tests has to be guaranteed to ensure accurate conclusions after the analysis of the results. Each setup is tested three times, and the results are compared. The method used is not strictly correct from a statistical point of view but gives some basis to work on, within the framework of this project. The previous students (Ponziani & Gardoni, 2017) performed a statistical analysis based on 16 replications of the same setup. Their results, average μ_b and standard deviation σ_b, are presented in Table 5.1 and Table 5.2. In this thesis, the standard deviation is involved further in the process as a percentage of the average, represented in the last row of the tables. This standard-deviation-to-average ratio results in various values within a group of sensors. To simplify the procedure, an average of the ratio, i.e. approximately 10 %, is considered for all the sensors apart of the landslide impact velocity, where 5 % is held. These two values form the limit ratio $(\sigma / \mu)_{limit}$ to consider a test reliable, as explained below.

Sensor n°	Wave gauge								
	1	2	3	4	5	6	7	8	9
μ_b	71.7	67.0	57.6	108.4	63.5	46.7	107.5	58.7	46.7
σ_b	5.6	10.1	1.8	5.9	8.9	8.9	6.4	3.5	1.6
σ_b / μ_b	8%	15%	3%	5%	14%	19%	6%	6%	3%

Table 5.1. Reliability statistics for the wave gauges results (Ponziani & Gardoni, 2017)

Sensor n°	Overtopping height			Landslide velocity	Overtopping volume
	11	13	16		
μ_b	71.7	67.0	57.6	108.4	63.5
σ_b	5.6	10.1	1.8	5.9	8.9
σ_b / μ_b	8%	15%	3%	5%	14%

Table 5.2. Reliability statistics for the overtopping height, landslide velocity, and overtopping volume results (Ponziani & Gardoni, 2017)

Once all three tests are performed in the same model setup, the average value μ_{test}, standard deviation σ_{test} and standard-deviation-to-average ratio $\sigma_{test} / \mu_{test}$ are computed for each sensor. If these ratios are within the limit ratio $(\sigma / \mu)_{limit}$, the group of tests is considered as reliable. If one sensor does not

pass the test, the value is not used for the analysis (red numbers in Appendix A). If a sensor has a ratio σ_{test} / μ_{test} of more than 25 %, the test is excluded and carried out again. In the analysis, the model is considered giving an accuracy of the results equal to 10 %. That is, a difference between two results is considered significant if the difference is higher than 10 %.

5.3   Table of performed tests

Over 200 tests were performed between February 2017 and May 2017, out of which 135 are reliable. Different parameters were changed: dam slope, dam profile, dam roughness, freeboard, block configuration and release height. A summary of the different setups tested is presented in Table 5.3. Until test 114, three tests were carried out and then compared to be defined as reliable. If the three similar tests had a too high standard deviation, a test with this setup was repeated, and a name identical to the worst test with a suffix "b" was assigned. From test 115 onwards, four tests were executed, and the best three ones were kept for the analysis. The ones discarded are in brackets.

Slope	Dam type	Freeboard [m]	Block configuration	Release height [cm]	Test number		
1 : 1.5	Rough dam (DR)	4.5	2H	150	1	2	3
				200	4	5	6
				100	7	8	9
			4	100	10	11	12
				50	13	14	15
				150	16	17	18
		6	4	150	19	20	21
				100	22	23	24
				50	25	26	27
			2H	200	28	29	30
				150	31	32	33
				100	34	35	36
	Smooth dam (SD)	4.5	2H	200	37	38	39
				150	40	41	42
				100	43	44	45
			2V	200	46	47	48
				150	49	50	51
				50	52	53	54
			4	150	55	56	57
				100	58	59	60
				50	61	62	63
			6	50	64	65	66
				100	67b	68	69
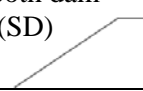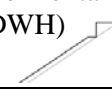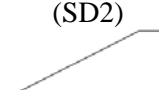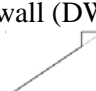
Slope	Dam type	Freeboard [m]	Block configuration	Release height [cm]	Test number			
1 : 1.5	Smooth dam (SD)	6	6	100	70	71	72	
				50	73	74	75	
			4	150	76	77	78	
				100	79	80	81	
				50	82	83	84	
			2H	200	85	86	87	
				150	88	89	90	
				100	91	92	93	
	Smooth dam (SD)	6	2V	200	94	95	96	
				150	97	98	99	
				50	100	101	102	
	Dam with wave wall and horizontal part (DWH)	4.5	4	150	103	104	105	
				100	106	107	108	
		6		150	109	110	111	
				100	112	113	114	
1 : 2	Smooth dam (SD2)	4.5	4	150	(115)	116	117	118
				100	(119)	120	121	122
		6		100	123	124	(125)	126
				150	127	128	129	(130)
1 : 1.5	Dam with wave wall (DW)	6	4	100	131	132	133	(134)
				150	135	(136)	137	138
		4.5		150	(139)	140	141	142
				100	(143)	144	145	146

Table 5.3. Planned tests with numbering, brackets signify the test was discarded

Chapter 6 Results analysis

The experiments carried out in the model resulted in a large data collection which is analysed in this chapter. The first part focuses on the different parameters varied over the tests. Afterwards, the wave generation and propagation are discussed, and a new way of predicting the wave speed and discharge over the dam in the model is presented. Furthermore, results of the tests considering the overtopping are commented. Finally, a comparison of the results of the tests with previous studies is presented. Besides, an experiment on a dimensional analysis with linear regression is added in the Appendix A.

6.1 Parametrical analysis

In the 135 reliable tests performed, the following parameters were changed. The dam structure was studied with different roughness, with two different slopes and different profiles. The reservoir water level, i.e. different freeboards, was adjusted according to different dam classes used in Norway. Finally, the landslide was parameterised by various shapes, volumes and speeds. In this first part of the collected data analysis, these parameters are analysed one by one.

6.1.1 Dam roughness

The first parameter to be investigated is the roughness of the dam. As seen in Section 4.3, different dam surfaces were tested on the model. First, the wooden slab was covered with 18-35 mm stones to simulate roughness on the upper side of the dam. Tests were performed with two freeboard heights and with the 4-block and 2H-block configurations. Later, the roughness was removed to leave a smooth wooden slab as an upper surface of the dam. The same tests were performed again. However, as mentioned in Section 4.1, the plexiglass guiding the landslide into the water broke and needed to be replaced before the 2H-blocks configuration could be tested. As the model could not be tested in the same conditions for the second configuration, the comparison is only made for the 4-block configuration.

Table 6.1 gives a comparison between smooth and rough upstream surface of the dam. The results presented here are coming from 4-block configuration tests with different freeboards and release heights. Each row corresponds to one test configuration where the results for the overtopping height and the overtopping volume are averages of 3 reliable tests (see Section 5.2). The overtopping height and volume vary mostly between ±10 %. As these values stay within the model uncertainty (10 %) and no significant trend can be observed, the roughness parameter is considered as having a negligible effect on the overtopping height and volume.

Freeboard	Release height	Overtopping height [mm]			Overtopping volume [l]		
		Rough	Smooth	Variation	Rough	Smooth	Variation
4.5 m	150	25.4	27.0	+ 6 %	60.79	62.73	+ 3 %
	100	24.5	26.3	+ 7 %	52.06	57.2	+ 10 %
	50	20.3	21.7	+ 7 %	42.6	44.7	+ 5 %
6 m	150	26.3	25.0	- 5 %	50.7	49.9	- 2 %
	100	25.3	22.0	- 13 %	41.6	44.4	+ 7 %
	50	18.8	17.5	- 7 %	30.2	31.3	+ 3 %

Table 6.1. Comparison of rough and smooth upstream dam surface (4-block configuration)

This result is explained by the wave length of impulse waves longer than 2.6 m (> 500m scaled up, see Section 6.2.2). On the local scale of the roughness, the wave is similar to a water level rise, and not a horizontal water displacement as for example in the case of wind generated waves with much shorter wave lengths.

6.1.2   Dam slope

The model used for this thesis allows the dam structure to be removed and replaced by another one. Two upstream dam slopes are tested: 1:1.5 and 1:2. The dam slope was tested under the 4-blocks configuration, for the two standard freeboards 4.5 m and 6 m and with two release heights. The results of the overtopping volume at the centre section of the dam, presented in Table 6.2 are average values of the three reliable tests. As the two setups used in this comparison are based on two different dams, it is not possible to compare the overtopping heights because the sensors cannot be positioned precisely on the maximal overtopping height on the dam (see Section 4.3).

Freeboard	Release height	Overtopping volume [l]		
		Slope 1:1.5	Slope 1:2	Variation
4.5m	150	62.7	77.2	+ 23 %
	100	57.2	65.0	+ 14 %
6m	150	49.9	61.8	+ 24 %
	100	44.4	49.8	+ 12 %

Table 6.2. Comparison of upstream dam slope 1:1.5 and 1:2 (4-block configuration)

The results of the tests show that a dam with a mild slope has a bigger overtopping volume (12 to 24 %). This phenomenon is increased with a higher release height of the landslide. However, the freeboard does not influence the variation of overtopping volume due to the release height. Bigger overtopping volume is caused by the smaller amount of energy being lost at the smaller change of slope. In our case, bigger overtopping occurs at the 1:2 dam compared to the 1:1.5 dam.

6.1.3 Dam profile

Three different dam profiles, illustrated in Figure 6.1, are studied in this part. First, a smooth embankment dam is compared to an embankment dam with a wave wall below the crest. In the second part, the influence of a horizontal part in front of the wave wall is analysed. All dam profiles have a constant slope 1:1.5. The impact of the dam profile was tested on the 4-blocks configuration with two freeboards and two release height.
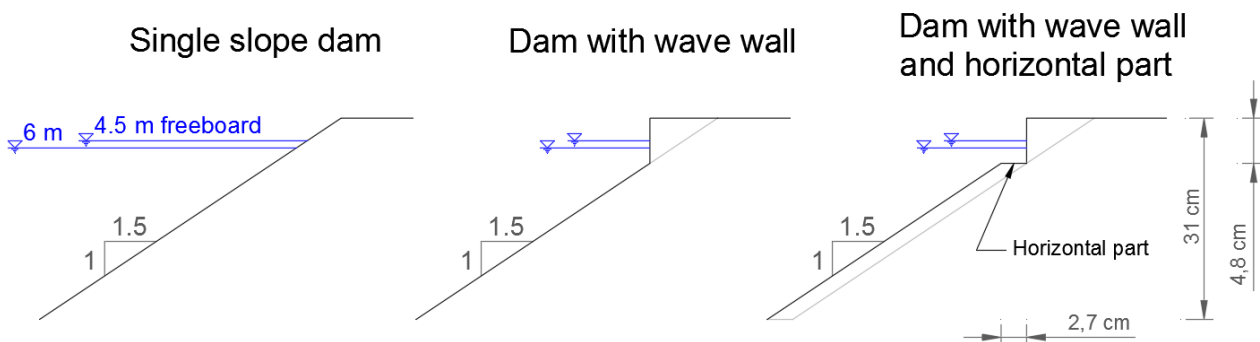
Figure 6.1. Recall of the different dam profiles analysed

The results of the first comparison between the smooth dam (SD) and the dam with a wave wall (DW) are given in Table 6.3. The wave wall reduces the overtopped water volume by 13 to 30 %. The first wave overtops both dams in the same way, but the waves arriving afterwards are influenced by the wave wall. With the single slope dam, water glides along the dam crest without meeting any obstacle. With the implementation of the wave wall, water deviates upwards to a vertical angle (Figure 6.2), and less water flows out of the reservoir.
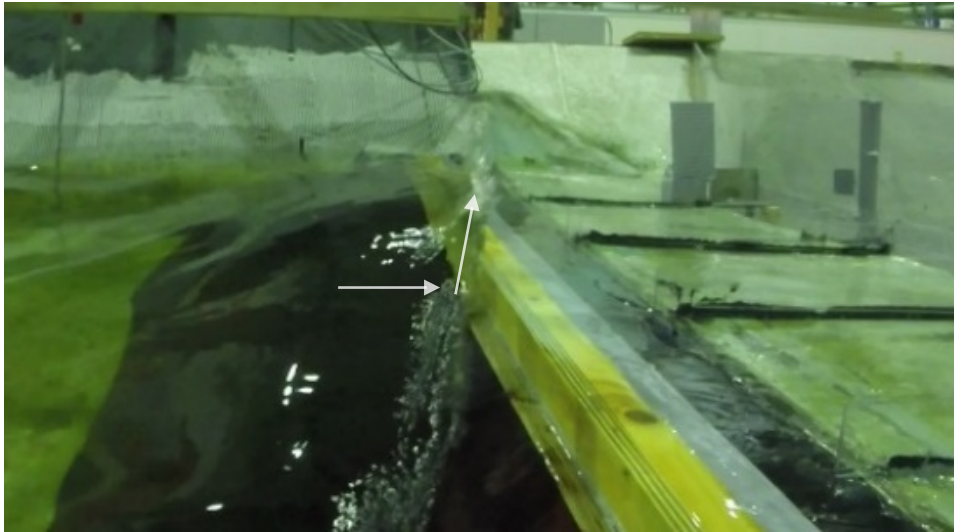
Figure 6.2. Splash of the water hitting the vertical part

Table 6.3 also shows that the more velocity the landslide has due to higher landslide release height, the less the wave wall reduces the overtopped water volume. This phenomenon happens because, in this case, the proportion between the wave wall height and the wave height is smaller.

Freeboard	Release height	Overtopping volume [l]		
		SD	DW	Variation
4.5m	150	62.7	54.5	- 13 %
	100	57.2	44.1	- 23 %
6m	150	49.9	42.1	- 16 %
	100	44.4	30.9	- 30 %

Table 6.3. Comparison of the smooth embankment dam with a dam with wave wall

The second comparison in this section studies the influence of an implementation of a horizontal part in front of the wave wall to increase the wave reflection (DW vs. DWH). Table 6.4 presents the results of these tests.

Freeboard	Release height	Overtopping volume [l]		
		DW	DWH	Variation
4.5	150	54.5	54.0	- 1 %
	100	44.1	44.7	+ 1 %
6	150	42.1	38.2	- 9 %
	100	30.9	31.4	+ 2 %

Table 6.4. Comparison of the embankment dam with wave wall, with and without horizontal part

This second setup with a horizontal part in front of the vertical wall gives approximately the same results as without the flat part. The results in Table 6.4 show variation within the standard deviation range ±10 % admitted as test imprecision. Therefore, it is concluded that this horizontal part in front of the vertical wave wall in the dam profile does not influence the overtopping volume.

6.1.4 Freeboard

Two different freeboards based on Norwegian regulation were tested. The influence of the freeboard parameter is analysed on the smooth dam with a 1:1.5 slope to avoid other parameters affecting the results. Table 6.5 presents the overtopping height measured by sensor 13 and the total overtopping volume ($\sum_1^5 V_i$) from tests number 37 to 102.

Configuration	Release height	Overtopping height [mm]			Overtopping volume [l]		
		4.5 m	6 m	Variation	4.5 m	6 m	Variation
2H	200	25.8	17.8	- 31 %	37.3	22.5	- 40 %
	150	22.4	16.3	- 27 %	28.7	16.9	- 41 %
	100	20.4	12.7	- 38 %	22.5	10.3	- 54 %
2V	200	35.7	28.2	- 21 %	39.3	28.0	- 29 %
	150	28.0	24.7	- 12 %	27.3	22.1	- 19 %
	50	23.1	19.8	- 14 %	17.7	10.5	- 41 %
4	150	27.0	25.0	- 8 %	62.7	49.9	- 20 %
	100	26.3	22.0	- 16 %	57.2	44.4	- 22 %
	50	21.7	17.5	- 20 %	44.7	31.3	- 30 %
6	100	36.3	37.9	+ 5 %	69.9	62.3	- 11 %
	50	38.9	31.6	- 19 %	66.9	50.6	- 24 %

Table 6.5. Comparison of 4.5 m and 6 m freeboard (slope 1:1.5, smooth dam)

The overtopping height is reduced by approx. 15-25 % for most of the cases with a 6m freeboard. In some tests, the results give smaller reduction or increase which are within the standard deviation and shouldn't be considered. For the overtopping water volume, two observations are made. First, the overtopping volume always decreases by values in a range from 11 to 54 % when the freeboard is 6 m. Second, for a lower release height, i.e. a lower landslide velocity at the impact with the water, variation between the two freeboards is bigger. This change is observed for all the tests apart from the test with a 2V-block configuration and 150 cm release height. However, if the ± 10 % accuracy is applied, the variation fits the other experiments. This means the freeboard has more significant impact on landslides of lower velocity. These results show the importance of a freeboard in the overtopping mitigation.

6.1.5 Landslide impact velocity

In each landslide simulation, the blocks hit the water and transmit their momentum, measured by the kinetic energy, mainly to the water. As known, velocity is squared in the kinetic energy formula $E_k = \frac{1}{2} m v^2$. According to this formula, the velocity should have a large influence on the results of the experiments, i.e. the overtopping of the dam. However, this influence is reduced before

reaching the dam by the reflections of the waves. In the model, the landslide impact velocity is modified by changing the length of the chain holding the blocks, and therefore changing the release height of the blocks. For each setup with three reliable tests, the average value of the overtopping height of sensor 13 and total overtopped volume are computed for a better clarity in the graphs. The results are presented in the following graphs (Figure 6.3 and Figure 6.4) where it can be observed that most of the curves are rising. These results are discussed below the plots.
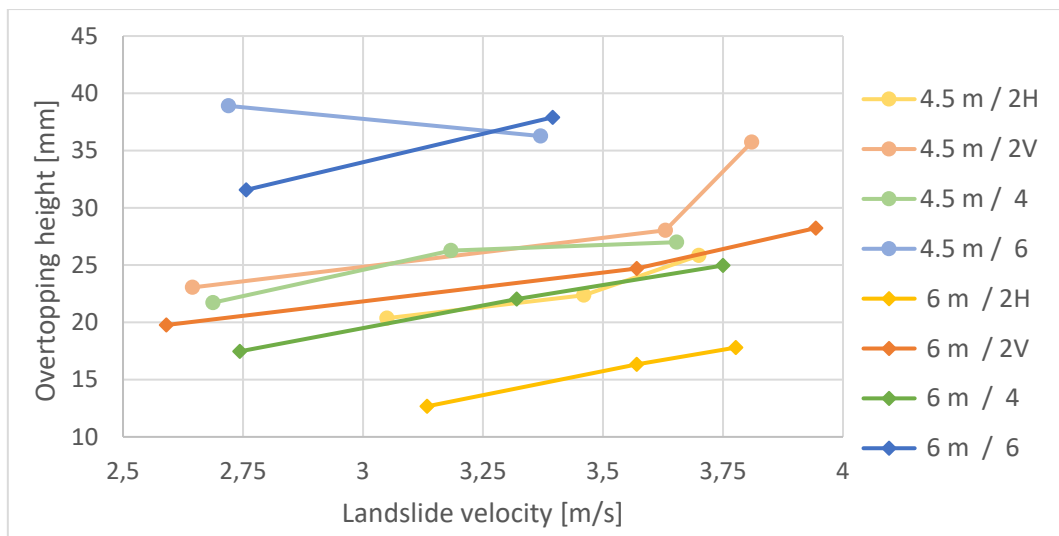
Figure 6.3. Dependency of the overtopping height on the landslide impact velocity (smooth dam, 1:1.5 slope)
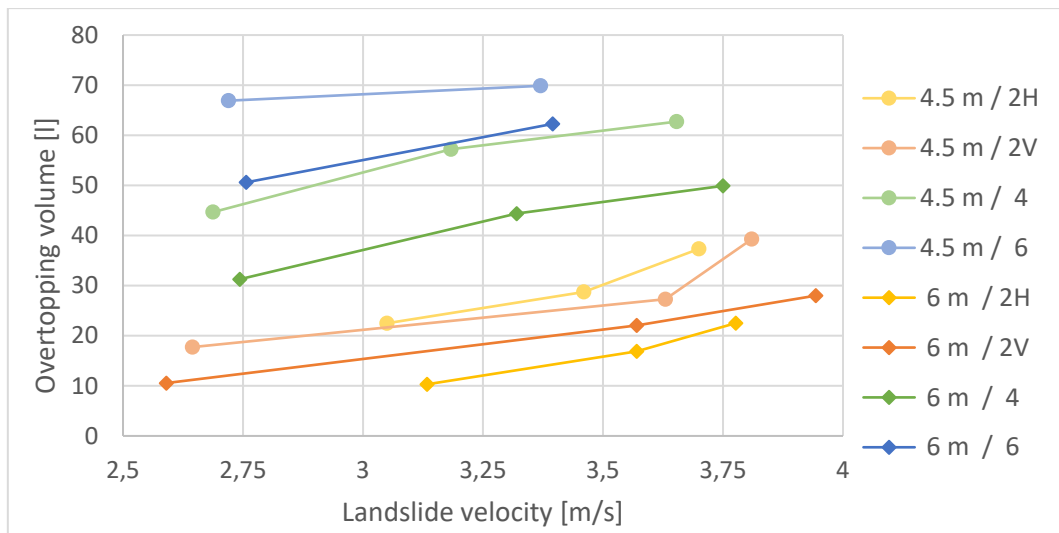
Figure 6.4. Dependency of the overtopping volume on the landslide impact velocity (smooth dam, 1:1.5 slope)

The first graph (Figure 6.3) shows the overtopping height as a function of the landslide velocity at the impact. All tests on the smooth dam with slope 1:1.5, apart from one, resulted in higher overtopping heights with higher velocities. The experiment (4.5 m / 6) giving the decrease of the overtopping

height does neither follow the trend of the other measurements nor can it be explained reasonably, thus it is not taken into consideration in the analysis. The second graph shows the influence of the landslide impact velocity on the overtopping volume. For all the block configurations tested the overtopping volume increases with the growth of the landslide impact velocity. In conclusion, the higher the velocity of the landslide, the higher the overtopping height and volume.

6.1.6　Landslide shape and volume

The landslide block configurations are varied to investigate the effect of the shape of the landslide. The tests analysed in this subsection are all carried out on the smooth dam with 1:1.5 slope. The different block configurations 2H, 2V, 4-blocks, 6-blocks are plotted in the graphs below (Figure 6.5). Previously, the release distance was used to characterise the tests. In this case, it is better to use the distance from the water level to the centre of mass, so as not to influence the tests by the dimensions of the landslides. In the graphs below, the overtopping height of sensor 13 is plotted towards the distance to the centre of mass, instead of release height.
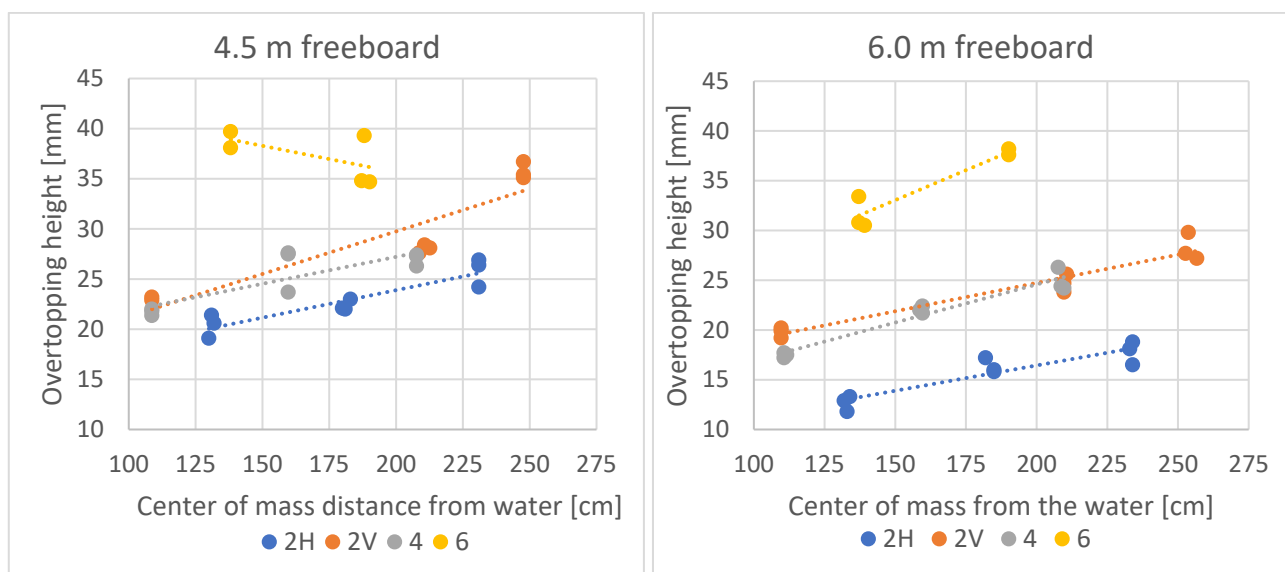
Figure 6.5. Impact of the landslide shape on the overtopping height (smooth dam, 1:1.5 slope)

The effect of the shape of the landslide is first analysed by observing its influence on the overtopping height. In both graphs above, the linear regression curves of the 2V and 4-blocks configurations are close to each other. The shape parameter identical in these two setups is the length of the landslide. The 2H configuration has a length of one block, the 2V and 4-block configurations have a length of two blocks, and the 6-block configuration has a length of three blocks. For both freeboards, a similar effect, i.e. the influence of length of the landslide on the overtopping height, is observed.

The position of the 2H and the 6-blocks curves in the graphs confirms this theory. The length of the landslide is, therefore, a parameter influencing the overtopping height positively, i.e. a longer landslide generates larger overtopping heights.
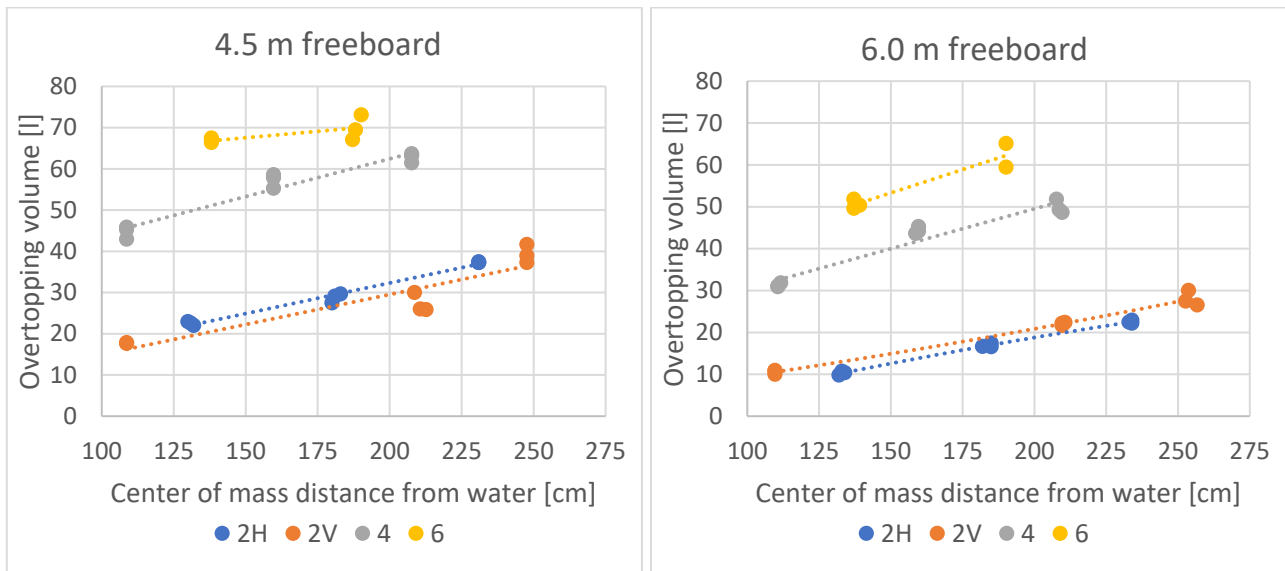
Figure 6.6. Impact of the landslide shape on the overtopping volume (smooth dam, 1:1.5 slope)

The graphs in Figure 6.6 show similar overtopping volumes for configurations with 2H and 2V blocks. Notice that these two two-block configurations have almost equal landslide volumes. Furthermore, the 4-block configuration generates larger overtopping volume than the two-blocks configurations, and the 6-block configuration causes the highest overtopping. The juxtaposition of these curves demonstrates a correlation between the landslide volume and the overtopping volume: the bigger the landslide volume, the larger the overtopping.

The relations of the landslide volume to the total overtopping volume and overtopping height from sensor 13 are plotted in Figure 6.7 for further investigation. In both graphs, the different block configurations are represented by one of the four columns. From the left, the first column illustrates the 2H configuration, the 2V, 4-block and 6-block configurations. The left graph shows that there is not as strong correlation between the landslide volume and the overtopping height, as it is the case for the overtopping volume (right graph).
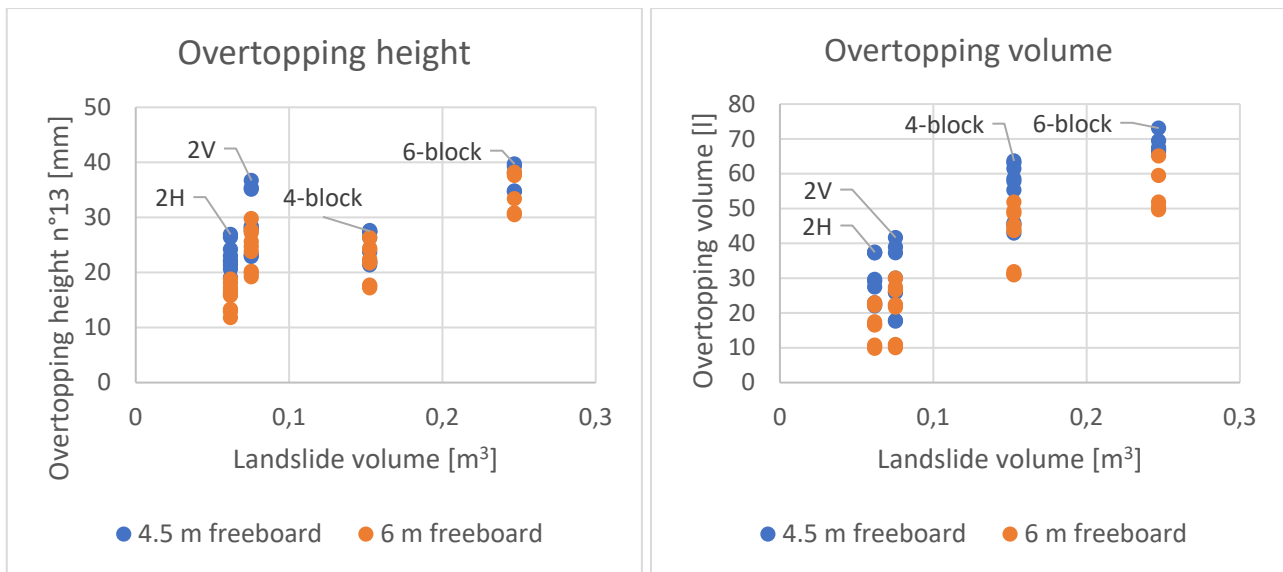
Figure 6.7. Impact of the landslide volume on overtopping height and volume, with linear regressions in the left graph (smooth dam, 1:1.5 slope)

Both freeboards, i.e. water levels, are shifted vertically, but the trend is the same in both cases. A doubling of the landslide volume corresponds approximately to the same increase of overtopping volume. However, this is not the case for a tripling of the volume. Therefore, this relation cannot be considered as linear. This confirms the conclusions of Ramírez (2016) in her bachelor thesis.

6.2 Wave generation and propagation

The wave generation and propagation patterns observed during the experiments are explained in this section and Figure 6.8. When the blocks enter the reservoir, water is pushed away and flows towards the opposite shore (1a). At the same moment, space in the water body is vacated behind the blocks. Water flows in this area from both sides (1b illustrated by Figure 6.9a), and the two water bodies collide (Figure 6.9b). Due to these two processes, the water level rises on both sides of the reservoir. This water level rise creates a first wave (2a and 3b) which propagates towards the dam and to the back of the reservoir. A second water level rise is observed subsequently on the reservoir side opposite to the landslide, creating a second wave (4), bigger on its left side. Finally, a third water level rise, on the right side of the reservoir engenders the last, third, big overtopping wave (5), higher on its left side.
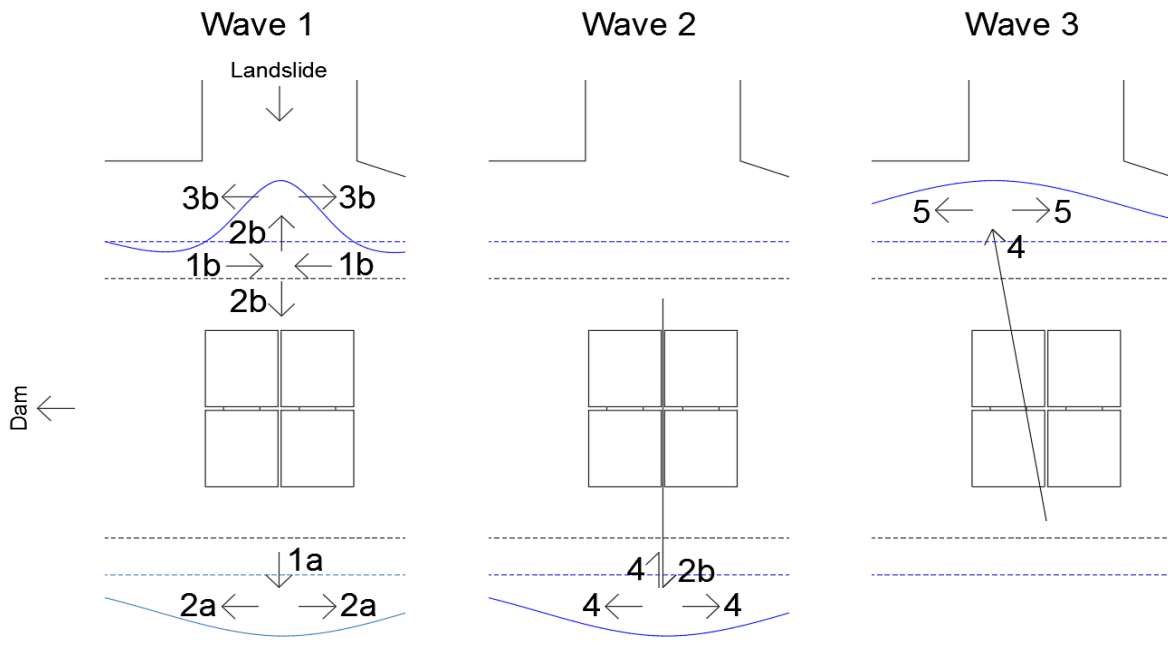
Figure 6.8. Scheme of the different wave generation
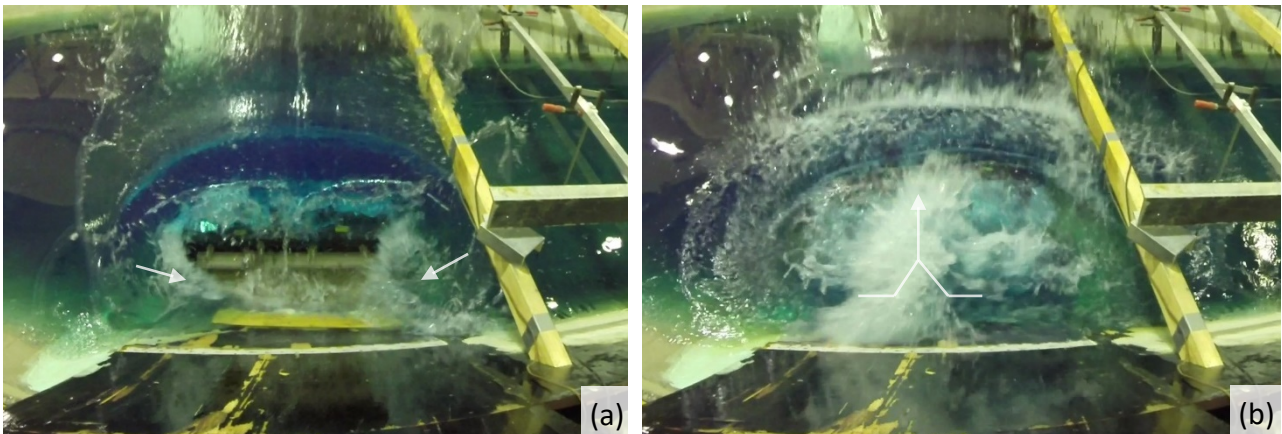
Figure 6.9. View from behind the landslide entering the water and leaving an empty space behind it. Water fills the space from both sides (a), and both water bodies collide resulting in a splash (b)

6.2.1 Wave pattern

Waves propagating through the basin are logged by the wave gauges. The recordings (Figure 6.10) show that the first wave is a solitary wave and following ones are different oscillatory waves generated by reflections in the reservoir. The wave pattern differs depending on the block configuration. When the landslide is arranged of two blocks (2H and 2V), the highest wave is the second one, followed by the third and fourth wave, whereas with four and six blocks the first wave, overtopping the dam, is the highest. This difference is explained as follows: in the case of the smaller landslide, the water displacement by the landslide is smaller than the wave generated behind the

landslide, whereas for 4 and 6-blocks landslides, the volume of the landslide is bigger, which generates a larger first wave.
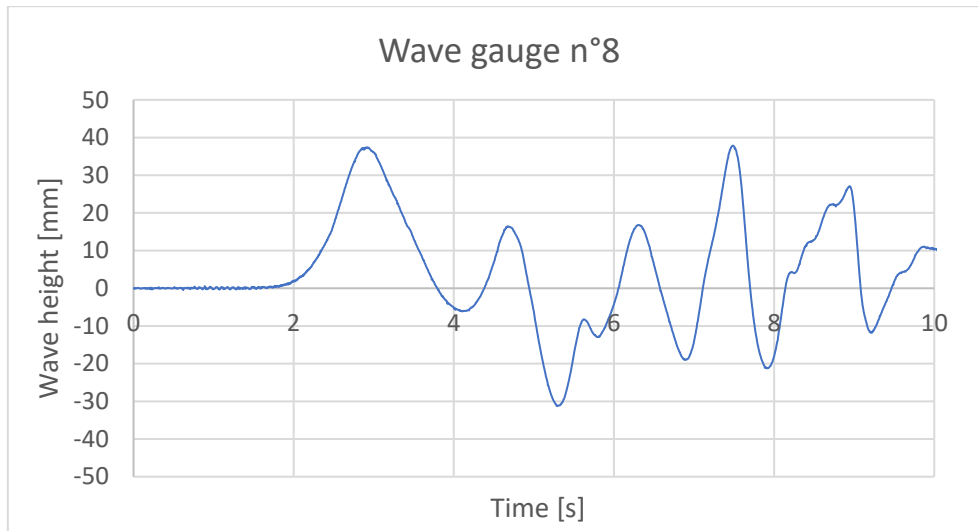
Figure 6.10. Wave height recording (test n° 20)

6.2.2   Wave length

The wave length is calculated from the recordings of sensors 1-9. As the wave is recorded passing the different sensors, the speed of the wave is calculated and compared to the theoretical wave speed Equation (6.8). The duration needed for one wave to pass one sensor is also known. The wave length is derived from these two indicators. In the model setup of 4-blocks released from 1 m (tests n° 58-60), the wave length of the first wave is 5.36 m, which corresponds to ≈1 km scaled up, and the next waves are shorter but still above 500 m in length. The waves generated by a landslide have a long wave length, which needs to be assimilated locally in the form of a temporary water level rise, rather than a water translation, which is, for example, the case with wind generated waves.

6.2.3   Wave speed

The speed of a wave in the reservoir is calculated from data collected by the wave gauge between the second line and the third line of sensors. The first line is not considered because it is too close to the landslide area and therefore the records are not very clear. The distance between sensor 5 and 8 is compared to the difference of time of the passing wave. The results, average speed and standard deviation, are presented for two completely different sets of reliable tests in Table 6.6.

Test	Wave	Average speed [m/s]	Standard deviation [m/s]
43 to 45 (SD / 4.5 m / 2H)	1	1.46	0.01
	2	0.66	0.00
	3	0.65	0.01
73 to 75 (SD / 6 m / 6-block)	1	1.47	0.03
	2	0.64	0.01
	3	0.69	0.00

Table 6.6. Wave speed measured between sensor 5 and 8 for two sets of reliable tests

The results show very similar wave speeds for both different configurations. Thus, it can be deducted that the wave speed is not depending on the landslide properties. The results show also higher speed for the first wave and lower speeds for the two next waves. All of these values are lower than the theoretical speed for an impulse wave, calculated with Equation (6.8) recalled below. The theoretical speed c for this setup varies between 1.70 and 1.80 m/s, depending on the still water depth h and the wave amplitude a.

$$c = [g(h + a)]^{1/2} \tag{6.8}$$

6.3 Dam overtopping

In this section, the results of the dam overtopping are discussed. First, the wave pattern is presented, and then the overtopping volume distribution is discussed. Finally, the overtopping speed is analysed, including a new method to derive it from the overtopping height measurements.

6.3.1 Overtopping pattern

The beginning of the overtopping always shows the same pattern (illustrated in Figure 6.11). The first wave overtops the dam in a straight way. Several overtoppings occur afterwards, with a higher wave on one side. It begins with the left bank and alternates until the last wave overtops the dam in a straight way again. The overtopping height is related to the wave pattern described in Section 6.2.1.
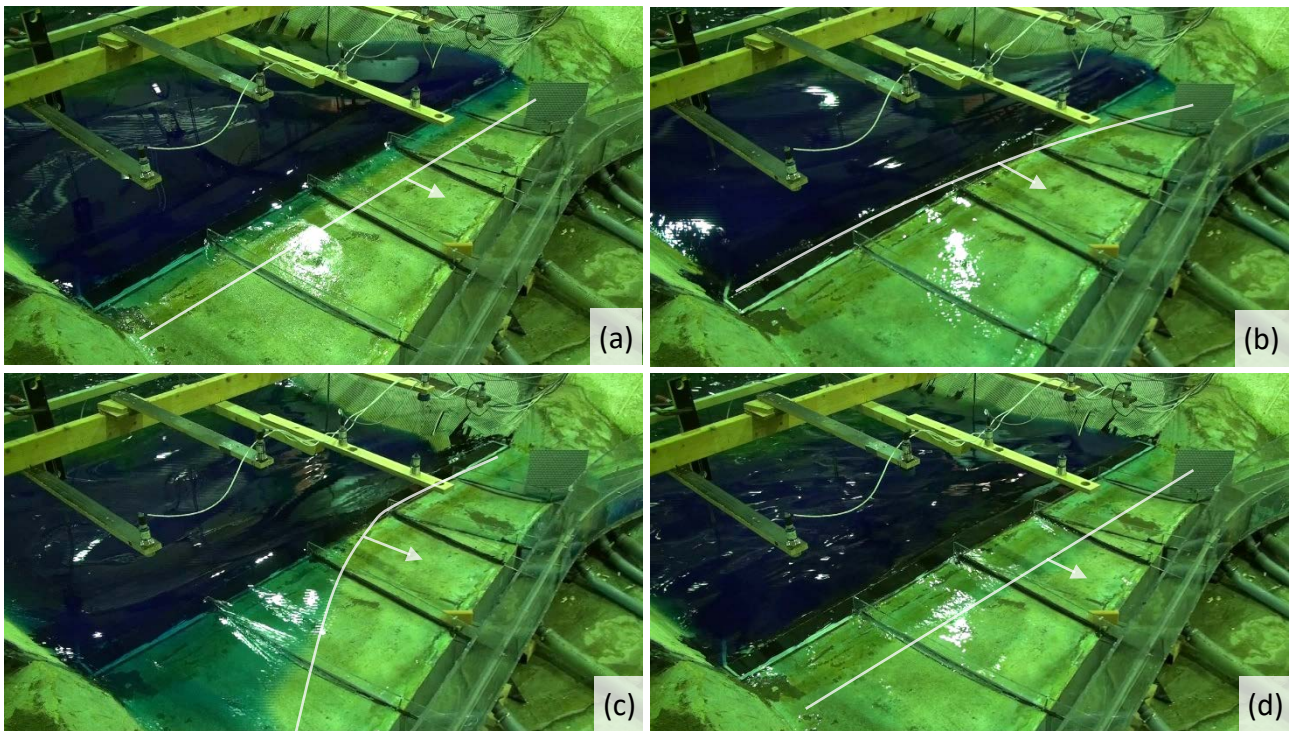
Figure 6.11. Overtopping pattern: first a straight wave overtops the dam (a), then several waves overtop in diagonal (b) & (c) and finally, a straight wave passes over the dam again (d).

6.3.2   Overtopping volume analysis

In the analysed model, the overtopping process is not uniform over the dam crest. As shown previously, the first wave overtops the dam crest in a straight way, but the next waves overtop diagonally (see Figure 6.11). This variation in overtopping process is reflected in the overtopping volume distribution (see Figure 6.12). On the sides of the dam, much more water overtops the dam than in its centre.
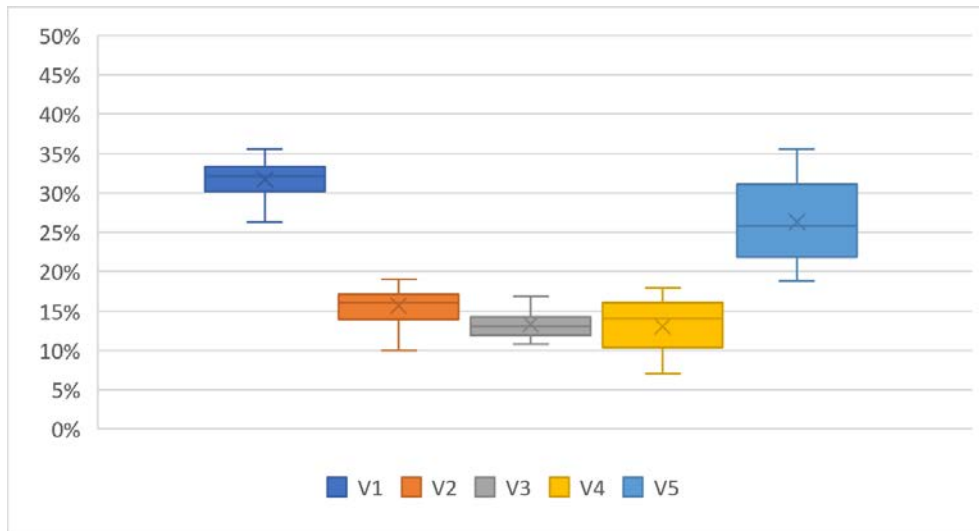
Figure 6.12. Overtopping volume distribution for the smooth dam (SD, all block configuration)

The slope of the dam has no influence on the overtopping distribution. On the other hand, the shape of the dam is found to have an influence. The results of the test carried out on the dam with wave wall (DW) are shown in Figure 6.13. The biggest changes in the overtopping distribution occur between the two dam profiles on section V1. It varies from 32 % to 40 %, whereas the centre section V3 it changes from 13 to 9 %. As seen previously (Chapter 6.1.2), the total overtopping volume is reduced by using a dam with wave wall. This reduction occurs mainly for the overtopping volume in section V3, whereas the overtopping volume in section V1 is similar in both cases.
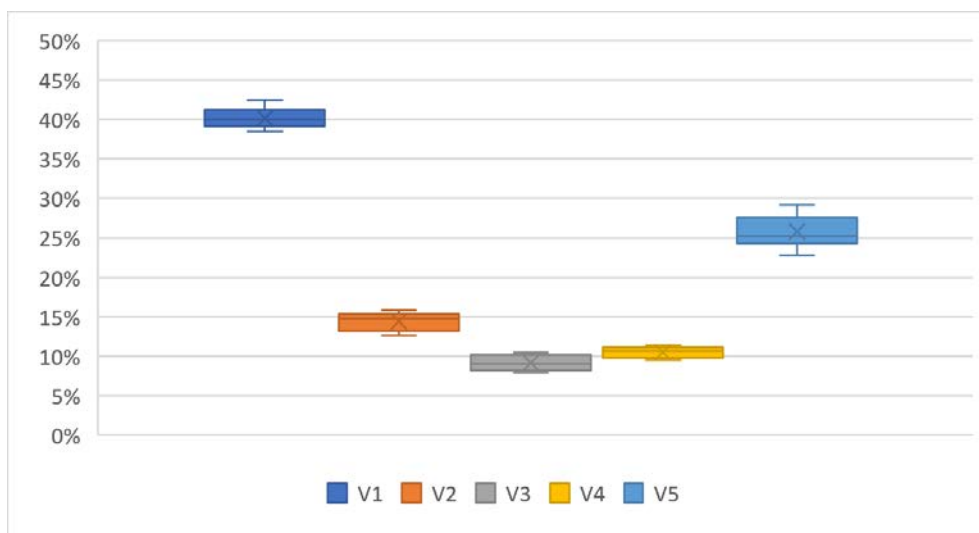
Figure 6.13. Overtopping volume distribution for the dam with wave wall (DW, 4-block configuration)

6.3.3   Overtopping speed and discharge analysis

The speed of the overtopping flow and the overtopping discharge is a valuable information needed to predict the erosion of an earth filled dam and to design the downhill riprap protection. In a previous study, (Mortensen, 2016) calculates the discharge per meter of dam per second by dividing the total overtopped volume by the overtopping time. A comparison between his result and the results of this thesis, based on this approach is given in Appendix G. In this thesis, a new and more precise method, based on the overtopping height and measured overtopping speed, is suggested to calculate the maximal overtopping discharge. The methodology developed as a part of this thesis is described in detail in Appendix E. The steps followed to get to it is presented here, as well as the results of this new method.

Overtopping speed analysis

At the beginning of the experiment period, two dam crest sensors aligned in the flow direction (sensor 13 and 14 in Figure 4.7) were installed to measure the speed of the wave. The distance between the sensors was 5.3 cm. The difference of times when the wave passes the sensors gives the speed of the overtopping wave. As the records of the waves show some different wave shape between these two points, it was decided to take the wave front as a measuring point. An example of recording by the two sensors is given in Figure 6.14.

The suggested method here is dependent on the time chosen to define the beginning of the wave at each sensor which is hard to set precisely. To reduce this sensitivity on the selected times, tests were carried out placing the sensors further apart from each other. However, the measurements were considerably different due to the influence of the flow surface after the dam crest on the wave. This observation confirms the results presented by Fuchs & Hager (2015), who claim that higher waves convert their potential energy into kinetic energy during the overland flow by decreasing the wave height and increasing the wave speed.

The result of the 50 first tests shows that the first wave is always the slowest one, with an average speed of 0.29 m/s ($\sigma = 0.05$) in the model, corresponding to 3.9 m/s, i.e. 14 km/h, scaled up. The second and third wave show higher speeds (0.48 and 0.50 m/s) with higher standard deviations (0.07 and 0.12 m/s). These speeds correspond to around 7 m/s, i.e. 25 km/h, scaled up. The three right boxplots in Figure 6.15 recall the presented values.

From test 51 on, interferences between the two ultrasonic sensors 13 and 14 were introduced into the monitoring data, and measurements lost their value. Sensor 14 was disconnected, and a new way of calculating the wave speed was elaborated: the new theoretical overtopping speed is derived from the overtopping height on sensor 13 and the total overtopped volume measured in the collecting bucket V3. Further details are available in Appendix E.
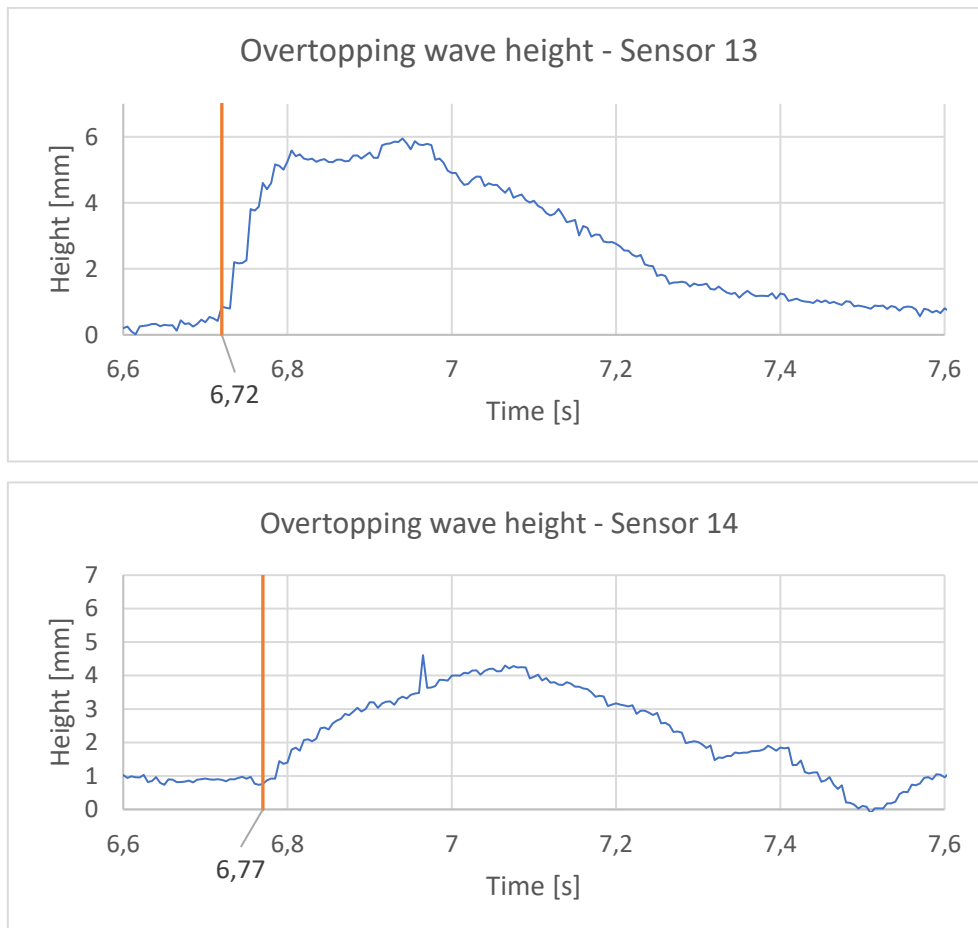
Figure 6.14. Example of overtopping wave height measurement by sensor 13 and 14
(here the second wave of test 20)

This procedure is validated by calculating the theoretical wave speed for the 50 first tests and comparing it to the results of the measurements. Figure 6.15 shows, starting from the left, the distribution of the measured overtopping speed for all three waves, the distribution of the theoretical overtopping speed and the first result displayed in separate boxes for each of the three waves. Even if the hypothesis of a constant overtopping speed for all the waves is not verified, the plot shows that the theoretical overtopping speed (red) should give a good indication of the average wave speed. This new procedure is confirmed because the box of the theoretical overtopping speed is contained within the box of all three waves.
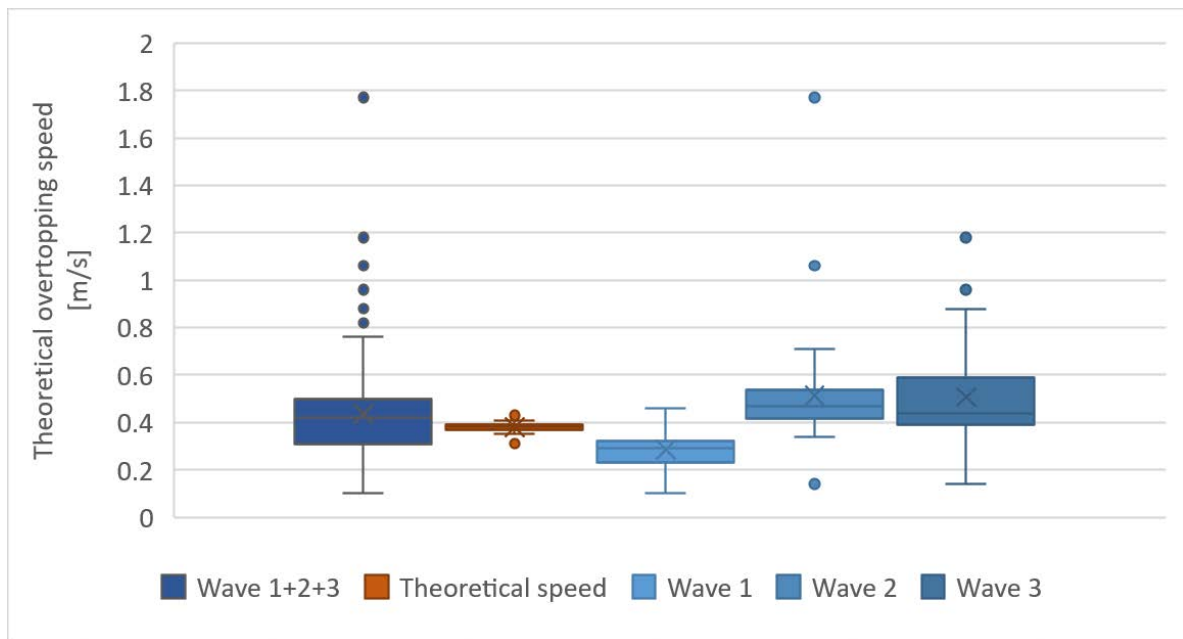
Figure 6.15. Measured overtopping speeds and theoretical wave speeds (Sensor 13, test n° 1-50)

The result of the theoretical overtopping speed is analysed to find any influence of the block configuration or the water level on it, but no effect on the overtopping speed is identified (Figures in the second part of Appendix E). The different dam profiles cannot be compared because the overtopping height sensors cannot be placed precisely on the maximal overtopping height (see Section 4.3). The distribution of theoretical overtopping speed for the smooth dam with 1:1.5 slope is shown in the boxplot in Figure 6.16. The three sensors are plotted next to each other. In the middle of the dam, sensor 13 is not influenced by the trapezoidal sides of the reservoir, and the results have less variation than on the dam sides. The speed of the wave is mainly dependent on the still water depth (Equation (6.8)), which has few changes over the different tests. Thus, the small interquartile range of sensors 11 and 13 is explained. Sensor 16 results are hard to explain and need to be further tested. In conclusion, the theoretical speed is verified to give an average value of the wave overtopping speed, and the theoretical speed has insignificant variation over the different test setup, i.e. is almost constant and independent of the setup in this particular model. This shows that the overtopping speed is not dependent on the landslide configuration, but probably on the still water depth. However, this last statement could not be shown within the small variation of the tested still water depths.
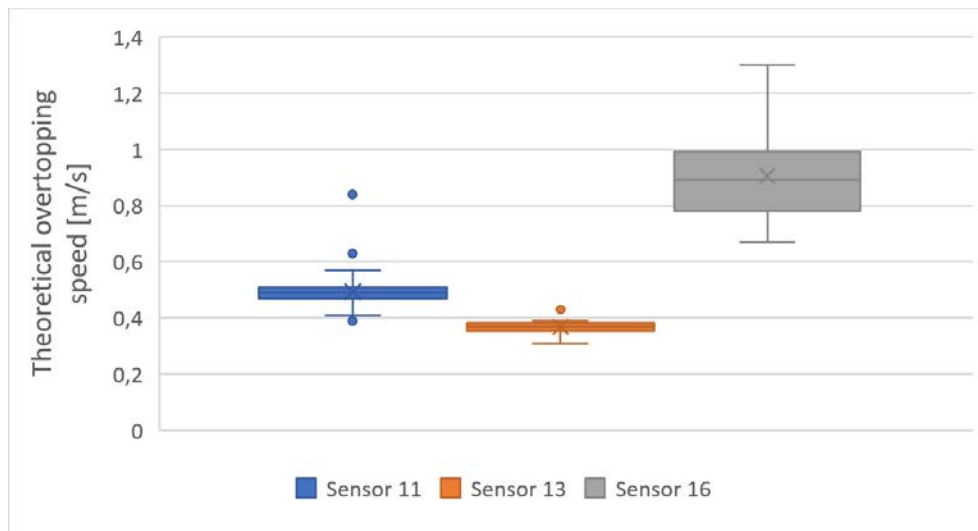
Figure 6.16. Theoretical overtopping speed for all tests with the smooth dam and slope 1:1.5

Average overtopping discharge analysis

The method used by Mortensen (2016) to calculate the average discharge consists of dividing the total measured overtopping volume measured by the total overtopping time. This second parameter is hard to define precisely, because the dam overtopping incorporates different waves with breaks in between as shown in Figure 6.17. The overtopping starts around at 3.5 seconds, but it is hard to define the end (either at 10 or 19.5 seconds). Mortensen (2016) consider an overtopping time around 14 seconds. In this thesis, the average overtopping discharge is an average of the discharges derived from the overtopping height and the theoretical overtopping speed. This method gives a more precise value. However, it considers a constant overtopping speed over time, which is not proven.
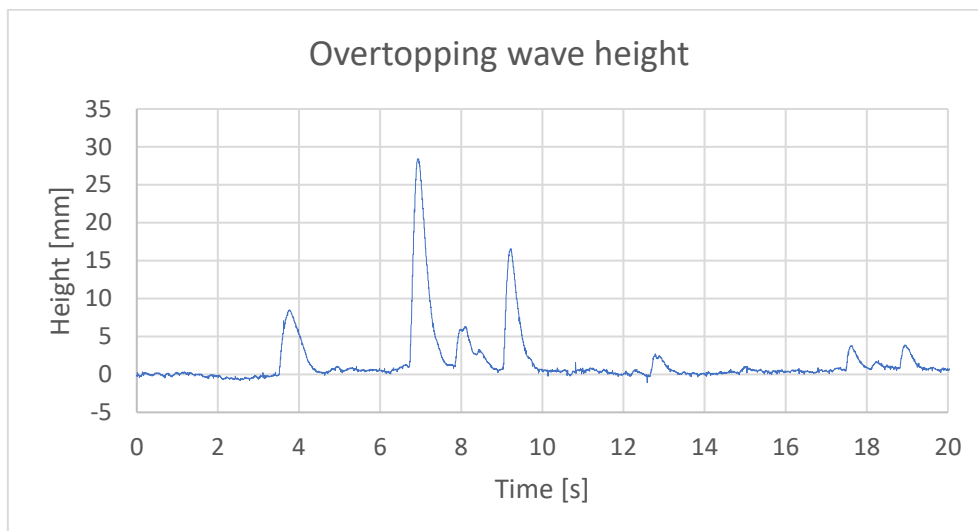
Figure 6.17. Overtopping height versus time (sensor 13, test n° 49)

The influence of the freeboard, the dam slope and the block configuration on the average overtopping discharge is investigated in Figure 6.18. In the left graph, only the 4-block configuration in the smooth dam 1:1.5 is taken into account, whereas in the right graph, all the block configurations are plotted. In the right chart, the interquartile range is large because data with different freeboards and release heights are considered. Different dam profiles cannot be compared because the sensors could not be placed precisely on the various dam profiles. The same dependency as for the overtopping height appears because the overtopping discharge is derived the overtopping height.
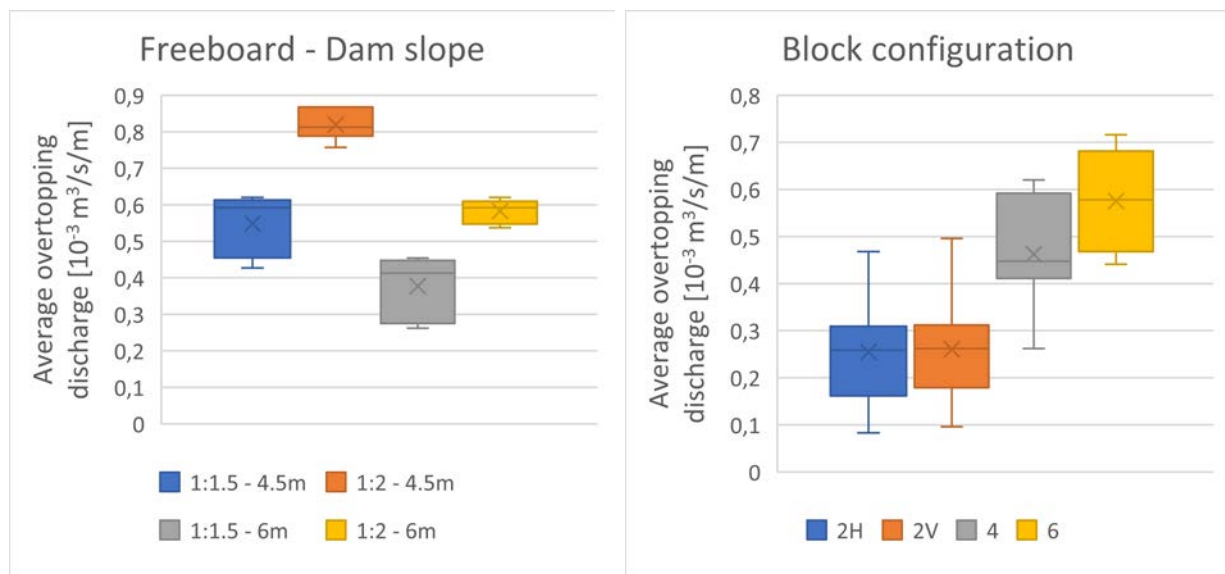
Figure 6.18. Influence of model parameters on average overtopping discharge
(section V3 in straight smooth dam with 1:1.5 slope)

A higher freeboard implies a lower average overtopping height, and a steeper upstream dam slope also reduces the average overtopping discharge. The left plot demonstrates that the average overtopping discharge is dependent on the landslide volume. The bigger the landslide is, the larger the average overtopping discharge is. These results correspond to the ones presented previously (see Subchapter 6.1.6), showing a logical correlation between the factor influencing the overtopping volume and the average overtopping discharge.

Furthermore, the distribution of the average overtopping discharge over the crest, plotted in Figure 6.19, is also giving an idea of the values on the prototype scale through the right axis. Higher average overtopping volumes are observed on the sides of the dam due to the unregular overtopping over the dam (see Subsection 6.3.2).
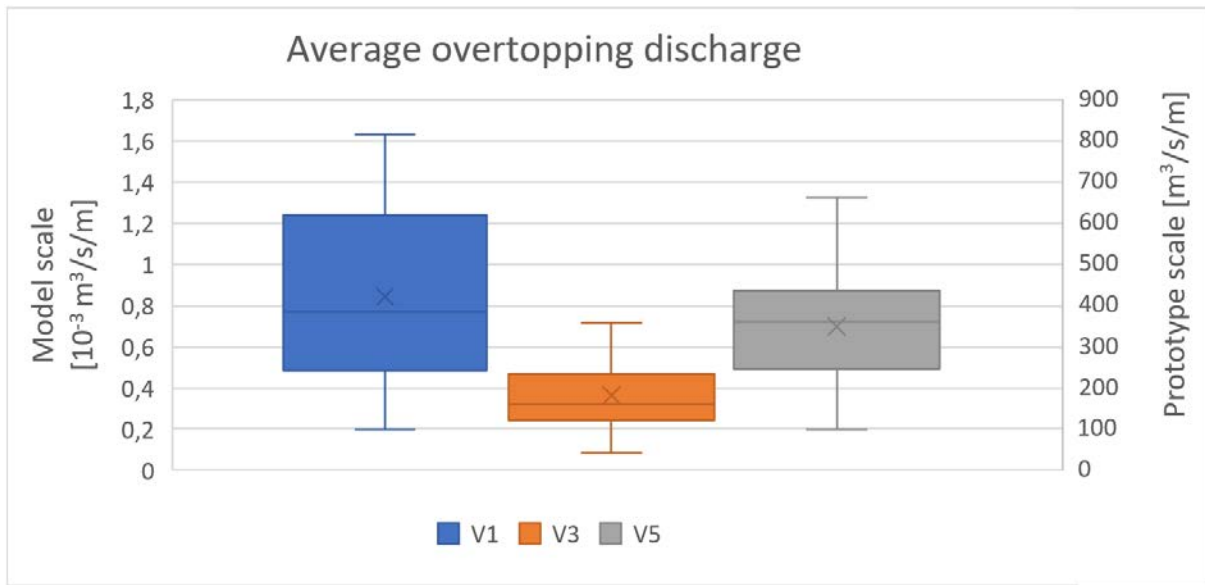
Figure 6.19. Average overtopping discharge distribution on the dam crest (smooth dam with 1:1.5 slope)

Maximal overtopping discharge analysis

A small analyse of the maximal overtopping discharge is presented here (Figure 6.20). The same trend is observed than for the influence of the freeboard and the dam slope on the average overtopping discharge, but with smaller variation. In the plot with the block configurations, the maximal overtopping discharge for the 2V block configuration is higher than for the 2H and the 4-block. This trend corresponds to the pattern of the overtopping wave height (Figure 6.7).
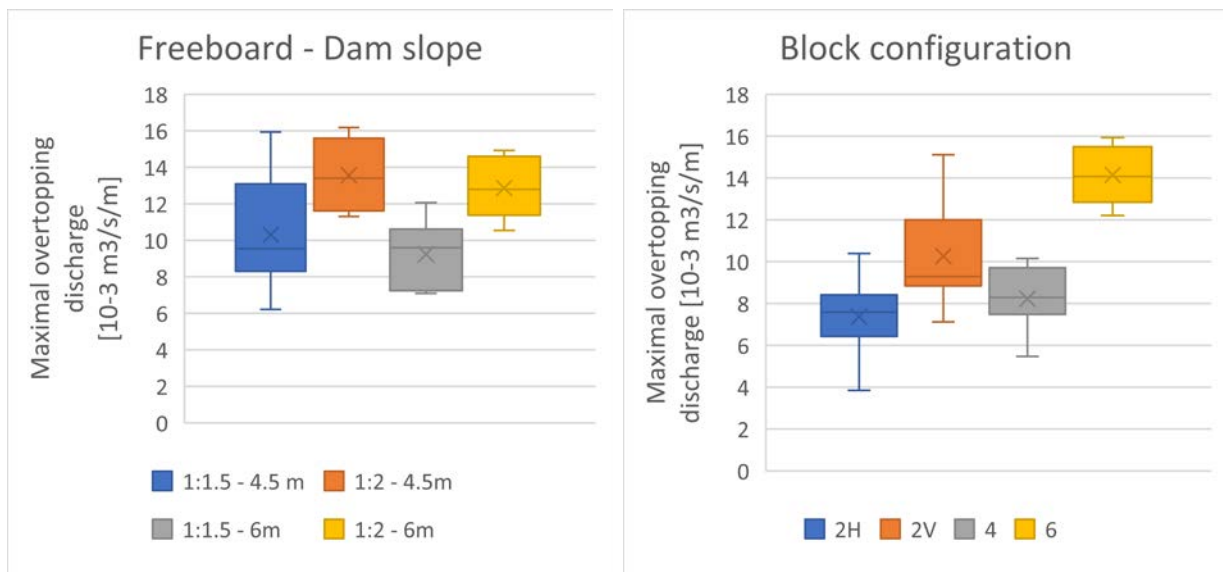
Figure 6.20. Influence of model parameters on maximal overtopping discharge
(section V3 in straight smooth dam with 1:1.5 slope)

The overtopping heights over the dam crest are not uniform and have higher values on the sides. Thereby, the maximal discharge over the dam follows the same trend. The Figure 6.21 gives the maximal overtopping discharge over the dam in the centre and on the two sides of the smooth dam (SD) setup and all the block configurations.
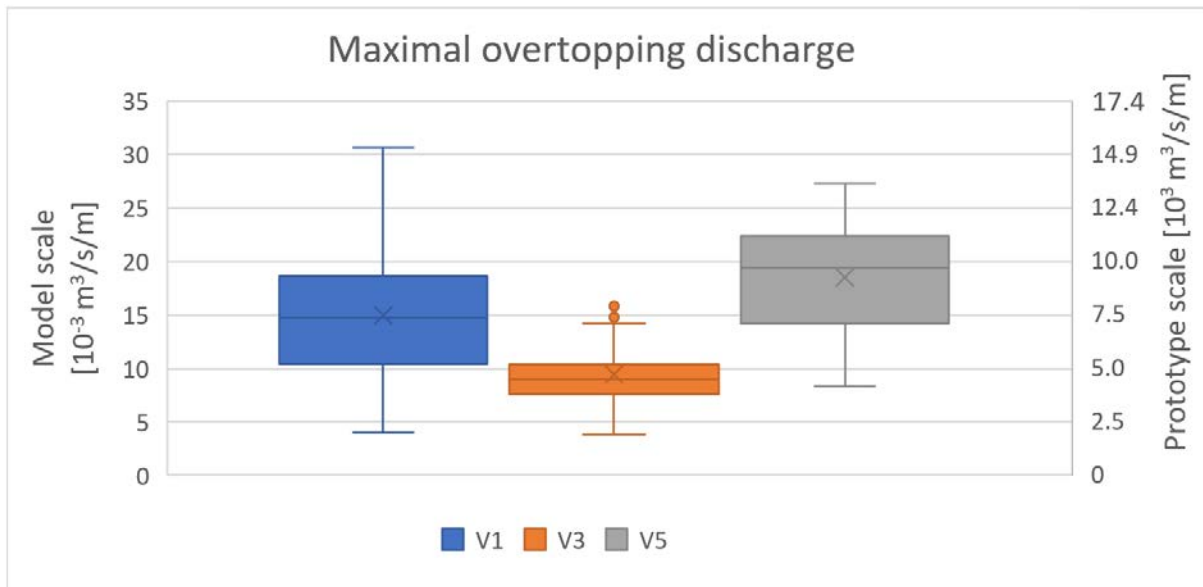
Figure 6.21. Maximal overtopping discharge distribution on the dam crest (smooth dam with 1:1.5 slope)

Finally, a comparison between the Figure 6.19 and Figure 6.21 demonstrates that the maximal overtopping discharge is 20-25 times bigger than the average overtopping discharge. This needs to be taken into consideration into the design if the dam needs to withstand such an event.

6.4   Comparison with previous studies

This section compares the results of the tests carried out in this thesis to the two studies from the literature review given in Chapter 2. First, the impulse product parameter formula is applied on the model, and further a comparison to the newly released study by Kobel et al. (2017) is given.

6.4.1   Impact product parameter

The impulse product parameter (IPP) was defined by Heller (2007) to estimate the wave generate by the landslide. For each test performed, the IPP was calculated to investigate if the IPP can be applied on this model. In this subsection, different wave heights, overtopping heights and overtopping volumes are compared to the impulse product parameter. Notice that for all the tests the limitations

for the calculation of the impulse product parameter are respected. Furthermore, in this analysis of the IPP only experiments with the smooth dam with 1:1.5 slope are compared.

Maximal wave height and maximal overtopping height

First, the maximal value recorded by all the wave gauge (sensor 1 to 9) during the whole event, i.e. several waves, is compared to the impulse product parameter. In the left graph of Figure 6.22, a slight rising trend is observed between the maximal wave height and the IPP. The right graph plots the same set of data, zooming in and distinguishing the different setups. All the setups follow a clear rising trend, apart from the 6-block configuration with 4.5 m freeboard which should not be considered as explained in Subsection 6.1.6. The IPP performs well within each setup with a generally good correlation (linear regression, $R^2 = 0.80$) but does not take well into account the different setups ($R^2 = 0.07$).
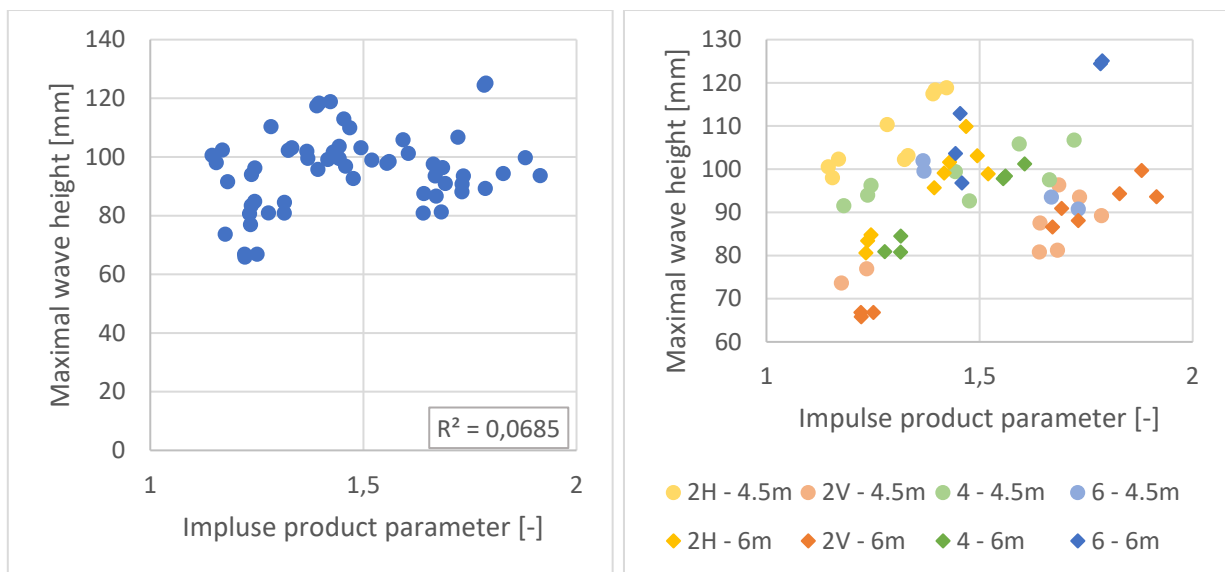
Figure 6.22. Impulse product parameter versus the maximal wave height (smooth dam with 1:1.5 slope)

The same conclusions are found when comparing the maximal overtopping height on the centre of the dam crest measured by sensor 13. Graphs are available in Appendix I, Figure I.1.

First wave height and first wave overtopping height

The fact that not always the first wave was the highest was observed in Subsection 6.2.1 "Wave pattern". Furthermore, only the first wave generated is an impulse wave. Therefore, more research on the first wave passing sensors 2, 5 and 13 was done by investigating their logs. All sensors are chosen in the centre of the reservoir to avoid side effects. Sensor 2 is the closest one to the impact

area, sensor 5 is behind the previous one and sensor 13 is on the dam crest (see Figure 4.7). The same results with slightly less scatter than for the maximal wave height (sensors 2 and 3) are obtained for the first wave. The maximal dam overtopping (sensor 13) appears more spread than previously. This is due to the low overtopping of the first wave in the 2H and 2V configurations. Further graphs are available in Figure I.2 and Figure I.3.
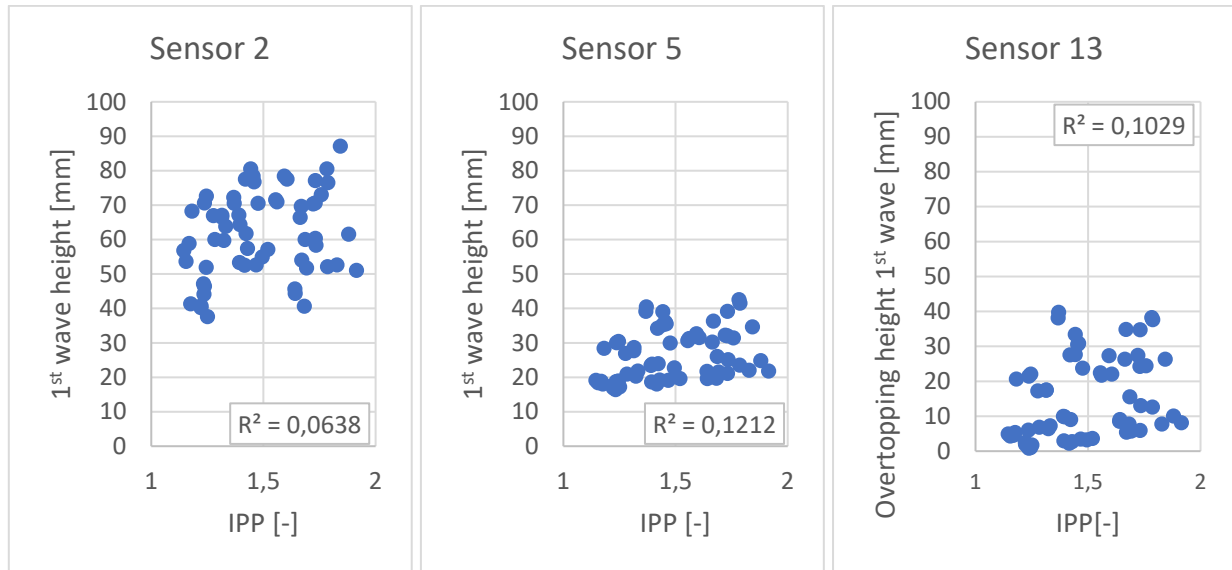
Figure 6.23. Measurements of 1ˢᵗ wave by sensor 2, 5, 13 versus IPP (smooth dam with 1:1.5 slope)

Overtopping volume

The overtopping volume is also plotted against the impulse product parameter. The same pattern is observed as previously with a trend but no correlation ($R^2 = 0.16$) in the left graph. When considering each setup separately the correlation varies between $R^2 = 0.49$ and 0.97, with 6 of 8 setups above $R^2 = 0.89$.
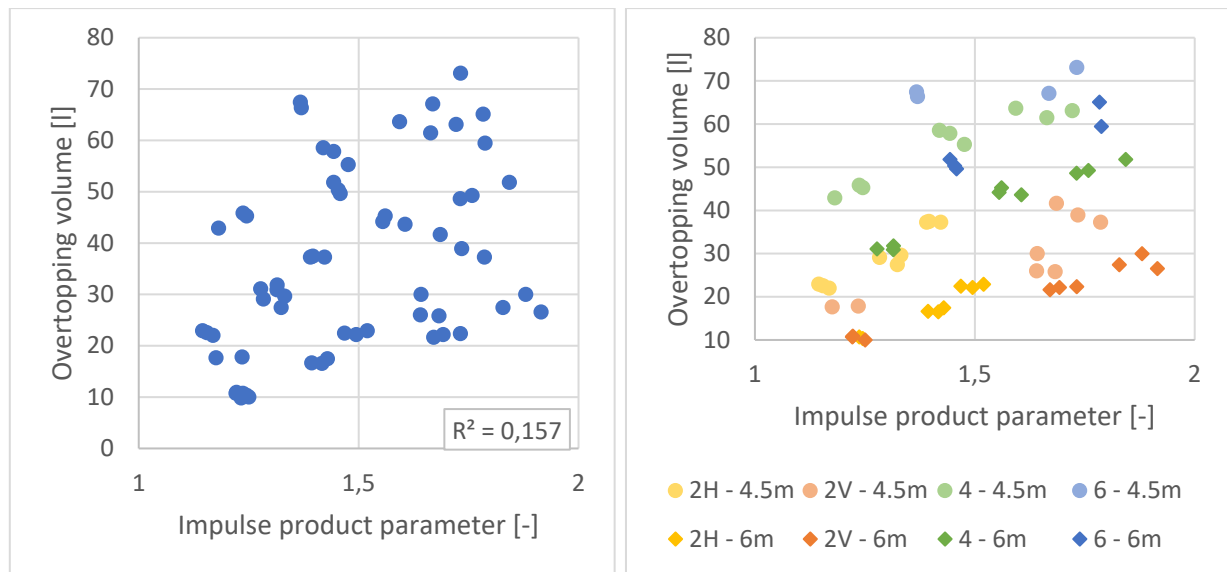
Figure 6.24. Total overtopping volume vs. impulse product parameter (smooth dam with 1:1.5 slope)

Conclusions about the impulse product parameter

The tests in this thesis confirm the results of Ponziani & Gardoni (2017) in their model B (same setup as this thesis). In the different test results analysed here, the IPP gives good results within a test setup; but does not manage well to take into account the different setups. When compared to the work done previously at the Laboratory of Hydraulics, Hydrology and Glaciology in Zurich (VAW), the model of this thesis differs in the setup. The analyses of landslide generated waves in reservoirs have extensively been conducted in two-dimensional (2D) laboratory-scale models. These setups consist of a flume with the landslide entering the water on the side and the overtopped reservoir on the other side. The third dimension (3D) was investigated at the VAW considering a wave propagation angle γ relative to the slide direction (Figure 6.25) in a basin. In all of these cases, the impulse wave generated by the landslide is considered propagating straight across the reservoir towards the reservoir. However, in the setup of this thesis, the main waves caused by the landslide are reflected on the opposite shore before moving towards the dam.
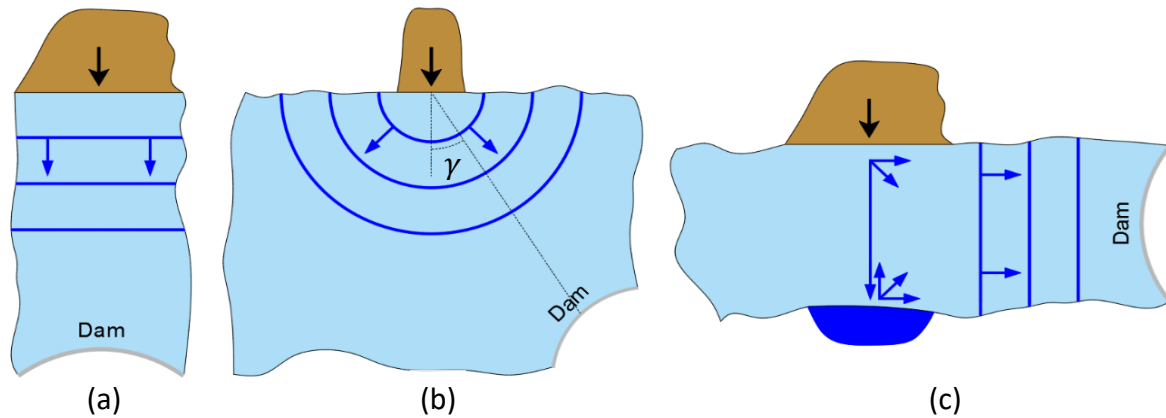
Figure 6.25. Different study setups in a flume (2D) (a), in a basin (3D) (b), and as the model of this thesis (c) Modified from (Heller et al., 2009)

Furthermore, the shape of the reservoir is not rectangular, as in most generic studies, but considers shores with an angle of 50°. These two differences imply different wave propagation processes, and therefore the impact product parameter cannot be easily applied to this model.

6.4.2   Normalised maximal overtopping depth

New equations for the overtopping volume and the maximum overtopping depth were published in the June 2017 edition of the Journal of Hydraulic Engineering by Kobel et al. (2017). These equations apply for impulse waves overtopping rigid structures. The recording of the wave gauges in the model shows that the first wave is close to a solitary-wave, as explained in Subsection 6.2.1 "Wave pattern". The comparison of the results of this thesis to these new equations is therefore going to be carried out only on the first wave, where overtopping is recorded.

The relations suggested by Kobel et al. (2017), giving the normalised value d_0/w, were applied on the first wave of 30 tests. This sample was selected among the test with a smooth dam with slope 1:1.5 and 1:2. The results of the comparison between the overtopping height measured by sensor 13 in the tests and the overtopping height calculated with Equations (2.6) and (2.7) based on data from sensor 8, are the following.

Equation (2.6) gives a good estimation (-10 % to +5 % of measured value) for the dam slope 1:2 with 4-block configuration. The predicted values for the dam slope 1:1.5 are overestimated. For the 4-block and 6-block configurations, the results of Equation (2.6) are 5 to 40 % too high, and the overestimation for the 2H and 2V configuration is between +66 % to +500 %. Equation (2.7) overestimates the waves created by the 4-block and 6-block configuration and underestimates the 2H

and 2V block configuration. Note that no other tests for the 1:2 slope are available for a different block configuration than 4-blocks. A table with the detailed results is available in Appendix J.

6.5   Dimensionless parameters analysis

By considering the main parameters affecting the impulse wave, dimensional analysis is carried out based on the work of Heller (2011) and Sleigh (1997). Six governing parameters were independently varied during the tests, namely the still water depth h, slide impact speed V_s, slide volume V_s, slide length l, slide density ρ_s, and dam slope β. Besides, gravitational acceleration g, slide impact angle α and water density ρ are also considered having an effect on the overtopping volume and height. All these parameters are described by three reference dimensions (length, mass and time). According to Buckingham's π-theorems, the relationship between the nine independent variables can be expressed as a relationship between six dimensionless parameters Π_i based on 3 repeating variables V_s, ρ_s, h. The

studied Π-parameters are the following ones: the relative slide volume $\Pi_1 = V_s/h^3$, relative slide length $\Pi_2 = l/h$, slide Froude number $\Pi_3 = V_s/(gh)^{1/2}$, relative slide density $\Pi_4 = \rho/\rho_s$, dam slope angle $\Pi_5 = \beta$ and the slide impact angle $\Pi_6 = \alpha$.

All these six dimensionless parameters were plotted against different measures done during the tests. All graphs showed either a likely linear regression possibility or no trend. Table 6.7 presents a summary of the coefficients of determination R^2 of all tested pairs. Only the tests with the smooth dam with slope 1:1.5 were taken into account in this table. Taking into account the 1:2 slope did not give better results. In the fitting for the Table 6.7, no coefficients are given for the dam slope angle Π_5 and the slide impact angle Π_6 because they are constant over the selected tests.

R2	Maximal wave height	Overtopping			1st wave height / overtopping		
		height 13	volume	speed	sensor 2	sensor 5	sensor 13
Π1	0,06	0,34	0,66	9E-06	0,58	0,87	0,87
Π2	7E-04	0,55	0,45	2,5E-03	0,21	0,58	0,62
Π3	0,15	0,02	6E-05	0,04	0,01	0,02	0,03
Π4	0,01	0,45	0,43	3,50E-03	0,19	0,52	0,58
Π5	-	-	-	-	-	-	-
Π6	-	-	-	-	-	-	-

Table 6.7. Coefficient of determination for fitting test of dimensionless parameters

The only parameter showing a high coefficient of determination is the relative slide volume on the impulse wave, i.e. the first wave. It is also interesting to highlight that the relative slide volume also

affects the overtopping volume and the relative slide length impact the overtopping height of the first wave. This last point confirms the observation about the influence of the landslide length on the overtopping height (see Subchapter 6.1.6). The graphs corresponding to the best fitting are plotted in Figure 6.26.
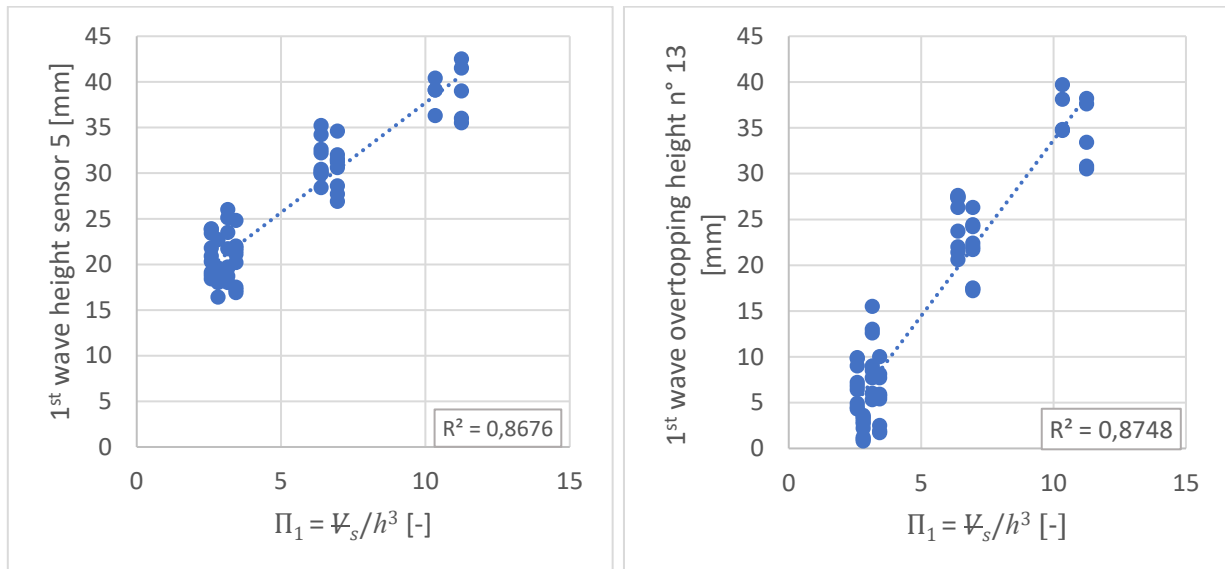
Figure 6.26. First wave versus relative slide volume

Chapter 7 Conclusion

This thesis studies an overtopping of a dam by landslide generated waves. A parametrical study, investigating the influence of reservoir and landslides properties, is carried out based on a laboratory model. It reproduces a typical situation of a reservoir in a valley with unstable hillsides. Therefore, the landslide enters the water from the reservoirs side and generates a run-up wave on the opposite shore, which propagates towards the dam. The overtopping volumes and heights are the main analysed results of the 135 reliable tests in this lateral landslide model, and following conclusions are drawn:

- A higher landslide impact velocity engenders a larger overtopping height and volume. The landslide shape influences the overtopping: its volume influences the overtopping volume, and its length influences the overtopping height. In previous studies, the landslide length was found to have a negligible impact on the wave generation and its relation to the overtopping height was therefore never highlighted. This new relation could be due to the lateral landslide position of this model.

- The higher the freeboard, the lower the overtopping height and volume.

- The dam roughness has a negligible impact on the overtopping properties, whereas the dam slope influences the overtopping volume. Steeper dam slope causes smaller overtopping volume. Moreover, a vertical wave wall below the crest reduces the overtopping volume as well.

- Besides these main observations, it is also interesting to point out that the overtopping speed measurements showed that the first wave is always the slowest one, while the second and third once are faster. However, these results for the overtopping speed have not significant variation over the different setups tested, and thus the overtopping wave speed can be considered to be approximately constant and independent of the setup tested. This observation is due to a similar still water depth over the tests.

In addition to the above, the wave propagation was observed and studied. Because the landslide is positioned on the side of the reservoir, water does not overtop the dam crest in a homogenous way, but more water flows on the sides. Furthermore, it is observed that the highest overtopping wave is not always the first solitary wave, but depending on the landslide properties, the successive reflected waves might be higher.

Moreover, comparison of the impulse product parameter from Heller with the laboratory tests from this thesis demonstrates a dimensionless parameter characterising well the wave generation and overtopping within a setup, but having trouble taking into account the different tested landslide shapes in this type of lateral landslide model. A second comparison with the equation of normalized maximal overtopping depth of Kobel et al. highlighted the same result. On of their equations give a good estimation with the 4-block configuration and 1:2 dam front slope, but other configuration, especially with small overtopping, result in lower overtopping depth than the predicted one.

In conclusion, the parameters influencing the overtopping the most are the landslide volume, landslide length and water level in the reservoir. Because no action can be taken on the landslide, the diminishing of the water level, i.e. an increased freeboard, is the best action to take to reduce the impact of a landslide generated impulse wave. The construction of a wave wall could be an additional mitigation measure. Besides, the model with the landslide positioned on the reservoirs side showed a complex wave reflection phenomenon leading to an uneven overtopping of the dam. Finally, equations from other studies aiming to estimate the overtopping appear to have troubles to deal with different landslide shapes.

Research gap

The main uncertainties of real cases are from the geological point of view. Even a completely mapped geological area leaves doubts about the exact behaviour of the landslide. In the catastrophe of Vajont, the velocity of the landslide was the parameter which was completely underestimated. Still, nowadays it is hard to precisely predict the velocity in order to design the protections properly. However, tests on simple, generic models bring a better understanding of the phenomenon's process.

The major equations in impulse wave research consider a rectangular flume channel or a large basin. Effects of the usually trapezoidal shape of a reservoir or fjord, with significant wave reflections, were not studied and thus not included in these equations. Therefore, it would be interesting to explore the case of a landslide entering a trapezoidal channel from the back of the reservoir, i.e. the opposite side

to the dam. Besides, the impulse wave generated by a landslide falling into a reservoir with bigger still water depth is known to have greater amplitude, but the effect of the lateral landslide configuration on the overtopping height and volume should be investigated. A further parameter of the reservoir to study is the distance between the landslide impact area and the dam. Finally, this thesis highlighted the beneficial effect of the wave wall to reduce the overtopping volume. A more detailed research could lead to an optimisation of the height of this structure by studying the optimal level for the bottom of this wall. Should it be above or below the still water level to decrease the overtopping?

References

Biedermann, J. (2017). *Overtopping of embankement dams from landslide generated waves - Prestudy for master thesis. Lausanne: EPFL (Ecole polytechnique fédérale de Lausanne).*

Bolzoni, M. (2015). *Physical model study on impacts of landslide generated wave action on embankment dams. Trondheim: NTNU.*

Fuchs, H., & Hager, W. H. (2015). *Solitary Impulse Wave Transformation to Overland Flow. Journal of Waterway, Port, Coastal, and Ocean Engineering, 141, 04015004. https://doi.org/10.1061/(ASCE)WW.1943-5460.0000294*

Gamlem, M. (2017, May 9). *Steinras i Geirangerfjorden. Retrieved 10 May 2017, from https://www.nrk.no/mr/steinras-i-geirangerfjorden-1.13507378*

Gamlem, M., & Brunstad, S. B. (2017, May 9). *Turistferga var like ved steinraset i Geiranger. Retrieved 10 May 2017, from https://www.nrk.no/mr/turistferga-var-like-ved-steinraset-i-geiranger-1.13509183*

Gardoni, M., & Ponziani, L. (2017). *Landslide generated impulse waves in dam reservoirs - Experimental investigation on a physical hydraulic model. NTNU, Trondheim.*

Hammeren, R. (2016). *Skred i magasin - Simulering av overtopping. Trondheim: NTNU.*

Harbitz, C. B., Glimsdal, S., Løvholt, F., Kveldsvik, V., Pedersen, G. K., & Jensen, A. (2014). *Rockslide tsunamis in complex fjords: From an unstable rock slope at Åkerneset to tsunami risk in western Norway. Coastal Engineering, 88, 101–122. https://doi.org/10.1016/j.coastaleng.2014.02.003*

Heller, V. (2007). *Landslide generated impulse waves – Prediction of near field characteristics (VAW-Mitteilungen No. 204). ETH Zurich, Zürich. Retrieved from https://www.ethz.ch/content/dam/ethz/special-interest/baug/vaw/vaw-dam/documents/das-institut/mitteilungen/2000-2009/204.pdf*

Heller, V. (2011). Scale effects in physical hydraulic engineering models. Journal of Hydraulic Research, 49(3), 293–306. https://doi.org/10.1080/00221686.2011.578914

Heller, V., Hager, W. H., & Minor, H.-E. (2008). Scale effects in subaerial landslide generated impulse waves. Experiments in Fluids, 44(5), 691–703. https://doi.org/10.1007/s00348-007-0427-7

Heller, V., Hager, W. H., & Minor, H.-E. (2009). Landslide generated impulse waves in reservoirs - Basics and computation (VAW-Mitteilungen No. 211). ETH Zurich, Zürich. Retrieved from https://www.ethz.ch/content/dam/ethz/special-interest/baug/vaw/vaw-dam/documents/das-institut/mitteilungen/2000-2009/211.pdf

Huang, B., Wang, S. C., & Zhao, Y. B. (2017). Impulse waves in reservoirs generated by landslides into shallow water. Coastal Engineering, 123, 52–61. https://doi.org/10.1016/j.coastaleng.2017.03.003

Hughes, S. A. (1993). Physical models and laboratory techniques in coastal engineering. Singapore ; River Edge, NJ: World Scientific.

ICOLD (International Commission on Large Dams). (2002). Reservoir landslides : investigation and management - Guidelines and case histories (Bulletin 124). Paris.

Jørstad, F. (1968). Waves generated by landslides in Norwegian fjords and lakes. Norwegian Geotechnical Institute, 79, 13–32.

Kamphuis, J., & Bowering, R. (1972). Impulse waves generated by landslides. In Proceedings of 12th ICCE (pp. 575–588). Vancouver, Canada: ASCE.

Kiersch, G. (1964). Vaiont reservoir disaster. Civil Engineering, 34, 32–39.

Kobel, J., Evers, F. M., & Hager, W. H. (2017). Impulse Wave Overtopping at Rigid Dam Structures. Journal of Hydraulic Engineering, 143(6), 04017002. https://doi.org/10.1061/(ASCE)HY.1943-7900.0001271

Lorås, S. (2014). Skred i magasin - Fastsettelse av relevante skredegenskaper for generering av bølger med hensyn til overtopping av fyllingsdam. Trondheim: NTNU.

Mortensen, R. (2016). Skred i vannmagasin - Overtopping av Damkrone. Trondheim: NTNU. Retrieved from https://brage.bibsys.no/xmlui/handle/11250/2433637

Müller, D. (1995). Auflaufen und Überschwappen von Imuplswellen an Talsperren (VAW-Mitteilungen No. 137). ETH Zurich, Zürich.

NVE. (2012, April). *Veileder for fyllingsdammer. NVEs hustrykkeri. Retrieved from http://publikasjoner.nve.no/veileder/2012/veileder2012_04.pdf*

Panizzo, A., De Girolamo, P., & Petaccia, A. (2005). *Forecasting impulse waves generated by subaerial landslides. Journal of Geophysical Research, 110(C12). https://doi.org/10.1029/2004JC002778*

Petley, D. (2017, May 10). *A significant rockslide on the flanks of Geiranger Fjord in Norway. Retrieved 11 May 2017, from http://blogs.agu.org/landslideblog/2017/05/10/geiranger-fjord-1/*

Ponziani, L., & Gardoni, M. (2017). *Landslide generated waves in dam reservoirs - Experimental investigation on a physical hydraulic model. Retrieved from https://brage.bibsys.no/xmlui/handle/11250/2442995*

Ramírez, M. J. (2016). *Studies on impacts of landslide generated wave action on embankment dams. Trondheim: NTNU.*

Ramsden, J. D. (1996). *Forces on a Vertical Wall due to Long Waves, Bores, and Dry-Bed Surges. Journal of Waterway, Port, Coastal, and Ocean Engineering, 122, 134–141. https://doi.org/10.1061/(ASCE)0733-950X(1996)122:3(134)*

Schleiss, A. J., & Pougatsch, H. (2011). *Les barrages: du projet à la mise en service. Lausanne: Presses Polytechniques et Universitaires Romandes.*

Sleigh, A. (1997). *Fluid Mechanics : Dimensional Analysis. Retrieved from http://www.efm.leeds.ac.uk/CIVE/CIVE1400/Section5/dimensional_analysis.htm*

Svendsby, J. N. (2014). *Skred i magasin - Test av Hellers beregningsmetode for estimering av skredgenererte impulsbølger mot forsøk i skalert modell med norske forhold. Trondheim: NTNU.*

Appendix A   Landslide properties

The landslide consists of blocks, which can be arranged in different configurations. Table A.1 gives the properties of the different blocks available. The blocks are always arranged in a defined order for a particular block configuration (see Figure A.1). The properties of these configurations are given in Table A.2.

Block number	Weight [kg]	Volume [cm^3]	Density [kg/m^3]
1	42.3	38250	1106
2	42.4	38250	1108
3	42.3	38250	1106
4	42.4	38250	1108
5	46.5	36000	1292
6	46.3	36000	1286
7 (front)	37.7	36000	1047
8 (front)	37.6	36000	1044

Table A.1. Landslide blocks properties
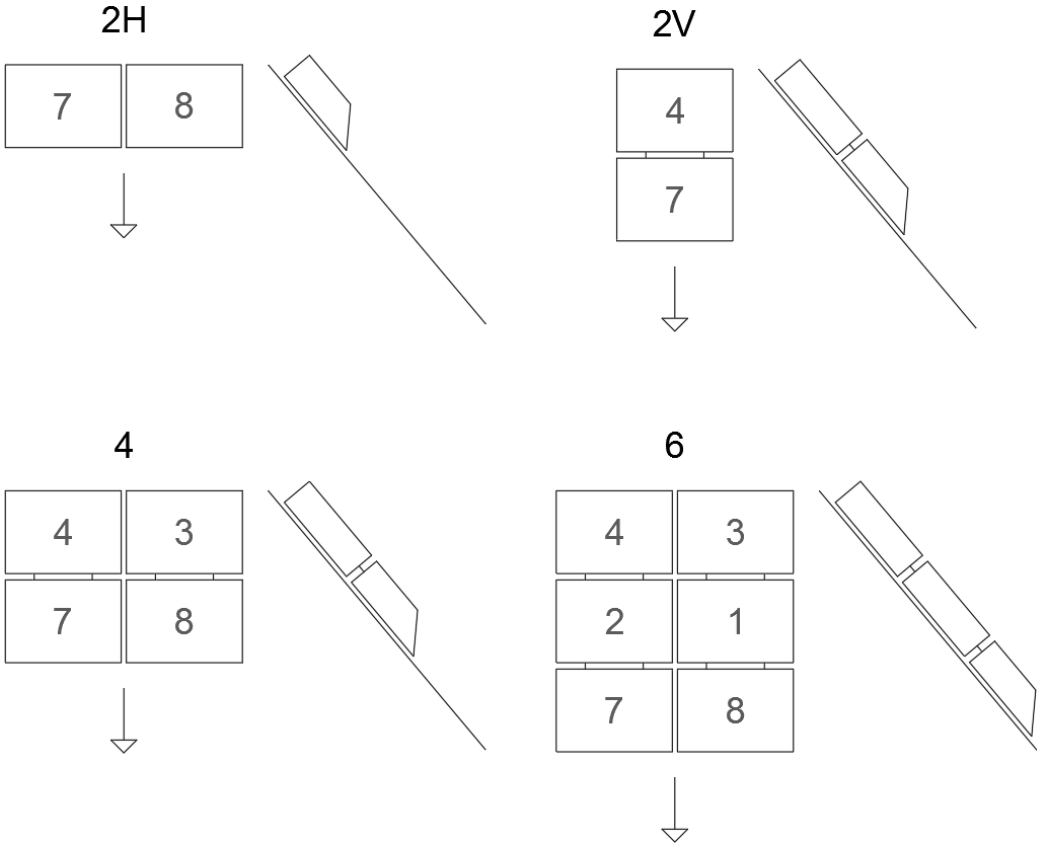
Figure A.1. Block configuration in the landslide

Landslide configuration			2H	2V	4	6
Model	Weight	[kg]	75.3	80.1	160	244.7
	Length	[cm]	50	109	109	170
	Width	[cm]	91	45	91	91
	Volume	[cm^3]	61880	75510	152698	247065
Scaled up volume		[10^6 m^3]	0.42	0.52	1.05	1.69

Table A.2. Landslide configuration properties

Appendix B   Sensors

Piezometer

A piezometer with a point gauge is used to set precisely the water level in the reservoir. Before each test, the reservoir level shall be adjusted to the desired level. The point gauge measures the distance with ± 0.01 mm precision but the reading of the water level is not that accurate. It is assumed having a precision of approximately 1 mm on the water level in the reservoir.

Figure B.1. Piezometer and point gauge used for setting the reservoir level

Start trigger

When the landslide is released, the start trigger sends a signal to Agilent to start recording data of the other sensors. Figure B.2 illustrates the detector in its positions, before and after the release of the landslide. The signal is sent when movement n° 2 happens.
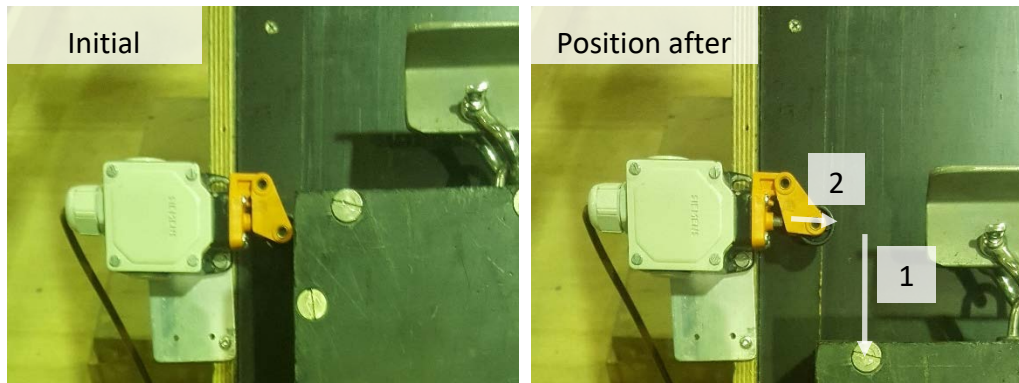
Figure B.2. Operation of start trigger

Landslide position sensor

The landslide position sensor continuously sends a value of voltage, corresponding to the position of the landslide, to the computer. This position of the landslide is measured by a string connected to it. A calibration of this sensor is carried out once a day by pulling the string to known distances and reading the voltage. By collecting several values and applying a linear regression, a value around -1.27 V per travelled meter is derived.
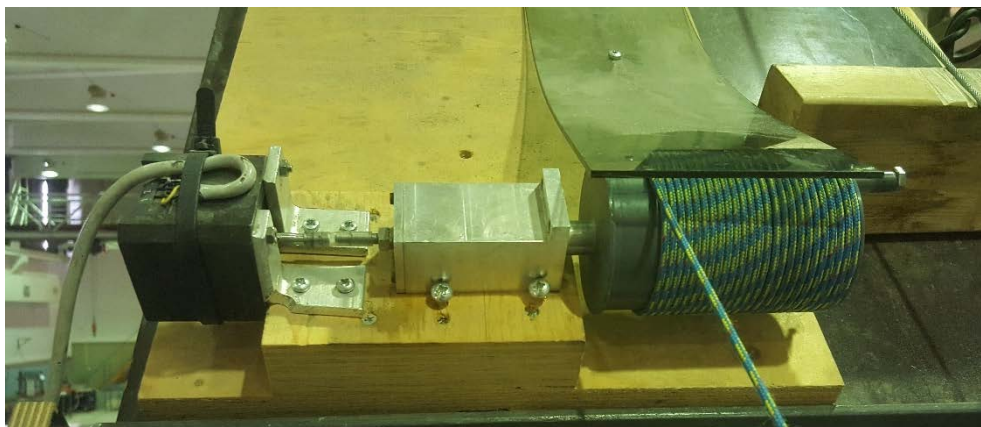
Figure B.3. Landslide position sensor with string going down to the blocks

Wave gauge

The measurement of wave gauge is based on conductivity. Information about the water height in the reservoir is transmitted to the software by mean of a voltage value. The wave gauge system needs to be recalibrated before each test. The procedure is following: once the water is completely still, the output voltage of each gauge is set to zero through the monitor modules. Then the structure with the wave probe attached to it is lifted 5 cm up. The reading of the output now corresponds to a voltage of a water level 5 cm lower than initially. By modifying the gain, the output value is set to 1V. Finally,

the level of the sensors needs to be reset to the initial position by lowering it 5 cm again. In the post processing, the conversion 1V = 5 cm is applied.

Overtopping height sensor

The ultrasonic sensors used for measuring the overtopping height are from Microsonic®. Type *MIC+35* is used in position 13, 14 and 16, *MIC+130* in position 11 and *MIC+340* in position 12 and 15 (see Figure 4.7 for the position numbers). The calibration of these sensors was carried out at the beginning of the tests by measuring the output voltage difference with and without an aluminium piece of 5 cm height. The results were applied in the post processing steps to derive the overtopping height.

Overtopping volume measurement

The overtopped water is collected in buckets behind the dam crest. The overtopping volume is obtained by measuring the distance between the edge of the bucket and the water level (see Figure B.3). The bottom of the buckets is uneven, which makes it difficult to read small volumes. This problem is solved by adding one litre of water into the empty buckets. The volume is measured by the freeboard reading of the buckets before and after each test. The buckets were calibrated by filling them three times up to 10 l by steps of 1 l. A linear function relating the distance measurement to the volume was derived from this step. The precision of the measurement is 1 mm, and the different calibrations show that the accuracy of the derived function is 1.8 mm. This corresponds to a volume of approximately 0.3 l, which corresponds approximately 2000 m^3 for each section when scaled up. Thus, the precision of the total volume (5 buckets) is around $\pm$ 10 000 m^3. A way to improve the accuracy of the measurement would be to use an accurate scale resistant to water, but none was available at the time of the tests.

Figure B.4. Overtopping volume measurement

Appendix C Model improvement and modifications

The first step after taking over the model from the previous students was to understand the model and carry out an analysis of possible improvements and changes that could be brought to the model. The aim was to improve the accuracy of the collected data and to reduce the time necessary per test. This Appendix first presents the modifications and then the various significant improvements made.

Dam shape

The dam used for the previous tests was the so-called Chevron dam. In order to enable easier comparison between results and between other analyses, it was decided to use a straight dam for the thesis. Two straight dams with roughness and slope 1:1.5 and 1:2 were available from prior studies. After the first tests, the glued stones were removed to test a smooth dam (without roughness). Other tested dam profiles are described in Section 4.3.

Chevron dam
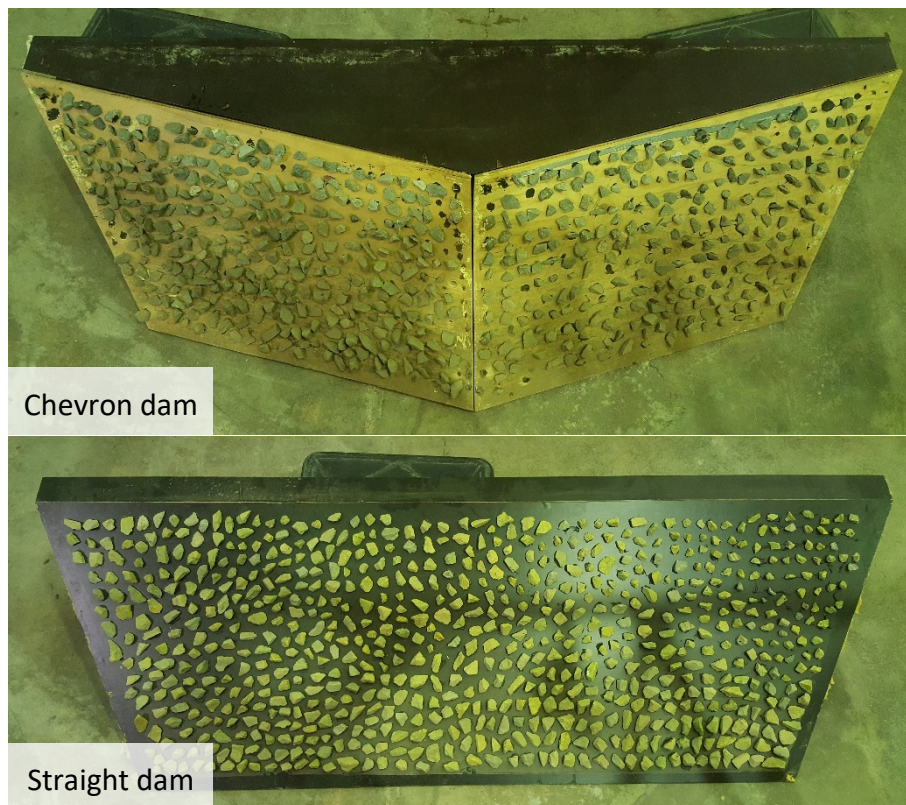
Straight dam

Figure C.1. Chevron and straight dam with roughness

It should be noted that the dam with slope 1:2 is 1 cm higher than the dam with slope 1:1.5. When comparing these two configurations, the freeboard is kept constant which involves a 3% higher water depth for the dam with 1:2 slope. This change is assumed to have negligible effects on the overtopping results.

Crest division

In the previous study, the dam crest was monitored by three overtopping height sensors and separated into four parts by small duct tape. Because the focus of this thesis is put on the overtopping of an embankment dam, the number of sections was increased to five, each with an overtopping height sensor. One more crest sensor was added in the centre section to investigate the overtopping speed. Furthermore, the separations of the five sections were improved by replacing the 1 cm high duct tape with 5 cm high rigid plexiglass. These enhancements are illustrated in Figure C.2.
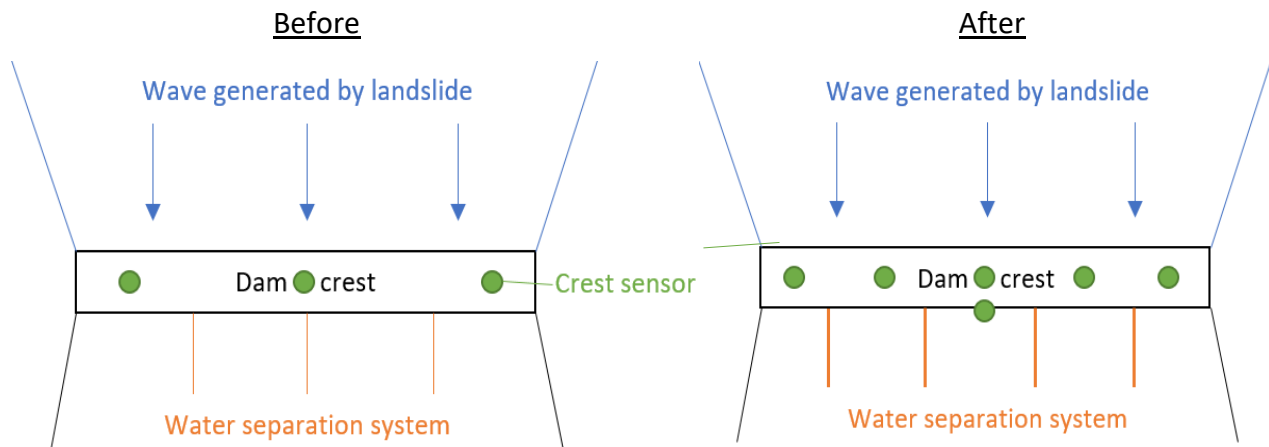
Figure C.2. Improvements of the dam crest

Distance sensor

During the initial period of understanding the model, the different test steps were explored independently. For the landslide, the velocity of the blocks is recorded by a rotational sensor as explained in Appendix B. By filming the landslide and analysing it in slow-motion, two conclusions were made. First, the string connecting the sensor to the landslide is oscillating and therefore degrading the precision of the measured velocity, and secondly, the landslide enters the water in a shifted way.

The first phenomenon happens due to the fall of the connection bar to which the string is attached (Figure C.3). When the chain is released, this bar, which is connecting the chain, the blocks and the

string of the landslide position sensor, falls onto the sliding surface, inducing the oscillation of the string. To avoid this drawback and get a regular unrolling of the string, the string is attached directly to the blocks. A before-after example is shown in Figure C.4.
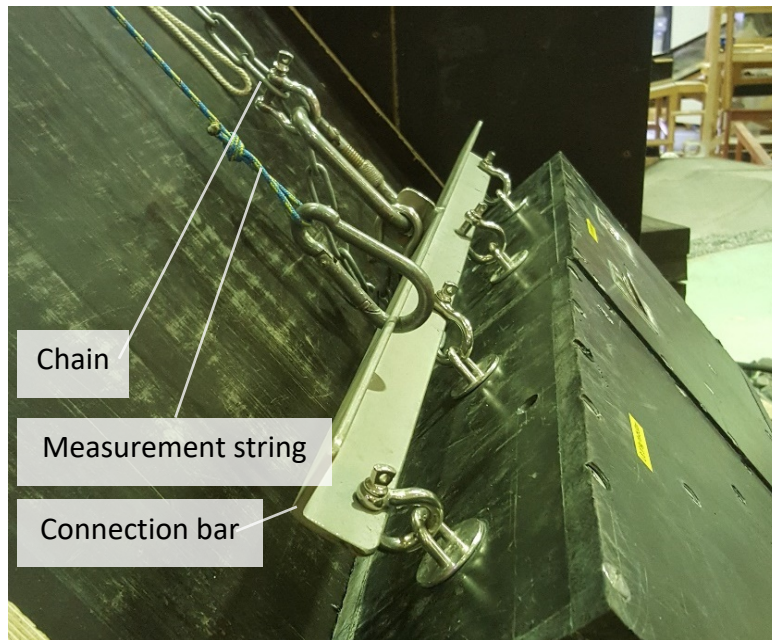
Figure C.3. Detail of the attachment of the blocks to the retaining chain and the measurement string (previous setup)

The second problem, concerning the block entering the water, happens due to a small tension force needed to get accurate position measurements. Tests showed that if the string is attached to the block on the right side (left in Figure C.4), the landslide enters the water in a straight way. This setup gives the string an angle which could imply wrong distance measurements. However, calibration tests of the device have shown that this parameter is negligible. Figure C.4 illustrates the setup with the corresponding details at the water impact moment.
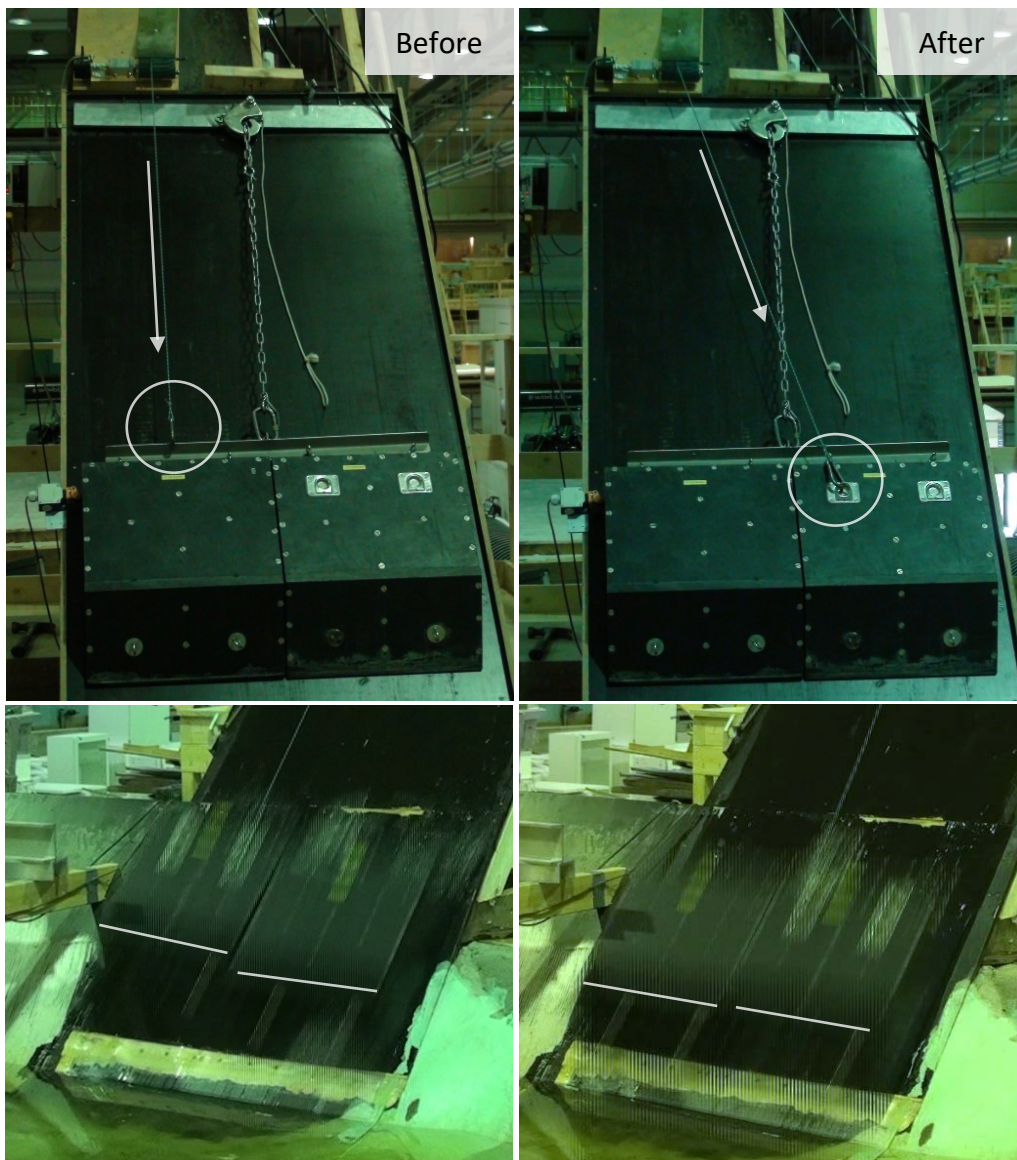
Figure C.4. Illustration of the change of distance/velocity measurement (above the modification of the fixing point of the string and below the details of blocks just before the impact with water)

Position to velocity conversion

The velocity of the landslide at the impact with the water is supposed to be one of the significant parameters influencing the wave generation and the dam overtopping. This maximal landslide impact velocity needs therefore to be measured in each test. By recording the position of the landslide (described in Appendix B) over time at a rate of 200 Hz, the velocity can be derived from it. In the previous study by Ponziani & Gardoni (2017), the position was derived to obtain the velocity (Figure C.5a), and then a 50 Hz filter was applied to reduce the oscillation. Finally, a polynomial regression (orange) was used to find a maximal velocity (Figure C.5b).
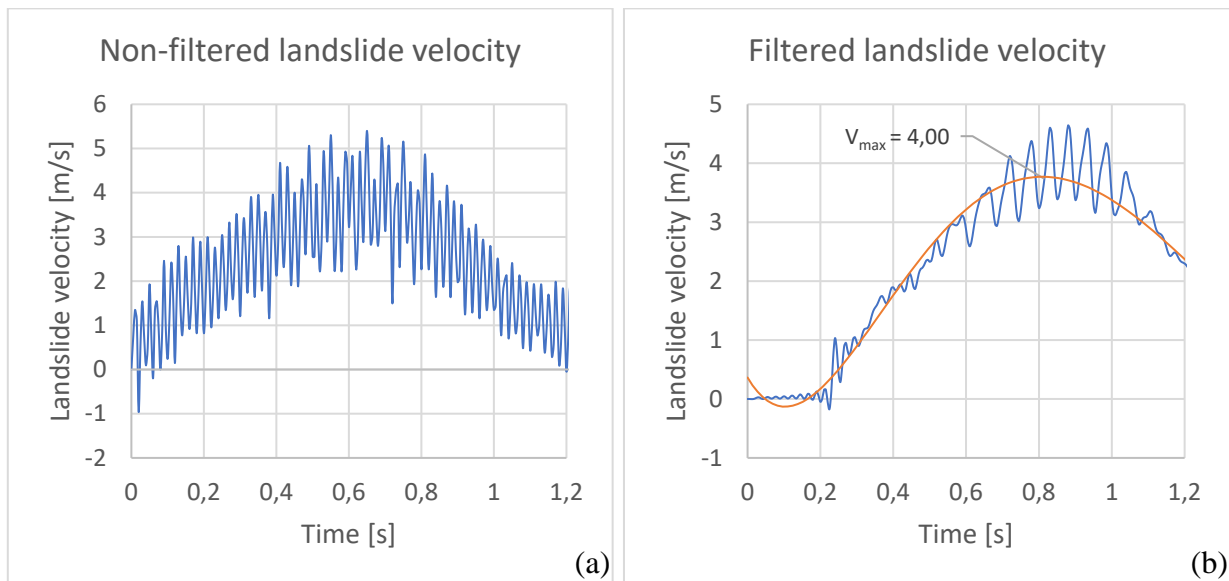
Figure C.5. Previous landslide impact velocity calculation method by Ponziani & Gardoni (2017) (test n° 20)

In this thesis, it was observed that the results of the landslide position are not a linear function but show some small oscillation (Figure C.6a). If a polynomial regression (orange) is applied to the position measurement and the velocity derived afterwards, the obtained velocity curve gives directly and more precisely the maximal speed (Figure C.6b). Both ends of the curves of the landslide impact velocity show strange behaviour. The cause is the polynomial regression. But the fit is good for the maximal velocity, which is the needed value.
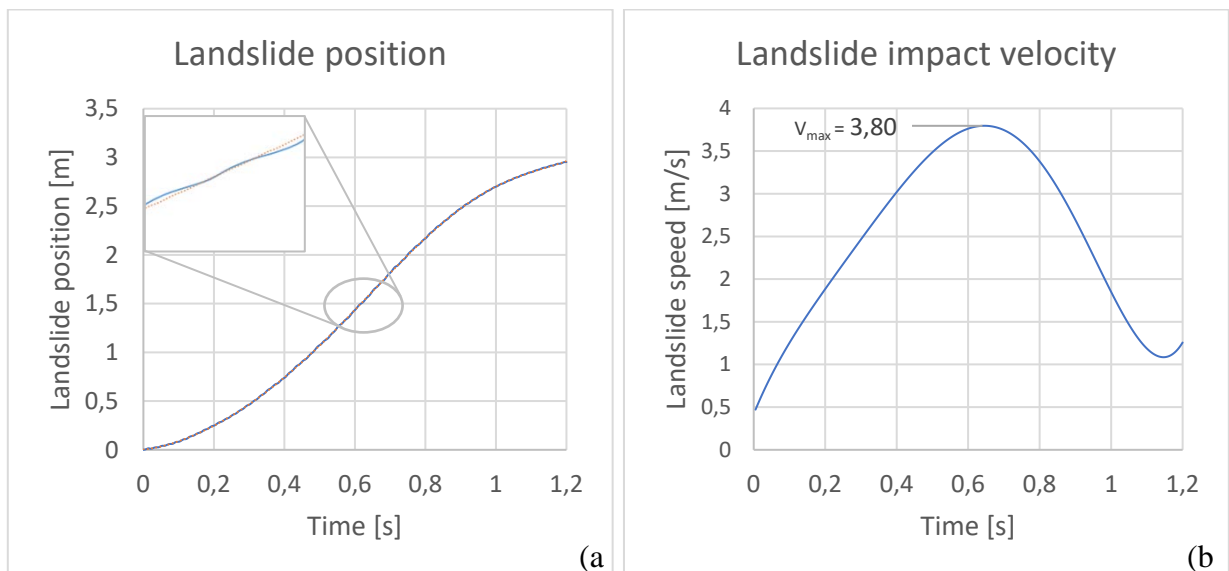
Figure C.6. Landslide position and derived velocity by the method used in this thesis (test n° 20)

This new way of deriving the velocity from the position gives results which should be more accurate, as they are not dependent on the filtering of oscillations which are hard to define precisely.

Appendix D   Standard graphical results from test n°20

The first graph (Figure D.1) illustrates the 6th polynomial regression of the measured position. The landslide run starts at the top of the ramp at position zero and slides for almost 3 m.
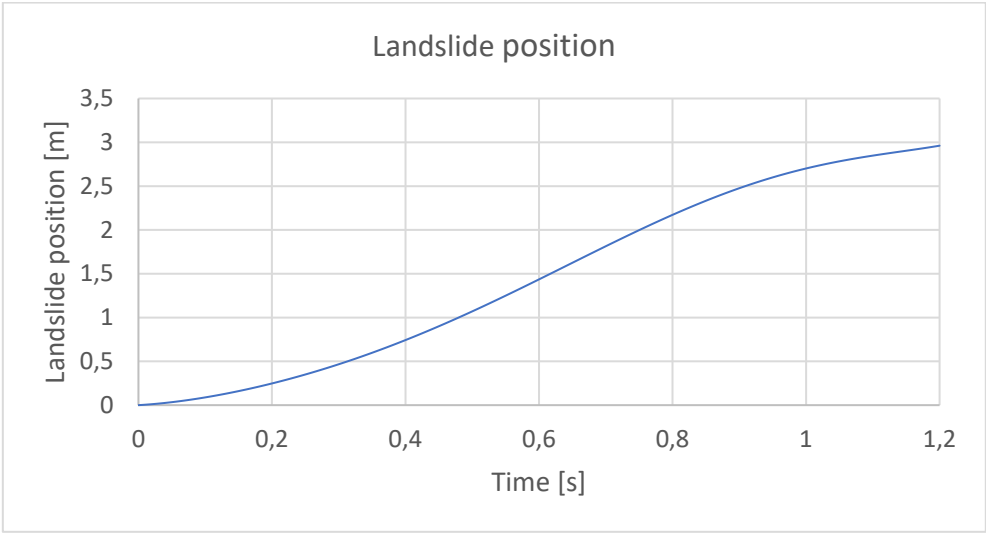
Figure D.1. Landslide position recording (test n° 20)

Figure D.2 shows the velocity curve derived from the previous graph. The value obtained from this curve is the maximal velocity which corresponds to the velocity at the impact with the water. Acceleration lasts for 0.65 s before the impact with the water. Maximal measured velocity is 3.8 m/s, corresponding to 52 m/s, i.e. 188 km/h, upscaled.
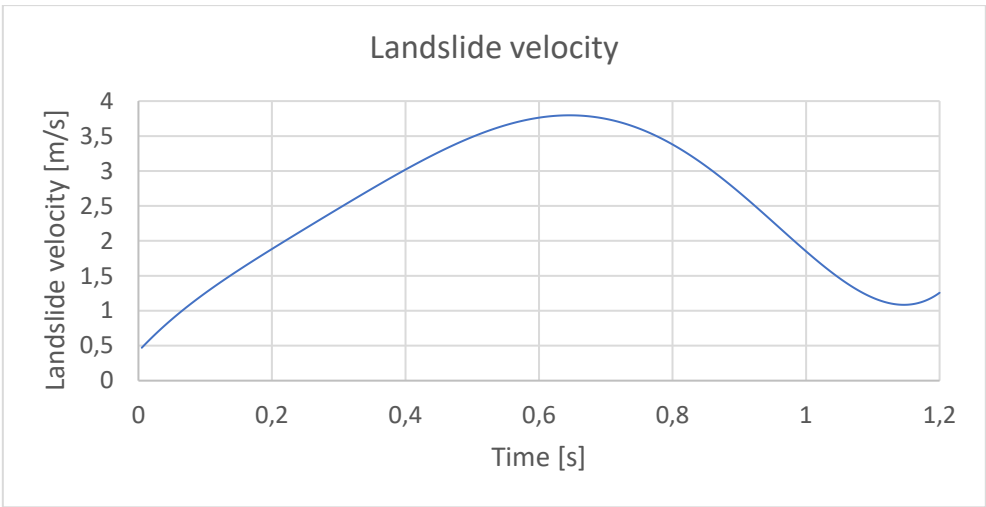
Figure D.2. Landslide impact velocity recording (test n° 20)

The wave propagation in the reservoir is represented through the three figures below. It can be observed that the wave propagation along the left shore is clear for the first wave, whereas propagation along the centre and the right shore is not that evident. This is due to the wave reflection process in the reservoir.
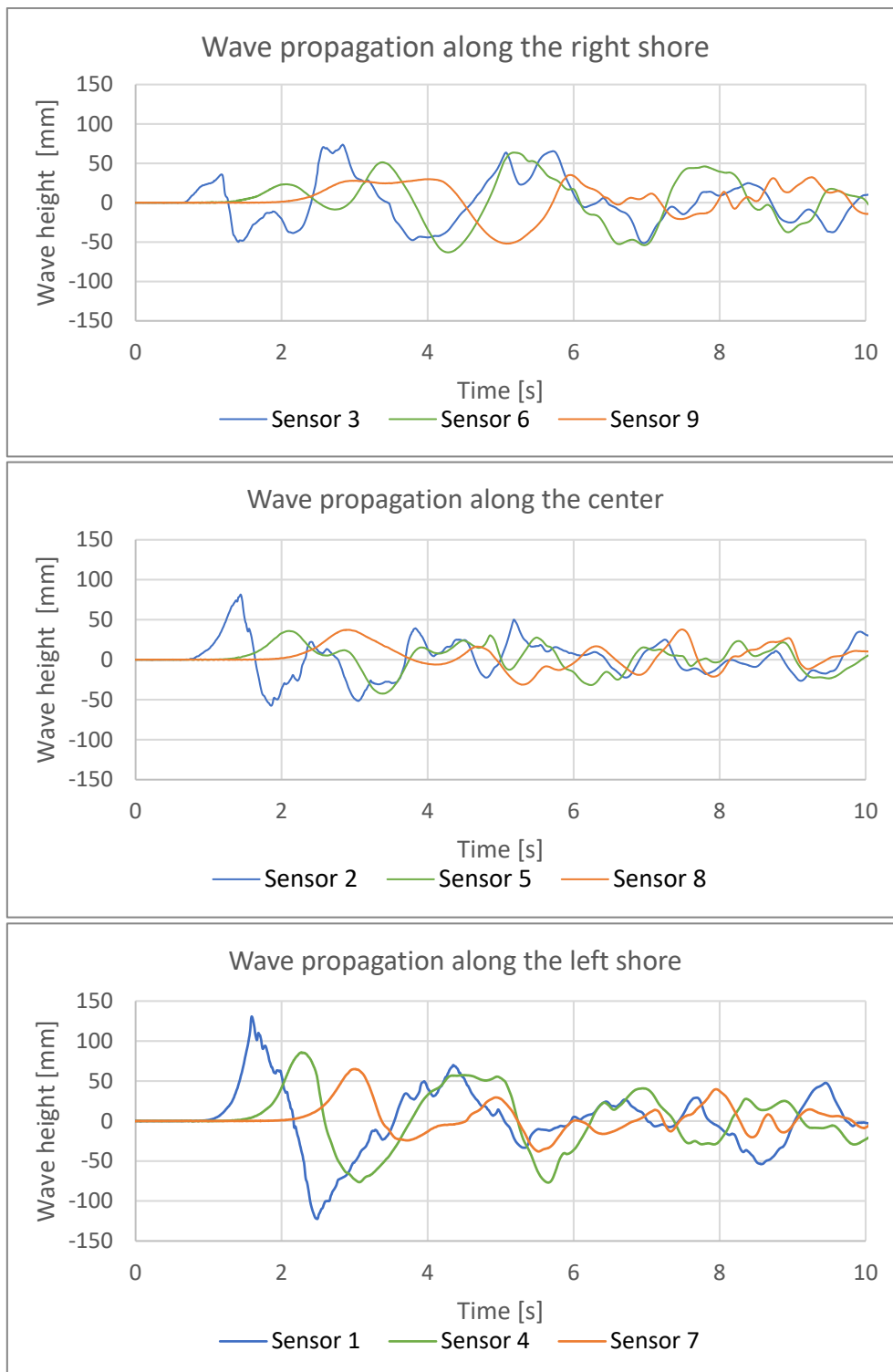
Figure D.3. Wave propagation curves through the reservoir along right shore, the centre and left shore (test n° 20)

The different overtopping heights measured are given in the graphs below. Sensor 15 and 16 have more scatter in the results. The reason could not be found.
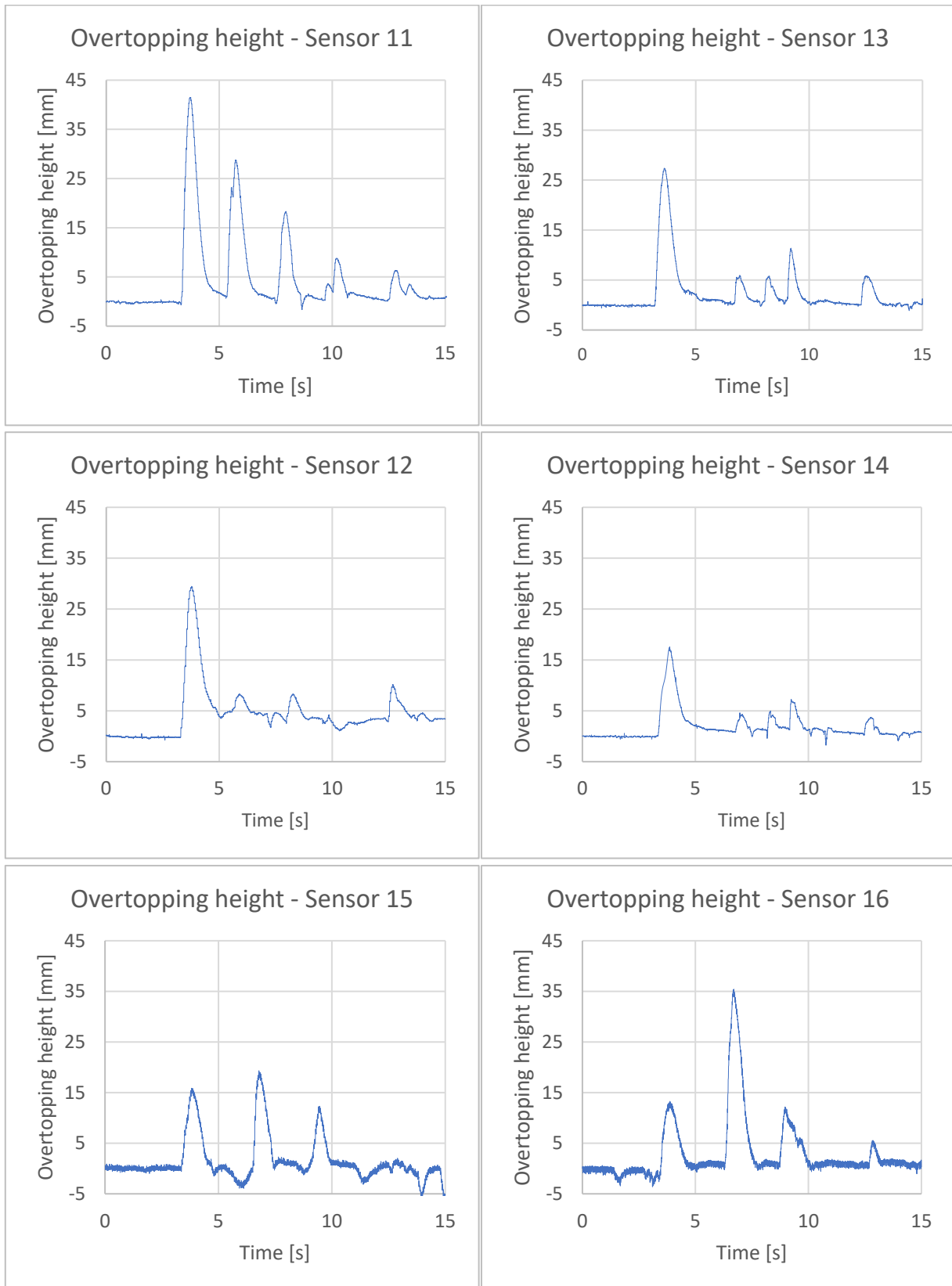
Figure D.4. Dam overtopping height recording (test n° 20)

Appendix E   Theoretical overtopping speed

E.1.   Calculation procedure

The overtopping speed was first measured by sensor 13 and 14 (Figure 4.7) which were subjected to interferences from test 51 on. A new way of calculating the overtopping speed based on the overtopping height (sensor 13) and the overtopping volume (bucket V3) was elaborated.

The initial step treats the overtopping height. Two filters are applied on the data from sensor 13 to take into account only the duration and the water height when the water is flowing over the dam crest. The first filter avoids taking into account the part without any dam overtopping (illustrated by the vertical red line in Figure E.2). The second filter is necessary to prevent considering values when a water film stays on the dam after a wave overtops. In the Figure E.2 below, this is illustrated by the red horizontal line. The wave height, taken into account after the filtering, is given in the following graph ().
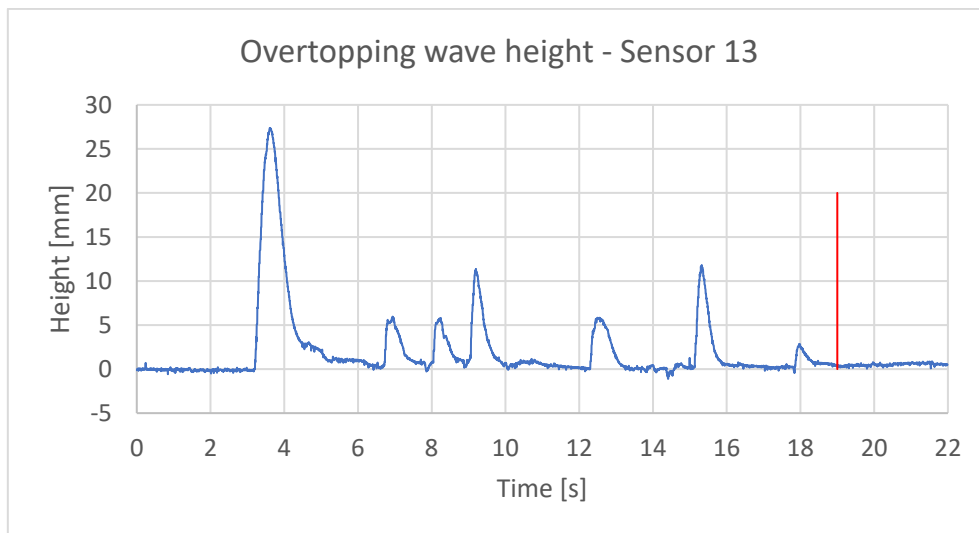
Figure E.1. Vertical filter in overtopping wave height treatment for overtopping speed calculation

Assuming a constant overtopping speed over time and the different wave heights, the filtered overtopping height is compared to the overtopping volume in bucket V13 to get the theoretical overtopping speed. This procedure is conducted by calculating the overtopping volume with 1 m/s speed. This overtopping volume is then compared to the one measured, and the speed is adapted to have both overtopping values fitting (formulas in Appendix A).
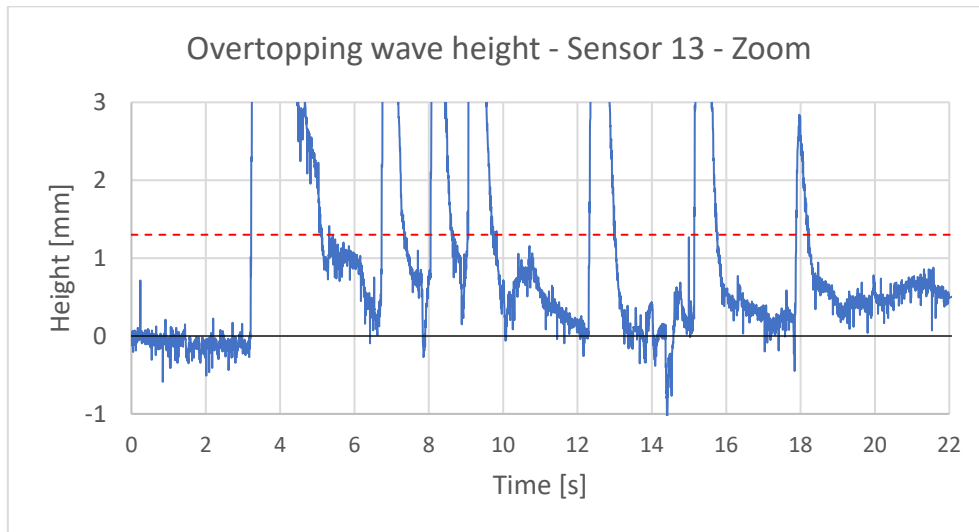
Figure E.2. Horizontal filter in overtopping wave height treatment for overtopping speed calculation
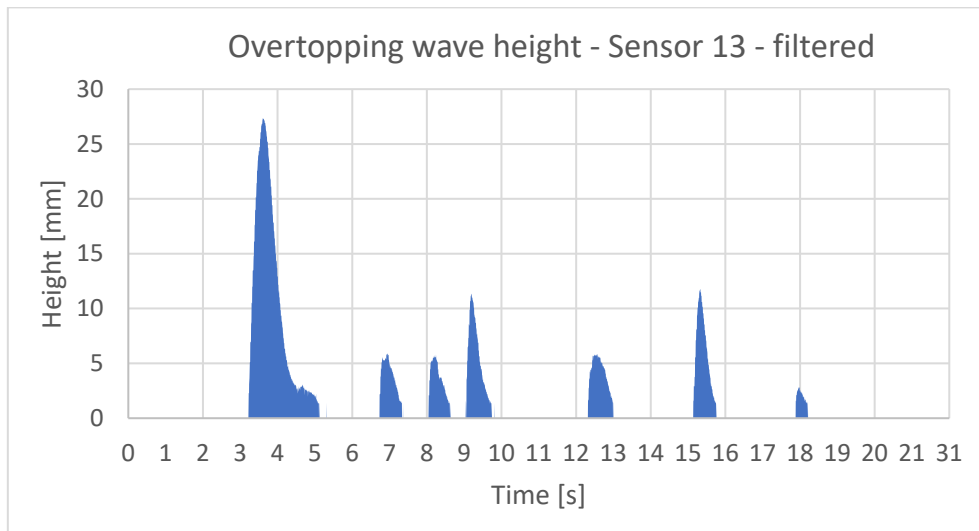
Figure E.3. Filtered overtopping height for overtopping speed calculations

E.2. Independence between theoretical overtopping speed and the freeboard and the block configuration

The influence of the freeboard and the block configuration on the theoretical overtopping speed were tested. Figure E.4 shows that these two parameters do not affect the overtopping speed for sensor 11. The same applies to sensors 13 and 16.
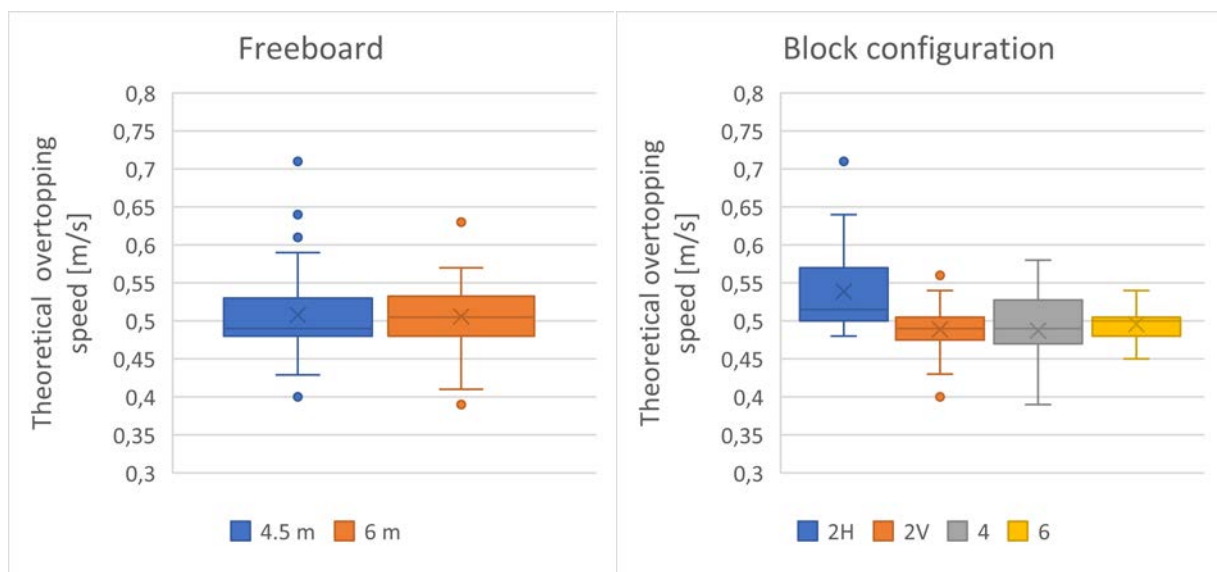
Figure E.4. Overtopping speed sensitivity to freeboard and block configuration (sensor 11)

Appendix F Formulas for theoretical overtopping speed and discharge calculations

To calculate the theoretical overtopping speed from the overtopping height, the following equations are followed, using the subscript c for "crest".

For each time step 1/200 sec, the volume which would overtop if the speed was 1 m/s is calculated:

$$h_c \cdot b_c \cdot t \cdot v_{1m/s} = V_{1m/s} \tag{F.1}$$

With the measured overtopping height h_c, the crest section width b_c, the time step $t = \frac{1}{200} sec$ and an assumed speed $v_{1m/s} = 1\,m/s$ which give the volume for an overtopping at 1 m/s with the measured overtopping height.

The sum of all the time steps i gives the volume which would overtop if the speed was 1 m/s:

$$\sum_{i=1}^{n}(h_{c,i} \cdot b_c \cdot t \cdot v_{1m/s}) = \sum_{i=1}^{n} V_{1m/s,i} \tag{F.2}$$

The volume with a 1 m/s overtopping speed $V_{1m/s}$ is compared to the one measured in the bucket V_{real}, and the average overtopping speed v_c is obtained, assuming as constant during an overtopping:

$$v_c = \frac{\sum_1^n V_{real} \cdot v_{1m/s}}{\sum_1^n V_{1m/s}} = \frac{\sum_1^n (V_{real}) \cdot v_{1m/s}}{\sum_1^n (h_c \cdot b_c \cdot t \cdot v_{1m/s})} \tag{F.3}$$

As the $v_{1m/s}$ is constant in the sum below, it can be taken out and simplified which gives:

$$v_c = \frac{\sum_1^n (V_{real})}{\sum_1^n (h_c \cdot b_c \cdot t)} \tag{F.4}$$

In a further step, the maximal overtopping discharge q_c is calculated:

$$q_{c,max} = v_c \cdot h_{c,max} \cdot b_c \tag{F.5}$$

With the maximal overtopping height $h_{c,max}$ and the crest width $b_c = 1m$ to get the discharge per meter dam crest.

The maximal discharge over the dam crest is, therefore:

$$q_{c,max} = \frac{\sum_1^n(V_{real})}{\sum_1^n(h_c \cdot b_c \cdot t)} \cdot h_{c,max} \cdot b_c \tag{F.6}$$

Appendix G   Comparison with Mortensen results

The model Mortensen (2016) tested is identical to the model used in this thesis, but some modifications were brought to it since then. Model A represents the previous model of Mortensen and Model B accounts for the actual model. The main difference is the position of the landslide. In Model A, the landslide is situated on the left shore behind a small wall allowing only the reflected waves to reach the dam and avoiding the direct impulse wave to propagate towards the dam. Furthermore, the still water depth is higher in this location, and the slide angle α is 40°. In Model B, the landslide is situated on the right shore, closer to the dam. The reservoir has a regular shape between the landslide impact zone and the dam. The slide angle is 50° in this case. This comparison is an investigation on the difference between the results of models A and B.

The comparison between the results of model A and model B is based on the overtopping volume, which is used to calculate the overtopping discharge by dividing it by the 420-m dam crest length as well as, approximately 14 seconds of overtopping. Table G.1 shows that the two models give different overtopping volumes. Model B usually allows less overtopping than Model A, which confirms the conclusion of Ponziani & Gardoni (2017) studying these models.

Model setup (smooth dam, 1:1.5 slope)			Model scale Overtopping vol. [l]		Prototype scale Overtopping vol. [10^3 m^3]		Difference Model B / Model A
Water level	Block config.	Release height [cm]	Model A	Model B	Model A	Model B	
4.5 m	2H	195	67	37	460	254	55%
	4	135	91	61	624	418	67%
	6	75	99	69	679	473	70%
6 m	2H	195	23	22	158	151	96%
	4	135	41	47	281	322	115%
	6	75	47	55	322	377	117%

Table G.1. Comparison between model A and model B

Appendix H   Summary of the results

Test code	Dam slope	Type	WL [mm]	Block setup	Freeboard [m]	Theo release [mm]	Release height [mm]	P [-]	Land. speed [m/s]	Max wave height [mm]	Wave 1		Wave 2		Wave 3		Ch. 1	Ch. 2	Ch. 3	Ch. 4
1	1,5	Straight rough	287	2H	4,5	150	147	1,37	3,59	96	3,4	0,21	6,6	0,34	7,93	0,34	96	50	48	55
2	1,5	Straight rough	287	2H	4,5	150	147	1,37	3,60	99	3,5	0,25	6,6	0,39	7,91	0,39	99	48	44	56
3	1,5	Straight rough	287	2H	4,5	150	146	1,33	3,50	98	3,4	0,31	6,7	0,53	7,93	0,46	98	47	50	58
4	1,5	Straight rough	287	2H	4,5	200	197	1,45	3,79	105	3,4	0,19	8,0	0,41	9,22	0,82	105	53	50	60
5	1,5	Straight rough	287	2H	4,5	200	197	1,41	3,70	108	3,4	0,20	6,7	0,46	8,01	0,38	108	59	51	62
6	1,5	Straight rough	287	2H	4,5	200	197	1,37	3,61	104	3,4	0,21	6,7	0,56	8,01	0,44	104	57	57	52
7	1,5	Straight rough	287	2H	4,5	100	98	1,18	3,08	85	3,3	0,23	6,5	0,53	7,85	0,41	85	44	45	47
8	1,5	Straight rough	287	2H	4,5	100	99	1,25	3,29	89	3,3	0,19	6,5	0,50	7,79	0,39	89	42	45	45
9	1,5	Straight rough	287	2H	4,5	100	96	1,22	3,21	85	3,4	0,20	6,6	0,50	7,87	0,31	85	45	45	49
10	1,5	Straight rough	287	4	4,5	100	97	1,49	3,26	95	3,1	0,37	6,5	0,53	7,8	0,44	95	45	44	65
11	1,5	Straight rough	287	4	4,5	100	97	1,49	3,25	95	3,1	0,31	6,5	0,42	9,0	0,44	94	47	51	66
12	1,5	Straight rough	287	4	4,5	100	97	1,42	3,10	99	3,0	0,26	6,5	0,37	9,0	0,35	99	46	48	65
13	1,5	Straight rough	287	4	4,5	50	47	1,32	2,88	89	3,1	0,32	6,4	0,62	7,9	0,46	89	56	55	52
14	1,5	Straight rough	287	4	4,5	50	47	1,17	2,57	91	3,0	0,25	6,4	0,66	7,9	0,50	91	54	49	57
15b	1,5	Straight rough	288	4	4,5	50	48	1,26	2,77	95	3,0	0,10	6,4	0,14	7,7	0,14	95	62	48	62
16	1,5	Straight rough	287	4	4,5	150	149	1,61	3,51	113	3,1	0,32	6,6	0,39	7,9	0,59	113	54	47	71
17	1,5	Straight rough	287	4	4,5	150	148	1,62	3,55	103	3,2	0,37	6,6	0,46	8,9	0,96	103	63	47	70
18	1,5	Straight rough	287	4	4,5	150	149	1,57	3,44	100	3,1	0,31	6,6	0,44	7,9	0,88	100	52	54	74
19	1,5	Straight rough	280	4	6	150	150	1,67	3,52	127	3,2	0,31	6,7	0,42	8,0	0,38	127	60	57	77
20	1,5	Straight rough	280	4	6	150	150	1,80	3,80	122	3,2	0,35	6,7	1,06	9,1	0,46	122	57	51	77
21	1,5	Straight rough	280	4	6	150	151	1,76	3,70	111	3,2	0,41	6,7	0,42	8,0	0,50	111	56	58	76
22c	1,5	Straight rough	280	4	6	100	97	1,45	3,07	102	3,2	0,44	6,6	0,46	7,9	0,66	102	54	46	73
23	1,5	Straight rough	280	4	6	100	98	1,50	3,17	99	3,1	0,29	6,6	0,44	9,1	0,50	99	50	46	72
24	1,5	Straight rough	280	4	6	100	98	1,57	3,30	93	3,2	0,35	6,6	0,38	8,0	0,62	93	55	49	72
25	1,5	Straight rough	280	4	6	50	48	1,36	2,86	93	3,1	0,29	6,4	0,34	7,8	0,29	93	53	41	64
26	1,5	Straight rough	280	4	6	50	50	1,31	2,76	95	3,1	0,37	6,4	0,35	7,7	0,44	95	58	42	63
27	1,5	Straight rough	280	4	6	50	49	1,33	2,80	99	3,1	0,32	6,4	0,41	7,8	0,42	99	56	42	65
28c	1,5	Straight rough	280	2H	6	200	198	1,47	3,72	109	3,5	0,23	6,8	0,48	8,0	0,46	109	60	49	71
29	1,5	Straight rough	280	2H	6	200	198	1,49	3,76	118	3,5	0,21	6,8	0,59	8,0	0,44	118	58	53	72
30	1,5	Straight rough	280	2H	6	200	197	1,50	3,80	121	3,5	0,35	6,8	0,56	8,0	0,66	121	67	50	72
31	1,5	Straight rough	280	2H	6	150	149	1,39	3,52	105	3,5	0,22	6,7	0,59	7,9	0,44	105	55	61	64
32	1,5	Straight rough	280	2H	6	150	149	1,39	3,51	100	3,5	0,27	6,7	0,59	7,9	0,42	100	56	50	63
33	1,5	Straight rough	280	2H	6	150	151	1,36	3,43	108	3,5	0,25	6,7	0,71	7,9	0,35	108	59	54	64
34	1,5	Straight rough	280	2H	6	100	101	1,24	3,13	96	3,5	0,19	6,6	0,42	7,9	0,34	96	47	49	57
35	1,5	Straight rough	280	2H	6	100	101	1,29	3,27	99	3,5	0,25	6,6	0,44	7,8	0,42	99	48	47	57
36	1,5	Straight rough	280	2H	6	100	98	1,26	3,18	99	3,4	0,17	6,6	0,41	7,9	0,42	99	50	52	56
37	1,5	Straight smooth	288	2H	4,5	200	198	1,40	3,68	118	3,3	0,25	6,7	1,77	7,9	0,59	118	69	46	73
38	1,5	Straight smooth	288	2H	4,5	200	198	1,39	3,67	117	3,3	0,29	6,7	0,44	7,8	1,18	117	67	47	71
39	1,5	Straight smooth	288	2H	4,5	200	198	1,42	3,75	119	3,4	0,31	6,7	0,50	7,9	0,59	119	67	56	70
40	1,5	Straight smooth	288	2H	4,5	150	150	1,33	3,51	103	3,3	0,25	6,6	0,53	7,8	0,44	103	57	55	64
41	1,5	Straight smooth	288	2H	4,5	150	147	1,32	3,49	102	3,4	0,31	6,6	0,50	7,8	0,42	102	52	49	61
42	1,5	Straight smooth	288	2H	4,5	150	148	1,28	3,38	110	3,2	0,26	6,4	0,38	7,7	0,39	110	60	53	62
43	1,5	Straight smooth	288	2H	4,5	100	98	1,16	3,05	98	3,3	0,35	6,5	0,50	7,8	0,76	98	48	50	55
44	1,5	Straight smooth	288	2H	4,5	100	97	1,15	3,02	101	3,3	0,27	6,5	0,50	7,7	0,62	101	46	46	56
45	1,5	Straight smooth	288	2H	4,5	100	99	1,17	3,08	102	3,3	0,27	6,5	0,53	7,7	0,59	102	48	48	56

Test code	Dam slope	Type	WL [mm]	Block setup	Freeboard [m]	Theo release [mm]	Release height [mm]	P [-]	Land. speed [m/s]	Max wave height [mm]	Wave 1		Wave 2		Wave 3		Ch. 1	Ch. 2	Ch. 3	Ch. 4
46	1,5	Straight smooth	288	2V	4,5	200	188	1,79	3,92	89	3,4	0,34	6,8	0,62	7,8	0,62	89	55	43	70
47	1,5	Straight smooth	288	2V	4,5	200	188	1,69	3,70	96	3,4	0,33	6,7	0,44	7,8	0,96	96	64	48	75
48	1,5	Straight smooth	288	2V	4,5	200	188	1,73	3,81	94	3,1	0,32	6,4	0,53	7,8	0,46	94	59	54	71
49	1,5	Straight smooth	288	2V	4,5	150	151	1,64	3,60	81	3,5	0,46	6,7	0,44	7,9	0,35	81	51	42	62
50	1,5	Straight smooth	288	2V	4,5	150	153	1,68	3,69	81	3,5	0,29	6,7	0,62	7,8	0,46	81	45	35	59
51b	1,5	Straight smooth	288	2V	4,5	150	149	1,64	3,60	88							88	48	42	61
52	1,5	Straight smooth	288	2V	4,5	50	49	1,18	2,58	74	3,4	0,44	6,49	0,53	7,64	0,28	74	36	39	51
53	1,5	Straight smooth	288	2V	4,5	50	49	1,24	2,71	77	3,3	0,44	6,44	0,56			77	36	34	52
55	1,5	Straight smooth	288	4	4,5	150	148	1,72	3,79	107							107	54	57	74
56	1,5	Straight smooth	288	4	4,5	150	148	1,59	3,51	106							106	54	49	75
57	1,5	Straight smooth	288	4	4,5	150	148	1,66	3,66	98							98	51	51	74
58	1,5	Straight smooth	288	4	4,5	100	100	1,48	3,25	93							93	58	50	64
59	1,5	Straight smooth	288	4	4,5	100	100	1,42	3,12	126							126	58	58	75
60	1,5	Straight smooth	288	4	4,5	100	100	1,44	3,18	99							99	58	43	73
61	1,5	Straight smooth	288	4	4,5	50	49	1,24	2,72	94							94	57	47	61
62	1,5	Straight smooth	288	4	4,5	50	49	1,25	2,74	96							96	54	46	61
63	1,5	Straight smooth	288	4	4,5	50	49	1,18	2,60	92							91	58	42	57
65	1,5	Straight smooth	288	6	4,5	50	50	1,37	2,73	100							100	38	49	61
66	1,5	Straight smooth	288	6	4,5	50	50	1,37	2,71	102							102	48	45	63
67	1,5	Straight smooth	288	6	4,5	100	100	1,70	3,37	91							91	67	50	57
67b	1,5	Straight smooth	288	6	4,5	100	99	1,67	3,31	94							94	46	53	59
68	1,5	Straight smooth	288	6	4,5	100	102	1,73	3,43	91							91	52	51	67
71	1,5	Straight smooth	280	6	6	100	102	1,79	3,40	125							125	61	60	61
72	1,5	Straight smooth	280	6	6	100	102	1,78	3,39	124							124	48	60	66
73	1,5	Straight smooth	280	6	6	50	49	1,46	2,77	97							97	45	62	55
74	1,5	Straight smooth	280	6	6	50	51	1,45	2,76	113							113	54	61	55
75	1,5	Straight smooth	280	6	6	50	49	1,44	2,74	104							104	48	60	54
76	1,5	Straight smooth	280	4	6	150	149	1,76	3,71	101							101	51	53	71
77b	1,5	Straight smooth	280	4	6	150	150	1,73	3,65	98							98	52	54	74
78	1,5	Straight smooth	280	4	6	150	148	1,84	3,89	123							123	53	65	71
79	1,5	Straight smooth	280	4	6	100	99	1,61	3,39	101							101	60	60	66
80	1,5	Straight smooth	280	4	6	100	100	1,56	3,29	98							98	58	48	65
81	1,5	Straight smooth	280	4	6	100	100	1,56	3,28	98							98	53	50	66
82	1,5	Straight smooth	280	4	6	50	51	1,31	2,77	81							81	46	54	49
83	1,5	Straight smooth	280	4	6	50	51	1,28	2,69	81							81	49	48	50
84	1,5	Straight smooth	280	4	6	50	52	1,32	2,77	85							84	52	53	53
85	1,5	Straight smooth	280	2H	6	200	200	1,47	3,71	110							110	55	51	56
85b	1,5	Straight smooth	280	2H	6	200	201	1,52	3,84	99							99	52	54	56
87	1,5	Straight smooth	280	2H	6	200	201	1,49	3,78	103							103	53	49	58
88	1,5	Straight smooth	280	2H	6	150	152	1,43	3,61	102							102	52	42	54
88b	1,5	Straight smooth	280	2H	6	150	149	1,39	3,52	96							96	47	51	51
89	1,5	Straight smooth	280	2H	6	150	152	1,42	3,58	99							99	49	42	51
91b	1,5	Straight smooth	280	2H	6	100	99	1,23	3,12	81							81	45	52	47
92	1,5	Straight smooth	280	2H	6	100	101	1,25	3,15	85							85	45	48	46
93	1,5	Straight smooth	280	2H	6	100	100	1,24	3,13	83							83	47	50	49

Test code	Dam slope	Type	WL [mm]	Block setup	Freeboard [m]	Theo release [mm]	Release height [mm]	P [-]	Land. speed [m/s]	Max wave height [mm]	Wave speed [s ; m/s] Wave 1	Wave 2	Wave 3	Max wave height [mm] Ch. 1	Ch. 2	Ch. 3	Ch. 4
94b	1,5	Straight smooth	280	2V	6	200	197	1,92	4,03	94				94	49	50	65
95	1,5	Straight smooth	280	2V	6	200	193	1,83	3,85	94				94	51	44	67
96	1,5	Straight smooth	280	2V	6	200	194	1,88	3,95	100				100	51	52	70
97	1,5	Straight smooth	280	2V	6	150	150	1,69	3,56	91				91	47	39	62
98	1,5	Straight smooth	280	2V	6	150	151	1,73	3,64	88				88	45	48	62
99	1,5	Straight smooth	280	2V	6	150	150	1,67	3,51	87				87	43	50	62
100	1,5	Straight smooth	280	2V	6	50	50	1,25	2,63	67				67	36	43	42
100b	1,5	Straight smooth	280	2V	6	50	50	1,22	2,57	66				66	37	42	42
101	1,5	Straight smooth	280	2V	6	50	50	1,22	2,57	67				67	40	39	43
103	1,5	Straight vert+horiz	290	4	4,5	150	150	1,57	3,50	156				156	83	71	77
104	1,5	Straight vert+horiz	290	4	4,5	150	150	1,69	3,77	149				149	82	76	79
105	1,5	Straight vert+horiz	290	4	4,5	150	150	1,68	3,73	137				137	81	63	76
106	1,5	Straight vert+horiz	290	4	4,5	100	101	1,52	3,37	122				122	77	60	69
107	1,5	Straight vert+horiz	290	4	4,5	100	102	1,46	3,24	124				124	83	78	73
108	1,5	Straight vert+horiz	290	4	4,5	100	101	1,44	3,21	121				121	81	64	71
109b	1,5	Straight vert+horiz	282	4	6	150	151	1,74	3,71	127				127	87	66	75
110	1,5	Straight vert+horiz	282	4	6	150	151	1,74	3,72	127				127	82	60	76
111	1,5	Straight vert+horiz	282	4	6	150	151	1,68	3,58	135				135	88	58	77
112	1,5	Straight vert+horiz	282	4	6	100	103	1,53	3,26	122				122	77	57	68
113	1,5	Straight vert+horiz	282	4	6	100	102	1,47	3,12	123				123	82	69	64
114	1,5	Straight vert+horiz	282	4	6	100	103	1,57	3,36	118				118	79	74	69
116	2	Straight smooth	300	4	4,5	150	150	1,49	3,48	133				133	66	94	90
117	2	Straight smooth	300	4	4,5	150	150	1,50	3,52	125				124	67	88	90
118	2	Straight smooth	300	4	4,5	150	150	1,50	3,51	125				125	74	84	39
120	2	Straight smooth	300	4	4,5	100	101	1,38	3,22	118				118	67	64	72
121	2	Straight smooth	300	4	4,5	100	101	1,40	3,27	121				121	67	63	77
122	2	Straight smooth	300	4	4,5	100	101	1,40	3,27	117				117	67	65	78
123	2	Straight smooth	292	4	6	100	100	1,46	3,29	118				118	64	64	
124	2	Straight smooth	292	4	6	100	99	1,48	3,33	115				115	64	65	
126	2	Straight smooth	292	4	6	100	100	1,46	3,28	119				119	67	66	
127	2	Straight smooth	292	4	6	150	151	1,62	3,63	130				130	65	94	88
128	2	Straight smooth	292	4	6	150	151	1,65	3,70	129				129	66	77	87
129	2	Straight smooth	292	4	6	150	151	1,71	3,84	136				136	68	97	85
131	1,5	Straight vertical	282	4	6	100	100	1,61	3,42	123				123	82	55	77
132	1,5	Straight vertical	282	4	6	100	100	1,61	3,42	118				118	73	61	72
133	1,5	Straight vertical	282	4	6	100	100	1,59	3,40	126				126	76	64	76
135	1,5	Straight vertical	282	4	6	150	150	1,86	3,97	138				138	86	65	85
137	1,5	Straight vertical	282	4	6	150	150	1,84	3,93	124				124	77	83	85
138	1,5	Straight vertical	282	4	6	150	150	1,80	3,84	129				129	79	74	84
140	1,5	Straight vertical	290	4	4,5	150	150	1,72	3,82	127				127	76	68	80
141	1,5	Straight vertical	290	4	4,5	150	150	1,75	3,89	128				128	77	74	80
142	1,5	Straight vertical	290	4	4,5	150	150	1,83	4,07	153				153	87	90	81
144	1,5	Straight vertical	290	4	4,5	100	100	1,57	3,49	125				125	74	63	74
145	1,5	Straight vertical	290	4	4,5	100	100	1,58	3,51	125				125	75	60	75
146	1,5	Straight vertical	290	4	4,5	100	100	1,55	3,45	117				117	72	64	71

Results

Test code	Max wave height [mm] Ch.5	Ch.6	Ch.7	Ch.8	Ch.9	Overtopping height max [mm] Ch.11	Ch.12	Ch.13	Ch.15	Ch.16	Overtopping volume model [l] Ch.11	Ch.12	Ch.13	Ch.14	Ch.15	Total	Calc. wave speed [m/s] Ch.11	Ch.13	Ch.16	Calc. Max discharge [m³/s/m] Ch.11	Ch.13	Ch.16	N° of highest crest wave highest	2nd highest	1st wave height [mm] Ch.2	Ch.5	Ch.13	Calc. average discharge [m³/s] Ch.11	Ch.13	Ch.16
1	40	45	33	26	46	11	5	14	17	24	4,73	2,36	2,73	2,36	7,45	19,64	0,64	0,39	0,74	6,70	5,52	17,63	2	3						
2	41	40	34	23	45	10	6	15	15	24	5,27	2,73	2,91	2,36	7,45	20,73	0,59	0,41	0,70	5,89	6,08	16,81	2	3						
3	42	43	36	25	45	10	7	14	17	24	4,91	3,09	2,55	2,55	7,64	20,36	0,71	0,39	0,75	6,91	5,52	17,87	2	3						
4	46	46	37	25	49	13	7	18	19	28	6,73	3,27	3,64	3,09	9,27	26,00	0,58	0,35	0,83	7,68	6,04	23,25	2	3						
5	49	45	36	26	48	15	8	17	18	28	6,73	3,27	3,64	3,45	9,09	26,18	0,59	0,36	0,72	8,82	5,96	19,85	2	3						
6	46	47	30	24	56	16	9	15	17	27	7,09	3,27	3,45	3,45	9,09	26,36	0,61	0,43	0,78	9,49	6,45	21,16	2	3						
7	40	40	25	20	46	10	8	13	12	18	4,00	2,18	2,18	1,64	5,09	15,09	0,57	0,37	0,65	5,46	4,93	11,71	2	3						
8	41	39	27	20	46	8	7	14	9	20	4,18	2,36	2,36	1,64	4,18	14,73	0,64	0,37	0,49	5,20	5,39	9,62	2	3						
9	40	38	27	21	44	11	9	14	13	16	3,73	2,18	2,18	1,64	4,73	14,45	0,54	0,38	0,60	5,65	5,40	9,33	2	3						
10	39	54	23	29	45	34	26	24	23	28	14,55	8,73	6,91	8,36	12,27	50,82	0,49	0,39	0,75	16,87	9,56	20,86	1	5						
11	40	48	21	30	47	36	26	24	23	26	15,27	8,73	7,00	8,18	12,36	51,55	0,49	0,32	0,68	17,56	7,66	18,04	1	2						
12	39	54	25	30	48	36	27	25	27	32	16,00	8,36	7,09	8,91	13,45	53,82	0,49	0,37	0,65	17,35	9,31	20,84	1	2						
13	38	48	21	29	37	29	21	20	22	25	12,91	6,73	5,45	7,09	9,82	42,00	0,48	0,38	0,74	13,73	7,41	18,54	1	2						
14	41	44	24	34	38	30	22	20	19	24	13,09	7,09	5,45	7,27	9,64	42,55	0,48	0,40	0,80	14,17	7,91	18,90	1	2						
15b	42	50	27	32	39	31	24	21	20	24	13,45	7,64	6,00	6,91	9,27	43,27	0,49	0,39	0,76	15,19	8,22	17,00	1	2						
16	38	54	29	26	50	37	27	25	22	33	17,45	9,27	6,73	8,73	15,27	57,45	0,51	0,35	0,79	18,84	8,71	25,80	1	4						
17	38	61	29	26	50	37	27	25	24	35	18,36	9,45	6,91	9,09	16,36	60,18	0,58	0,38	0,82	21,52	9,69	28,69	1	0						
18	39	59	31	27	49	38	28	26	23	35	19,45	10,18	8,73	9,82	16,55	64,73	0,53	0,43	0,83	20,03	11,28	29,25	1	5						
19	39	54	27	25	53	38	27	25	23	31	15,64	7,27	6,00	6,64	12,00	47,55	0,48	0,33	0,78	18,18	8,34	24,05	1	5						
20	42	63	38	31	52	42	30	27	19	35	17,09	8,36	6,18	7,64	13,27	52,55	0,54	0,39	0,79	22,29	10,80	27,83	1	4						
21	40	63	31	28	58	40	28	26	23	38	17,09	7,27	5,64	7,64	14,36	52,00	0,52	0,37	0,81	20,65	9,88	30,93	1	4						
22c	39	50	21	29	46	38	26	26	18	24	14,36	7,45	5,09	6,00	9,82	42,73	0,53	0,39	0,79	20,47	10,05	18,77	1	2-4						
23	37	51	25	31	47	40	28	26	18	23	13,82	7,09	5,64	6,00	9,55	42,09	0,54	0,46	0,76	21,53	12,06	17,38	1	5						
24	39	49	23	30	47	36	25	24	16	23	13,73	6,91	5,09	5,64	8,73	40,09	0,55	0,39	0,72	19,90	9,30	16,56	1	5						
25	43	48	26	33	41	29	20	18	16	18	9,09	5,45	3,64	4,18	5,64	28,00	0,47	0,39	0,78	13,44	7,09	13,79	1	5						
26	43	47	26	32	40	29	20	18	16	18	10,18	5,64	3,82	4,55	6,00	30,18	0,49	0,39	0,74	14,19	7,13	13,35	1	5						
27	43	52	26	32	41	30	21	20	19	21	11,09	5,82	4,18	4,73	6,73	32,55	0,51	0,38	0,72	15,28	7,57	14,80	1	5						
28c	39	54	30	32	59	21	10	18	15	27	8,18	3,82	3,64	2,55	7,27	25,45	0,52	0,39	0,84	11,07	7,20	22,64	2	3						
29	40	54	32	31	58	20	10	19	14	28	8,36	3,64	4,00	2,36	7,64	26,00	0,57	0,39	0,95	11,60	7,39	25,43	2	3						
30	46	55	31	32	59	22	11	18	13	28	7,82	4,18	3,82	2,36	7,45	25,64	0,54	0,41	0,88	11,93	7,36	24,68	2	3						
31	38	50	30	25	46	17	8	15	13	23	6,18	2,18	2,18	1,64	6,00	18,18	0,56	0,39	0,80	9,34	5,69	18,55	1	2						
32	40	52	31	25	55	17	9	15	14	22	6,00	2,36	2,36	1,82	6,27	18,64	0,51	0,39	0,81	8,85	5,79	18,14	2	3						
33	41	51	32	28	55	17	9	14	13	23	6,18	2,18	2,18	1,82	6,55	18,91	0,50	0,45	0,86	8,28	6,21	20,01	2	3						
34	42	42	33	30	47	13	8	10	11	15	4,36	1,82	1,64	0,91	4,18	12,91	0,51	0,38	0,83	6,42	3,91	12,73	2	3						
35	41	41	32	30	45	11	9	12	9	15	3,82	1,82	1,64	1,18	4,00	12,45	0,53	0,37	0,74	5,91	4,34	11,34	2	3						
36	39	42	31	28	45	12	9	10	10	16	4,18	2,00	1,64	0,91	4,18	12,91	0,50	0,38	0,77	6,03	3,82	12,49	2	3						
37	44	47	41	33	59	28	14	26	19	25	10,55	5,45	6,18	4,18	11,09	37,45	0,48	0,36	1,08	13,50	9,54	27,26	2	3	64	24	10	0,76	0,47	0,86
38	47	53	31	32	64	30	13	27	19	25	10,73	5,64	6,18	4,18	10,55	37,27	0,49	0,39	1,09	14,85	10,39	27,20	2	3	67	23	10	0,78	0,47	0,82
39	46	51	34	29	64	28	12	24	18	23	11,09	5,45	5,64	4,00	11,09	37,27	0,51	0,38	1,13	13,98	9,18	25,88	2	3	62	24	9	0,80	0,43	0,86
40	39	45	34	27	56	22	11	23	18	21	8,18	4,00	4,36	3,82	9,27	29,64	0,49	0,38	1,07	10,48	8,76	21,82	2	3	64	22	7	0,59	0,33	0,72
41	47	40	34	26	54	20	11	22	16	20	8,18	3,82	3,82	3,27	8,36	27,45	0,52	0,38	0,91	10,22	8,30	21,37	2	3	60	20	6	0,59	0,29	0,65
42	43	49	35	25	55	21	13	22	17	17	8,36	4,00	4,00	3,45	9,27	29,09	0,49	0,38	1,19	10,41	8,29	20,56	2	3	60	21	7	0,61	0,30	0,72
43	45	40	38	33	46	16	15	21	14	19	6,00	4,18	3,82	2,18	6,36	22,55	0,48	0,37	0,83	7,53	8,03	15,31	3	2	54	18	4	0,44	0,29	0,49
44	41	41	37	32	47	17	14	19	14	19	6,55	4,00	3,64	2,36	6,36	22,91	0,50	0,33	0,77	8,58	6,21	14,46	3	2	57	19	5	0,47	0,28	0,49
45	45	42	39	32	47	17	14	21	14	20	6,00	4,00	3,45	2,36	6,18	22,00	0,48	0,31	0,71	8,04	6,50	14,03	2	3	59	19	5	0,44	0,26	0,48

Results

Test code	Max wave height [mm]					Overtopping height max [mm]					Overtopping volume model [l]						Calc. wave speed [m/s]			Calc. Max discharge [m³/s/m]			N° of highest crest wave		1st wave height [mm]			Calc. average discharge [m³/s]		
	Ch. 5	Ch. 6	Ch. 7	Ch. 8	Ch. 9	Ch. 11	Ch. 12	Ch. 13	Ch. 15	Ch. 16	Ch. 11	Ch. 12	Ch. 13	Ch. 14	Ch. 15	Total	Ch. 11	Ch. 13	Ch. 16	Ch. 11	Ch. 13	Ch. 16	highest	2nd highest	Ch. 2	Ch. 5	Ch. 13	Ch. 11	Ch. 13	Ch. 16
46	42	51	39	34	61	32	15	35	16	16	11,27	6,91	6,18	3,27	9,64	37,27	0,47	0,37	1,13	15,35	13,09	18,14	2	4	52	24	13	0,82	0,47	0,75
47	48	57	37	35	62	34	17	37	19	19	12,91	6,73	6,55	4,36	11,09	41,64	0,50	0,39	1,09	16,96	14,14	21,18	2	4	60	26	16	0,94	0,50	0,86
48	46	55	34	33	60	31	15	35	19	17	12,18	6,18	6,18	3,82	10,55	38,91	0,48	0,43	1,21	14,96	15,11	20,03	2	4	58	25	13	0,88	0,47	0,82
49	43	40	32	30	50	27	10	28	12	14	8,55	4,91	3,82	2,00	6,73	26,00	0,47	0,33	0,93	12,60	9,27	13,32	2	4	46	22	9	0,62	0,29	0,52
50	38	40	33	29	50	22	10	28	11	16	8,18	4,91	3,82	1,82	7,09	25,82	0,50	0,33	1,05	11,24	9,29	16,30	2	4	41	20	8	0,59	0,29	0,55
51b	36	51	30	28	59	32	12	28	14	15	9,45	5,09	4,18	2,55	8,55	30,00	0,49	0,37	1,30	15,64	10,25	19,40	2	3	44	20	9	0,69	0,31	0,66
52	28	40	24	27	40	19	8	23	17	15	5,82	2,36	2,18	2,73	4,55	17,64	0,43	0,37	0,78	8,24	8,49	11,65	2	1	41	18	5	0,42	0,17	0,35
53	27	39	25	29	38	19	8	23	17	14	5,82	2,36	2,55	2,91	4,18	17,82	0,40	0,39	0,70	7,72	8,95	9,58	2	1	44	19	6	0,42	0,19	0,32
55	34	58	28	29	55	41	30	27	25	27	20,36	10,73	8,18	9,09	14,73	63,09	0,47	0,36	0,96	19,61	9,87	25,95	1	2	70	32	27	1,48	0,62	1,14
56	39	54	31	26	56	41	30	27	24	29	20,36	10,73	8,18	9,09	15,27	63,64	0,53	0,36	0,89	21,47	9,94	25,37	1	2	78	33	27	1,48	0,62	1,18
57	35	62	26	28	52	39	27	26	26	27	19,64	9,64	7,82	9,09	15,27	61,45	0,46	0,37	0,98	18,12	9,66	26,65	1	2	66	30	26	1,42	0,59	1,18
58	35	57	27	35	50	35	24	24	26	24	17,45	10,00	7,45	8,55	11,82	55,27	0,44	0,36	0,74	15,52	8,56	17,78	1	2	71	30	24	1,26	0,57	0,92
59	39	48	25	33	51	41	30	28	26	24	19,09	10,73	7,82	8,73	12,18	58,55	0,43	0,36	0,90	17,71	9,89	21,79	1	2	78	34	28	1,38	0,59	0,94
60	39	53	26	34	49	41	29	28	25	23	18,73	10,18	8,00	8,55	12,36	57,82	0,49	0,37	0,96	20,11	10,15	22,39	1	6	78	35	28	1,36	0,61	0,96
61	41	51	19	32	43	32	23	21	24	21	14,73	7,64	6,18	7,82	9,45	45,82	0,43	0,38	0,87	13,70	8,02	18,35	1	6	71	30	21	1,07	0,47	0,73
62	40	51	26	33	45	32	23	22	26	21	14,73	7,64	5,82	7,09	10,00	45,27	0,47	0,34	0,89	15,06	7,49	19,38	1	6	73	30	22	1,07	0,44	0,78
63	39	53	26	32	41	30	22	22	23	21	13,82	7,27	5,64	6,91	9,27	42,91	0,46	0,34	0,85	13,66	7,44	17,79	1	6	68	28	21	1,00	0,43	0,72
65	34	45	22	39	36	58	41	40	30	24	21,82	11,09	9,45	11,09	13,27	66,36	0,50	0,40	0,76	28,98	15,81	18,53	1	2	71	40	40	1,58	0,72	1,03
66	35	39	23	39	34	56	40	38	28	24	21,82	11,64	9,45	11,27	13,27	67,45	0,50	0,42	0,69	27,66	15,93	16,50	1	2	72	39	38	1,58	0,72	1,03
67	26	37	31	31	40	57	40	39	28	23	21,27	12,18	11,45	11,45	14,91	69,45	0,48	0,39	0,91	27,13	15,39	21,42	1	5						
67b	37	50	27	29	44	49	35	35	26	24	21,45	11,09	7,82	10,73	16,00	67,09	0,51	0,40	0,83	24,88	13,93	20,19	1	2	70	36	35	1,55	0,59	1,24
68	38	47	22	35	46	32	36	35	26	23	22,55	11,82	8,55	13,09	17,09	73,09	0,84	0,39	1,03	26,45	13,56	23,57	1	2	77	39	35	1,63	0,65	1,33
71	33	49	36	32	45	55	38	38	26	24	20,00	9,45	7,27	9,45	13,27	59,45	0,50	0,38	0,84	27,83	14,20	20,07	1	3	77	42	38	1,45	0,55	1,03
72	23	50	39	32	46	57	39	38	28	27	22,00	9,82	7,64	10,55	15,09	65,09	0,54	0,39	0,90	30,66	14,78	24,34	1	4	81	43	38	1,59	0,58	1,17
73	44	42	25	37	41	45	32	31	22	18	16,91	8,00	5,82	5,82	10,18	49,64	0,48	0,40	0,71	21,50	12,21	13,12	1	2	77	36	31	1,23	0,44	0,79
74	45	41	28	38	43	45	31	31	24	19	17,09	8,36	6,00	5,36	10,18	50,36	0,50	0,42	0,71	22,43	12,80	13,24	1	2	78	36	31	1,24	0,45	0,79
75	44	45	25	40	42	49	33	33	24	21	17,45	8,36	6,36	7,45	10,73	51,82	0,45	0,39	0,75	21,81	12,86	15,57	1	2	81	39	33	1,26	0,48	0,83
76	39	49	24	34	54	39	26	24	21	22	16,55	8,18	5,82	5,82	11,82	49,27	0,48	0,38	1,05	18,60	9,14	23,57	1	2	73	31	24	1,20	0,44	0,92
77b	35	51	29	29	56	38	25	24	24	19	17,27	7,82	5,36	6,55	11,64	48,64	0,49	0,35	0,91	18,60	8,47	23,08	1	2	71	32	24	1,25	0,41	0,90
78	41	51	26	35	54	41	28	26	23	21	17,27	8,36	6,00	7,45	12,73	51,82	0,55	0,35	0,83	22,59	9,19	22,58	1	4	87	35	26	1,25	0,45	0,99
79	39	51	24	34	52	34	26	24	24	22	14,36	7,82	6,00	6,36	9,09	43,64	0,48	0,34	0,80	16,57	7,60	17,84	1	4	78	32	22	1,04	0,45	0,70
80	37	59	25	34	51	34	23	22	24	22	14,91	7,82	6,73	6,73	10,36	45,27	0,47	0,37	0,98	16,12	8,12	21,30	1	4	71	31	22	1,08	0,41	0,80
81	36	58	23	34	51	35	24	22	23	21	14,73	7,82	6,55	6,55	9,64	44,18	0,48	0,34	0,92	16,56	7,68	19,09	1	4	72	31	22	1,07	0,41	0,75
82	37	45	25	34	39	28	19	18	18	16	10,91	5,45	3,64	3,64	5,82	30,91	0,41	0,32	0,78	11,26	5,67	12,35	1	4	67	28	17	0,79	0,28	0,45
83	39	44	27	36	40	27	18	17	19	15	10,55	5,27	3,64	3,64	6,18	31,09	0,39	0,32	0,86	10,48	5,47	13,09	1	4	67	27	17	0,76	0,28	0,48
84	39	49	27	40	40	28	19	18	19	18	10,91	5,45	3,45	3,45	6,55	31,82	0,39	0,32	0,76	10,94	5,69	13,65	1	4	67	29	18	0,79	0,26	0,51
85	51	50	25	31	59	22	8	18	15	23	6,73	2,91	3,36	2,36	7,09	22,45	0,50	0,42	0,84	10,69	7,59	19,49	2	3	53	19	3	0,49	0,26	0,55
85b	56	46	29	34	62	23	6	19	14	22	7,27	3,09	3,27	2,36	6,91	22,91	0,51	0,40	0,99	11,60	7,55	21,61	2	0	57	20	4	0,53	0,25	0,54
87	61	46	26	31	60	20	7	17	14	24	6,55	2,91	2,91	2,36	7,45	22,18	0,57	0,46	0,90	11,61	7,59	21,56	2	0	55	23	3	0,47	0,22	0,58
88	47	42	29	30	54	17	6	16	15	18	5,45	2,36	2,18	1,82	5,64	17,45	0,50	0,44	0,79	8,30	7,08	14,15	2	0	57	19	3	0,40	0,17	0,44
88b	46	44	27	25	55	16	5	17	13	16	5,36	2,00	2,00	1,82	5,45	16,64	0,63	0,39	0,88	10,07	6,69	14,45	2	0	53	19	3	0,39	0,15	0,42
89	45	44	30	28	54	15	7	16	13	16	4,73	2,18	2,18	1,82	5,45	16,55	0,51	0,48	0,99	7,49	7,60	15,90	2	0	53	18	2	0,34	0,17	0,42
91b	43	37	26	21	46	8	8	13	10	12	2,91	1,45	1,09	0,91	3,45	9,82	0,49	0,30	0,67	4,04	3,85	8,33	2	0	47	16	1	0,21	0,08	0,27
92	39	38	29	24	45	8	8	13	9	13	2,73	1,64	1,27	1,09	3,64	10,36	0,52	0,37	0,78	4,25	4,86	9,98	2	0	52	19	1	0,20	0,10	0,28
93	40	36	29	24	44	9	8	12	10	12	2,91	1,45	1,27	1,27	3,82	10,73	0,51	0,39	0,82	4,41	4,56	10,20	2	0	46	18	1	0,22	0,10	0,30

Test code	Max wave height [mm]					Overtopping height max [mm]					Overtopping volume model [l]						Calc. wave speed [m/s]			Calc. Max discharge [m³/s/m]			N° of highest crest wave		1st wave height [mm]			Calc. average discharge [m³/s]		
	Ch.5	Ch.6	Ch.7	Ch.8	Ch.9	Ch.11	Ch.12	Ch.13	Ch.15	Ch.16	Ch.11	Ch.12	Ch.13	Ch.14	Ch.15	Total	Ch.11	Ch.13	Ch.16	Ch.11	Ch.13	Ch.16	highest	2nd highest	Ch.2	Ch.5	Ch.13	Ch.11	Ch.13	Ch.16
94b	43	54	32	36	66	30	12	27	15	19	8,36	4,00	3,45	2,18	8,55	26,55	0,48	0,35	1,16	14,72	9,43	21,53	2	3	51	22	8	0,61	0,26	0,66
95	42	52	33	29	66	31	10	28	15	26	8,55	4,18	3,45	2,73	8,55	27,45	0,51	0,39	0,98	15,56	10,91	25,34	2	3	53	22	8	0,62	0,26	0,66
96	45	53	32	31	66	31	12	30	17	19	9,64	4,18	2,55	2,55	9,45	30,00	0,56	0,45	1,10	16,95	13,57	21,23	2	4	62	25	10	0,70	0,31	0,73
97	31	53	31	25	62	29	9	24	15	26	7,45	3,45	2,55	1,64	7,09	22,18	0,50	0,38	0,86	14,52	9,17	22,44	2	4	52	22	6	0,54	0,19	0,55
98	36	50	28	26	62	28	9	26	14	24	7,6	2,9	2,9	1,8	7,1	22,4	0,5	0,4	1,0	13,9	10,0	23,5	2	0	60	21	6	0,55	0,22	0,55
99	41	51	30	27	59	28	9	25	12	25	7,3	3,3	2,6	1,6	6,9	21,6	0,5	0,4	1,0	15,3	9,0	24,6	2	3	54	20	5	0,53	0,19	0,54
100	25	38	24	26	42	13	5	19	15	10	3,5	1,1	1,3	1,6	2,6	10,0	0,5	0,4	0,8	6,3	7,9	8,5	2	0	38	17	2	0,25	0,10	0,20
100b	24	44	22	27	43	15	4	20	16	12	3,6	1,1	1,5	1,8	2,9	10,9	0,5	0,4	0,7	7,4	8,7	8,8	2	0	41	17	2	0,26	0,11	0,23
101	25	44	21	27	44	15	4	20	16	12	3,8	1,1	1,3	1,6	2,9	10,7	0,5	0,4	0,7	7,5	7,1	8,7	2	0	40	18	3	0,28	0,96	0,23
103	48	70	56	35	35	44	31	42	27	27	18,0	7,8	7,3	6,9	13,3	53,3	0,5	0,3	0,8	22,3	13,1	22,5	3	1		33				
104	54	76	58	44	36	46	34	120	34	27	20,2	9,5	8,2	7,8	14,6	60,2	0,5	0,2	1,0	23,5	28,2	27,6	3	0		32				
105	56	59	56	40	39	45	32	46	30	24	18,6	8,6	7,1	7,1	13,5	54,7	0,5	0,3	1,0	21,7	13,4	23,0	2	4		33				
106	49	58	49	40	43	38	29	24	26	19	15,3	7,3	6,2	5,6	9,6	44,0	0,5	0,3	0,8	18,4	8,0	15,6	1	3		29				
107	49	65	50	47	49	39	29	26	28	21	16,0	6,9	6,0	5,5	11,1	45,5	0,5	0,3	0,9	18,7	7,8	18,0	0	0		29				
108	48	67	50	44	48	39	28	57	25	21	15,6	7,5	6,4	5,6	10,7	45,8	0,5	0,3	0,8	18,7	17,5	17,7	3	1		29				
109b	52	64	53	35	40	37	30	30	20	21	13,1	4,4	4,4	4,0	7,8	35,8	0,5	0,3	0,8	18,9	8,9	16,0	4	3		30				
110	54	77	55	40	36	39	27	35	28	20	13,8	4,6	4,6	4,6	8,7	37,8	0,5	0,3	0,9	19,4	11,2	17,3	2	1		29				
111	56	60	56	39	34	41	29	55	29	18	15,1	5,1	5,1	5,1	8,9	41,1	0,5	0,3	0,8	21,5	15,6	15,2	5	2		31				
112	37	62	48	31	42	33	26	19	19	16	10,7	4,9	3,6	3,8	6,4	29,5	0,4	0,4	0,7	13,4	7,0	11,6	1	2		31				
113	48	57	50	41	49	35	24	20	25	17	12,2	5,3	3,8	3,8	7,6	32,7	0,5	0,4	0,8	16,6	7,6	13,9	1	0		32				
114	44	67	49	34	40	34	24	25	30	17	11,3	5,1	4,0	4,2	7,5	32,0	0,5	0,3	0,8	16,4	7,7	14,0	2	1		32				
116	40	75	66	61	30	48	38	35	28	52	22,4	13,1	11,5	11,8	18,9	77,6	0,5	0,5	0,7	25,7	16,2	36,9	1	2	66	33	35	1,62	0,87	1,47
117	38	74	65	54	30	48	38	35	28	53	22,7	13,1	10,7	11,8	18,6	76,9	0,5	0,4	0,7	25,5	15,4	35,0	1	2	67	32	35	1,65	0,81	1,44
118	33	64	62	52	30	47	37	34	29	49	21,6	12,7	11,5	12,0	19,1	76,9	0,5	0,4	0,7	24,8	14,0	36,0	1	0	74	33	34	1,57	0,87	1,48
120	51	67	53	32	32	39	31	28	30	38	17,5	10,4	10,7	10,7	14,6	63,8	0,5	0,4	0,7	21,0	11,3	27,6	1	4	67	29	28	1,26	0,81	1,13
121	48	67	53	33	28	40	32	29	30	39	18,2	10,7	10,0	10,7	15,6	65,3	0,5	0,4	0,7	20,3	11,7	26,9	1	4	67	29	29	1,32	0,76	1,21
122	49	61	53	32	28	41	33	30	30	40	18,4	10,9	10,6	10,7	15,3	65,8	0,5	0,4	0,7	20,4	12,8	27,7	1	4	67	29	30	1,33	0,80	1,18
123	62	65	56	33	29	39	29	27	25	36	14,2	8,0	7,1	7,8	11,5	48,6	0,5	0,4	0,7	19,3	10,5	24,1	1	4	64	30	27	1,03	0,54	0,89
124	50	61	56	32	34	38	29	26	25	38	14,7	8,6	7,3	7,8	11,6	50,0	0,5	0,5	0,6	20,1	11,8	22,2	1	4	64	29	26	1,07	0,55	0,90
126	43	64	56	33	28	39	30	27	26	40	14,4	8,4	7,8	8,4	12,0	50,9	0,5	0,4	0,6	21,1	11,7	25,3	1	4	67	31	27	1,04	0,59	0,93
127	39	72	54	36	36	47	32	32	24	50	19,3	10,0	8,0	9,1	15,8	62,2	0,6	0,5	0,7	26,3	14,9	35,0	1	0	65	31	32	1,40	0,61	1,23
128	40	77	53	37	37	47	35	32	24	48	18,9	8,2	9,3	9,3	15,5	62,0	0,6	0,5	0,7	25,9	14,5	32,9	1	0	66	32	32	1,37	0,62	1,20
129	52	71	54	31	31	45	34	31	26	50	18,2	9,5	7,8	9,5	16,0	61,3	0,6	0,4	0,7	25,3	13,7	34,2	1	0	69	32	31	1,32	0,59	1,24
131	46	51	56	32	40	44	21	24	25	39	12,4	4,7	2,7	3,5	7,5	30,7	0,3	0,2	0,4	15,0	5,1	14,1	1	0						
132	40	50	36	36	37	44	20	26	23	38	12,4	4,7	2,7	3,5	7,5	30,7	0,4	0,2	0,4	16,1	5,2	13,6	3	1						
133	44	54	32	33	37	45	22	24	18	38	13,1	4,7	2,6	3,1	7,8	31,3	0,3	0,2	0,4	15,2	5,4	13,8	1	0						
135	51	61	37	44	44	54	28	31	19	69	17,8	5,5	3,5	4,0	11,3	42,0	0,4	0,2	0,4	21,9	7,2	25,4	1	0						
137	46	70	45	46	46	52	27	41	16	74	16,6	5,3	3,3	4,0	12,0	41,1	0,4	0,2	0,4	19,7	8,6	27,5	3	1						
138	49	64	40	48	48	53	27	38	16	79	18,0	5,5	3,5	4,2	12,2	43,3	0,4	0,2	0,4	21,3	9,3	33,4	3	1						
140	47	64	62	40	45	55	30	33	16	70	20,6	7,3	4,9	5,5	14,4	52,6	0,4	0,2	0,5	20,0	7,2	32,1	1	0						
141	39	64	63	35	42	55	30	42	22	82	21,3	7,8	5,1	5,8	15,3	55,3	0,4	0,2	0,4	20,7	8,8	33,8	3	1						
142	48	68	64	43	38	56	31	34	19	73	21,6	8,2	5,8	6,0	14,2	55,8	0,4	0,3	0,4	20,8	8,6	30,1	1	3						
144	37	59	54	38	34	48	24	27	15	44	17,1	6,5	4,5	4,7	10,7	43,6	0,3	0,3	0,4	16,4	6,8	15,6	1	2						
145	43	57	55	36	33	48	25	41	13	42	17,8	7,1	4,6	5,1	10,2	44,7	0,4	0,2	0,4	18,0	8,9	14,8	3	1						
146	44	58	53	32	26	47	24	43	31	43	17,3	6,6	4,4	4,7	10,6	43,5	0,4	0,2	0,4	17,3	8,9	18,1	3	1						

Appendix I   Impulse parameter analysis complement

Maximal overtopping height

These two graphs illustrate remarks formulated in Subsection 6.4.1 about the relation between the maximal overtopping height and the impulse product parameter.
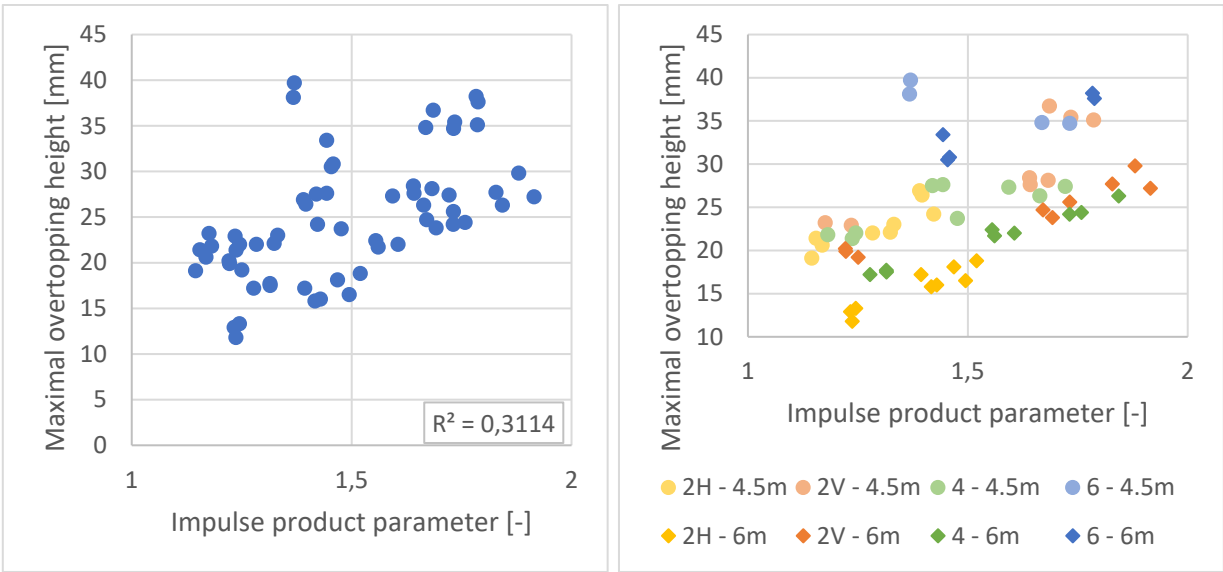

Figure I.1. Impulse product parameter versus the maximal overtopping height (sensor 13, smooth dam with 1:1.5 slope)

First wave height and first wave overtopping height

These three graphs illustrate remarks formulated in Subsection 6.4.1 about the relation between the first wave height, the first overtopping wave and the impulse product parameter.
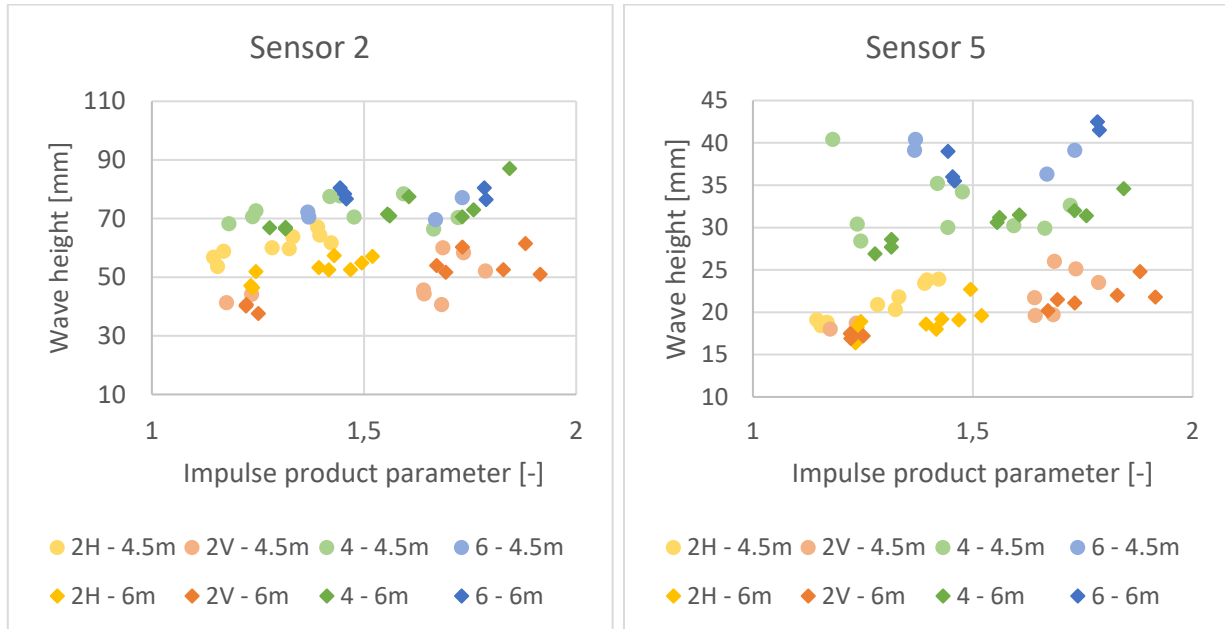

Figure I.2. Wave height of the first wave at sensor 2 and 3 versus the IPP (smooth dam with 1:1.5 slope)
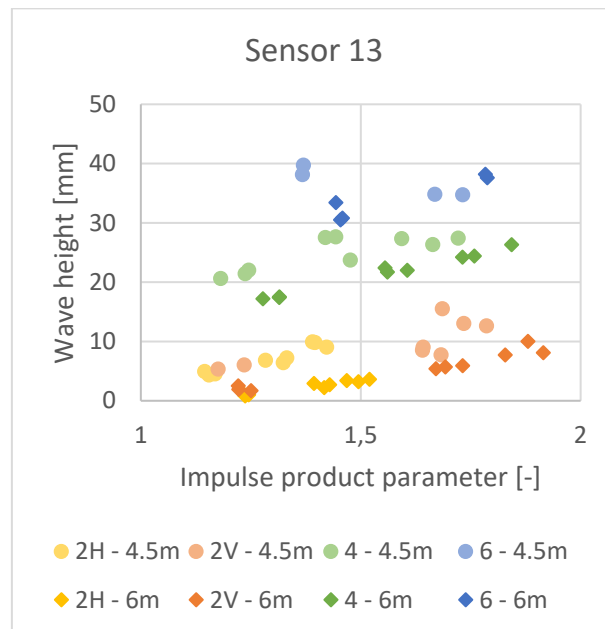

Figure I.3. Overtopping height of the first wave at sensor 13 versus the IPP (smooth dam with 1:1.5 slope)

Appendix J   Kobel et al. equations test

| Test n° | Dam slope | Dam type | Block setup | Freeboard [m] | Release height [mm] | a [m] | h [m] | w [m] | β [°] | Maximal overtopping depth [mm] | | | | |
| | | | | | | | | | | Measured by sensor 13 | Equation (2.6) | | Equation (2.7) | |
											Value	Rel. error	Value	Rel. error
100b	1,5	Straight smooth	2V	6	50	0,0167	0,28	0,34	33,69	3	15	511%	9	256%
88b	1,5	Straight smooth	2H	6	150	0,0165	0,28	0,34	33,69	3	15	439%	9	214%
85b	1,5	Straight smooth	2H	6	200	0,0174	0,28	0,34	33,69	4	16	342%	9	158%
43	1,5	Straight smooth	2H	4,5	100	0,0172	0,288	0,34	33,69	4	16	282%	10	144%
99	1,5	Straight smooth	2V	6	150	0,0202	0,28	0,34	33,69	5	18	242%	11	100%
52	1,5	Straight smooth	2V	4,5	50	0,0172	0,288	0,34	33,69	5	16	203%	10	93%
94b	1,5	Straight smooth	2V	6	200	0,0222	0,28	0,34	33,69	8	20	151%	12	47%
40	1,5	Straight smooth	2H	4,5	150	0,0192	0,288	0,34	33,69	7	18	149%	11	59%
49	1,5	Straight smooth	2V	4,5	150	0,0204	0,288	0,34	33,69	8	19	127%	12	45%
38	1,5	Straight smooth	2H	4,5	200	0,0218	0,288	0,34	33,69	10	20	105%	13	31%
48	1,5	Straight smooth	2V	4,5	200	0,0232	0,288	0,34	33,69	13	22	67%	14	6%
82	1,5	Straight smooth	4	6	50	0,0265	0,28	0,34	33,69	17	24	39%	14	-18%
80	1,5	Straight smooth	4	6	100	0,0303	0,28	0,34	33,69	22	28	28%	16	-25%
63	1,5	Straight smooth	4	4,5	50	0,0278	0,288	0,34	33,69	21	26	26%	17	-19%
77b	1,5	Straight smooth	4	6	150	0,0325	0,28	0,34	33,69	24	30	23%	18	-28%
72	1,5	Straight smooth	6	6	100	0,0495	0,28	0,34	33,69	38	45	19%	27	-29%
58	1,5	Straight smooth	4	4,5	100	0,0300	0,288	0,34	33,69	24	28	18%	18	-24%
74	1,5	Straight smooth	6	6	50	0,0377	0,28	0,34	33,69	30	34	13%	20	-33%
56	1,5	Straight smooth	4	4,5	150	0,0324	0,288	0,34	33,69	27	30	11%	19	-29%
124	2	Straight smooth	4	6	100	0,0322	0,292	0,34	26,57	26	29	11%	19	-27%
20	1,5	Straight rough	4	6	150	0,0327	0,28	0,34	33,69	27	30	10%	18	-35%
126	2	Straight smooth	4	6	100	0,0327	0,292	0,34	26,57	27	29	7%	19	-30%
65	1,5	Straight smooth	6	4,5	50	0,0449	0,288	0,34	33,69	40	42	6%	27	-32%
67b	1,5	Straight smooth	6	4,5	100	0,0394	0,288	0,34	33,69	35	37	5%	24	-32%
128	2	Straight smooth	4	6	150	0,0370	0,292	0,34	26,57	32	33	4%	22	-31%
120	2	Straight smooth	4	4,5	100	0,0320	0,3	0,34	26,57	28	29	3%	21	-26%
127	2	Straight smooth	4	6	150	0,0371	0,292	0,34	26,57	32	33	3%	22	-32%
121	2	Straight smooth	4	4,5	100	0,0317	0,3	0,34	26,57	29	29	-1%	21	-29%
118	2	Straight smooth	4	4,5	150	0,0355	0,3	0,34	26,57	34	32	-5%	23	-31%
117	2	Straight smooth	4	4,5	150	0,0366	0,3	0,34	26,57	35	33	-5%	24	-31%

Appendix K Multiple linear regression experiments

This is an experimental multiple regression which needs to be confirmed. The multiple regression was first applied to the set of data collected during the tests of the smooth dam to investigate which parameters significantly influence the generated waves, overtopping volume and overtopping height from a statistical point of view. In the second step, the same procedure is applied to the dimensionless parameters.

K.1. Model parameters

The following subsections present the data pre-treatment carried out to fit the underlying assumptions of multiple linear regression, as well as the results of the analysis for the measured wave height in position eight, overtopping height and overtopping volume.

Assumptions

This multiple linear regression is based on four assumptions: independency, normality and linearity of the data, as well as homogeneity of variances. Therefore, the data need to be pre-treated. First, the correlation between the different parameters characterising the tests, namely the landslide volume, length, weight and impact velocity, the reservoir water level, freeboard and the dam slope, was tested (Table K.1).

| | | Water level | Freeboard | Dam slope | Landslide | | | |
					volume	length	weight	velocity
	Water level	1,00	-0,68	-0,73	0,12	0,04	0,13	0,04
	Freeboard	-0,68	1,00	0,00	0,00	0,00	0,00	0,09
	Dam slope	-0,73	0,00	1,00	-0,16	-0,05	-0,18	-0,13
Landslide	**volume**	0,12	0,00	-0,16	1,00	0,86	1,00	0,28
	length	0,04	0,00	-0,05	0,86	1,00	0,83	-0,28
	weight	0,13	0,00	-0,18	1,00	0,83	1,00	-0,28
	velocity	0,04	0,09	-0,13	0,28	-0,28	-0,28	1,00

Table K.1. Correlation matrix of the predictors

The results show a correlation between the landslide volume and weight ($\rho = 0.998$), as well as between landslide weight and length ($\rho = 0.83$), freeboard and water level ($\rho = -0.68$), and water level and dam slope ($\rho = 0.73$). The weight of the landslide, the freeboard and the dam slope are not

considered in the regression to avoid multicollinearity between the predictors. A choice between the volume and the length has also to be made depending on which of measured values is analysed. *Homogeneity of the variances* is obtained by standardizing the data, i.e. subtracting the mean of the data set and dividing it by the standard deviation ($\mu = 0$, $\sigma = 1$). The condition of n*ormality* and *linearity* are assumed in the regression. Besides, not enough tests were carried out for 1:2 slope to be able to include it in these statistical tests.

Maximal generated waves height

The generated waves were analysed by applying multiple linear regression with maximal wave height measured by sensors n° 8 as the response variable. After removing the correlated and insignificant predictors, the main governing predictors found are the water level and the landslides volume. However, the regression only explains 43 % of the results variability (adjusted $R^2 = 0.43$). The maximal water height of sensor 5 was also tested. Governing predictors changed to length a speed of landslide, but with an even lower $R^2 = 0.33$. These two results show that the maximal generated wave height cannot be explained linearly with the predictors available for these tests.

Overtopping height

In the case of the overtopping height as a response variable, the volume of the landslide is shown to be statistically insignificant, which corresponds to the observations in Section 6.1.6. Therefore, it is not considered as influencing parameters for the overtopping height. Fitting the model to the standardised values of the water level, the landslide length and impact velocity gives the result in Equation (K.1).

$$Overtopping\ height \approx$$
$$26.8 + 3.9 \cdot water\ level + 5.9 \cdot landslide\ lenght + 2.8 \tag{K.1}$$
$$\cdot landslide\ velocity$$

This result shows that the overtopping height of the dam is not influenced by one main parameter. All three chosen predictors have a significant impact the overtopping height, and the landslide length has the largest impact. The results of model fitting on non-standardized predictors is presented in Equation (K.2). It enables to predict the overtopping height in this model. Notice that the adjusted coefficient of determination is relatively good ($R^2 = 0.85$), and the mean of absolute residuals is 2.11 mm.

$$Overtopping\ height\ [mm]$$
$$= -195.3 + 0.6 \cdot water\ level\ [mm] +$$
$$5.9 \cdot landslide\ lenght\ [m] + 2.8 \cdot landslide\ velocity\ [m/s]$$

(K.2)

Overtopping volume

For the overtopping volume, the statically insignificant value amongst the correlated landslide length and volume is found to be the length. Statistically significant predictors of overtopping volume are the water level, the landslide impact velocity and landslide volume. Equation (K.3) presents the regression equation for the overtopping volume, taking into account the standardised parameters.

$$Overtopping\ volume \approx$$
$$41.8 + 9.2 \cdot water\ level + 16.8 \cdot landslide\ volume + 6.4$$
$$\cdot landslide\ velocity$$

(K.3)

This equation shows that the statistically significant predictors of the overtopping volume are the landslide volume, which has 1.4 times larger impact than the water level and 2.6 times greater impact than the landslide impact velocity. According to the kinetic energy equation, it was assumed that the speed of the landslide has the most significant impact. But apparently, the landslide volume has more influence as it rises the water level by filling up the reservoir. This result is based on tests of this thesis, where the landslide volume is rather significant compared to the reservoir size. Regression Equation (K.4) is a result of model fitting on non-standardised values for this model. The adjusted R^2 has a value of 0.94, and the mean absolute residual is 3.14 l, which is good.

$$Overtopping\ volume\ [l] \approx -482.5 + 1.5 \cdot water\ level\ [mm] +$$
$$259.1 \cdot landslide\ volume\ [m^3] + 15.4$$
$$\cdot landslide\ velocity\ [m/s]$$

(K.4)

K.2.   Dimensionless parameters

The same dimensionless parameters as in Section 6.5 are analysed here: the relative slide volume $\Pi_1 = V_s/h^3$, relative slide length $\Pi_2 = l/h$, slide Froude number $\Pi_3 = V_s/(gh)^{1/2}$, relative slide density $\Pi_4 = \rho/\rho_s$, dam slope angle $\Pi_5 = \beta$ and the slide impact angle $\Pi_6 = \alpha$. Here data for the smooth dam with slope 1:1.5 and 1:2 were investigated. The slide impact angle is identical for all

the tests; thus, it is not taken into account in this fitting. Besides, the magnitude of the following suggested coefficients concerning the dam slope angle β have to be take cautiously, because only few tests were done in the 1:2 slope setup. Correlations between the relative slide volume, the relative slide length and the relative slide density were highlighted (Table K.2). Therefore, the relative slide density Π_4 was discarded. A significance tests of the other two Π-parameters are carried out for the overtopping height and the overtopping volume. The less relevant is then discarded.

	Π_1	Π_2	Π_3	Π_4	Π_5	Π_6
Π_1	1,00	0,86	-0,29	0,79	-0,06	-
Π_2	0,86	1,00	-0,28	0,95	-0,01	-
Π_3	-0,29	-0,28	1,00	-0,26	-0,17	-
Π_4	0,79	0,95	-0,26	1,00	-0,07	-
Π_5	-0,06	-0,01	-0,17	-0,07	1,00	-
Π_6	-	-	-	-	-	1,00

Table K.2. Correlation matrix of the dimensionless parameters

The statistically significant predictors for the *overtopping height* are the relative slide length, the slide Froude number and the dam slope angle. The fitting of standardised values results in Equation (K.5) with a relatively low $R^2 = 0.67$. Thus, this result needs to be taken with caution.

Overtopping height
$$\approx 11.26 + 4.3 \cdot l/h + \ 9.7 \cdot V_s/(gh)^{1/2} - 35.6 \cdot \beta \qquad \text{(K.5)}$$

The *overtopping volume* is governed by the relative slide volume, the slide Froude number and the dam slope angle. The result of model fitting is Equation (K.6) and adjusted $R^2 = 0.75$.

Overtopping volume
$$\approx 41.1 + 15.5 \cdot V_s/h^3 \ + 5.0 \cdot V_s/(gh)^{\frac{1}{2}} - 8.2 \cdot \beta \qquad \text{(K.6)}$$

In both cases, the fitting does not represent a significant amount of the tests. Therefore, it is concluded that the multiple linear regression of the Π-parameters is not good, and more complex equations should be studied to find better fitting of the dimensionless parameters or more tests should be carried out.